Parameters design and the operation simulation of a pneumatic dispensing system for biomaterial 3D printing

By

Wenqi Zhou

A thesis submitted to
the Faculty of Graduate Studies
in partial fulfilment of
the requirements for the degree of
Master of Science

Department of Mechanical Engineering
Faculty of Graduate Study
University of Manitoba
Winnipeg, Manitoba

August 2016

© Copyright
2016, Wenqi Zhou

Abstract

Tissue engineering (TE) combines methods of cells, engineering and materials to improve or replace biological functions of native tissues or organs. Fabricating scaffolds is a vital process in TE for the mechanical support of the cells proliferation with desired functions and intricate structures. A pneumatic dispensing system of 3D printing is used to build soft scaffolds with controllable pore sizes in this research. An effective method is required to help users to systematically select proper parameters to print hydrogel strands with desired widths to fabricate scaffolds. In this research, printing parameters are classified first to build a simplified mathematical model to identify the significant parameters. A factorial experiment is then conducted to investigate effects of selected parameters and their interactions on the strand width. The solution is further verified using single variable experiments with the regression test. Based on the results, a parameters selection method is proposed and evaluated using two verification tests. A comparison test of the scaffolds fabrication is conducted to verify the analytic solution of the proposed theory. It is found that the nozzle sizes, dispensing pressure, and moving speed of a printer head all statistically affect strand widths. Among them, the nozzle size has the most significant influence on strand widths. Factors interactions are mainly embodied in between the nozzle size - moving speed and the nozzle size - dispensing pressure. In addition, a statistical significant linear relationship is found between the moving speed - strand width and the dispensing pressure - strand width. Furthermore, due to the high cost of bio-materials and the high pressure threat of air compressor in the dispensing system, a

3D bio-printing simulation system is developed to demonstrate the system configuration and operation procedures to help new users avoiding operation mistakes in the real world. A haptic-based 3D bio-printing simulation system with the haptic feedback is presented by means of the Phantom Omni haptic interface. The virtual environment is developed using the Worldviz software. The haptic force feedback is calculated based on the spring-damper model and the proxy method. This system is verified using questionnaire survey to provide a flexible, cost-effective, safe, and highly interactive learning environment.

Acknowledgments

I would like to take this opportunity to thank my advisor, Dr. Qingjin Peng. Without his constant support and great patience, I would not be able to complete this thesis. His encouragement is very important for me to complete my degree. I wish to acknowledge that this research has been supported by the University Research Grants Program (URGP) from the University of Manitoba, Discovery Grants from the Natural Sciences and Engineering Research Council (NSERC) of Canada and GETS Grant from the University of Manitoba. I would also like to give my thanks to my colleagues in the Virtual Manufacturing Lab and friends who helped me for my research and thesis. Finally, I would like to thank my parents. They are the most important people in my life. Without their support and understanding, it is impossible for me to obtain this degree.

Contents

Front Matter

List of Tables

List of Figures

List of Appendices

Chapter 1
Introduction

1.1 Research Background

The advancement of medical infrastructures makes it possible for early detection of organ failures or malfunctioning that often requires full organ transplantations (Ghosal et al., 2014). However, two problems of organ transplantations are the organs shortage and the immune rejection. Tissue engineering has recently emerged as a promising alternative that integrates methods of cells, engineering and materials to improve or replace biological functions of native tissues or organs (Nerem et al., 1995). It has the potential to regenerate any kind of tissues or organs without the immune rejection since living tissues can be grown in vivo (in patients' body) using patients' own cells to be accepted as a natural part of patient's body (Ghosal et al., 2014; Katari et al., 2015; Murphy et al., 2014; Yoo, 2015). In the process of Tissue Engineering, scaffolds play a vital role to provide the intricate tissue structure and mechanical support for patient's cells proliferation with desired functions (Hutmacher, 2000). Generally, scaffolds can be grouped into hard scaffolds and soft scaffolds based on the material property (Weibin, 2014). The hard scaffolds are normally used for the fabrication of artificial bones (Motamedian et al., 2015) while the soft scaffolds are suitable for soft tissues or organs (Kumbar et al., 2008). Many

technologies have been used for the scaffolds fabrication, including conventional methods and 3D bio-printing methods. The conventional technologies mainly include the solvent casting/particle leaching (Murphy et al., 2002), thermally-induced phase separation, melt moulding (Thomson et al., 1995), and emulsion freeze-drying (Whang 1995). The disadvantages of these approaches include i) it is hard to control the porosity, pore sizes, pore interconnectivity and spatial distribution of pores within scaffolds, ii) cells and proteins cannot be incorporated in the fabrication process because scaffolds are normally built under harsh conditions such as high temperature or in the presence of organic solvents (Janik et al., 2015). To overcome these disadvantages, 3D bio-printing techniques have been introduced for the scaffolds fabrication in TE. CAD (Computer-aided design) technologies are used to design customized three-dimensional (3D) scaffolds models to drive a 3D printer to deposit biomaterials layer-by-layer to form scaffolds in desired 3D shapes (Mironov et al., 2006). As 3D bio-printing methods can fabricate scaffolds with designed microstructures to allow the incorporation of living cells and protein/growth factors during the fabrication process, they are currently widely employed in TE (Murphy et al., 2014). Among the 3D bio-printing technologies, extrusion-based systems are widely used for the soft scaffolds fabrication since they can print materials with a wider range of viscosity than inject print and laser assisted printing (Chang et al., 2011), thus making it possible to print high cell density bio-materials that are similar to physiological cell densities in tissue-engineered organs, which is a major goal in the bio-printing field (Marga et al., 2012). In the fabrication process, cell encapsulation bio-materials are extruded from a printer head to pile up layer-by-layer to form a 3D scaffold which is comprised of multiple hydrogel strands. The width of a single strand largely affects the printing quality (Weibin, 2014). In an extrusion-based

system, it is reported that a range of factors have influence on the strand width. Thus, understanding effects of process parameters on the strand width is important for the scaffold fabrication.

Although many research activities have been conducted to fabricate scaffolds using extrusion-based systems, there are still two problems in the process of printing soft scaffolds including (1) there is a lack of relationships of process parameters and their interactions on strand widths. (2) random trails and errors are commonly used to decide parameters for the desired strand width (Li et al., 2009a). There is not an efficient and scientific method for researchers to select appropriate parameters for a desired strand width using customized materials in various viscosities.

In addition to the parameter investigation in the scaffold fabrication, the bio-printing process using an extrusion-based system is a challenge as variable biomaterials, especially cells materials. There is a need to develop a cost-effective method to best use of these materials. Also, a dispensing system uses an air compressor that would be dangerous if the air pressure is over the limit. Any faults in the operation of machines may cause the material loss or even hazard to operators. Therefore, it is necessary to develop a simulation system of 3D bio-printing to demonstrate the system configuration and operation procedures to help users avoiding operation mistakes in the real world. Considering these problems, this research proposed a scientific method for parameters selection based on the experimental design and regression analyse. In addition, a 3D printing simulation system incorporated with a haptic device is built for the system demonstration and operation training, which is a different research filed from parameter investigation.

1.2 Research Objectives

The objectives of this research are to propose a parameters selection method for users to efficiently and systematically set appropriate parameters in printing strands with the required accuracy using customized materials in various viscosity, and to develop a 3D bio-printing simulation system for the operational demonstration and training purpose. Based on the literature review of both 3D printing technologies and parameter investigation methods, advantages and disadvantages of 3D bio-printing systems and related parameter investigation methods are summarized. A pneumatic dispensing system for 3D bio-printing is used in the research to establish parameters relationships for the customized material. At first, factors that have potential effects on printing result are identified and classified to build a mathematical model to descript the deposition process. A factorial experiment is carried out based on the mathematical model to investigate relationships of selected parameters and their interactions on the strand width. A single variable experiment is then conducted with the regression test to further search relationships of the printing speed and strand width, the pressure and strand width. Also, a data table that includes a series of experimental results is built for researchers to make an initial parameter selection for a targeted magnitude of a strand width. Based on experimental results and the data table, a parameter selection method is proposed and evaluated using two verification tests. A series of comparison experiments of the scaffolds fabrication are implemented to verify parameter relations and measure their degrees of the influence. Additionally, based on the literature review of the Virtual Reality and haptic technology, requirements of a VR system and haptic modeling methods are summarized. The SolidWorks software is used to build the virtual machine models, the virtual environment is developed using the Worldviz software. A spring-damper model and the proxy method are implemented to achieve the haptic

force feedback. A VR-based 3D printing simulation system is presented and evaluated using a questionnaire survey method.

1.3 Thesis Contents and Structure

As shown in Fig.1-1, the thesis is organized as follows. Chapter 1 introduces the research background, research objectives and thesis structure. Based on the literature review of both 3D printing technologies and parameter investigation methods, advantages and disadvantages of 3D bio-printing systems and parameter investigation methods with related challenges are summarized in Chapter 2. A pneumatic dispensing system for 3D bio-printing is chosen in the study for the parameters research. The printing parameters research is introduced in Chapter 3, which includes the parameter classification, mathematical modeling, a full factorial experiment, and single variable experiments with regression tests. Through the theoretical analysis and experiments, corresponding results of the significant parameters and their interactions are analysed and discussed. According on the conclusions summarized in Chapter 3, Chapter 4 proposes a parameter investigation method with two verification experiments. A series of scaffolds comparison tests are described in Chapter 5 to both further evaluate the proposed parameters selection method and verify effects of printing parameters on the printing quality of scaffolds. Chapter 6 is another research for bio-printing system training operation. Firstly, the importance of 3D bio-printing system simulation for the demonstration and training purpose is identified. Based on the review of VR technology and Haptic technology, a haptic-based simulation system for 3D bio-printing is built and a questionnaire survey is conducted to evaluate the simulation system. Chapter 7 concludes the thesis and identifies contributions of the research. Future work is also discussed.

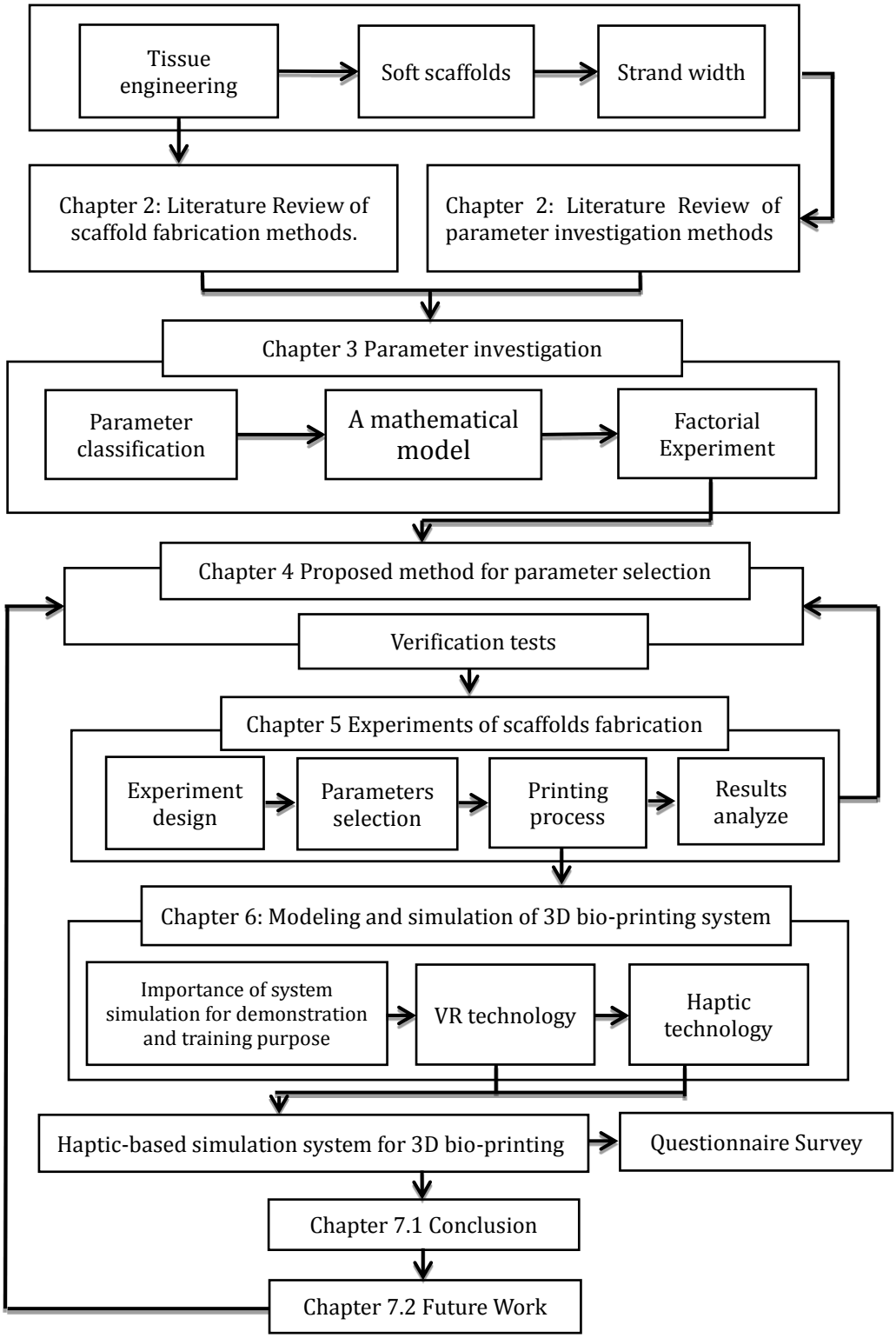

Figure 1-1. Thesis outline

Chapter 2
Literature review

2.1 3D bio-printing technologies

Different methods have been used for preparing porous structures to be employed as scaffolds in Tissue Engineering (TE). The conventional methods are limited to control the porosity and pore sizes of scaffolds while the 3D bio-printing technologies (Li et al., 2009a) integrate computer-aided design and manufacturing techniques into Tissue engineering, making it possible to design a three-dimensional (3D) structure in different sizes and porosity (Mironov et al., 2006). 3D bio-printing technologies are classified into inkjet printing, extrusion-based printing and laser-assisted printing as shown in Fig. 2-1 (Lee et al., 2015; Murphy et al., 2014).

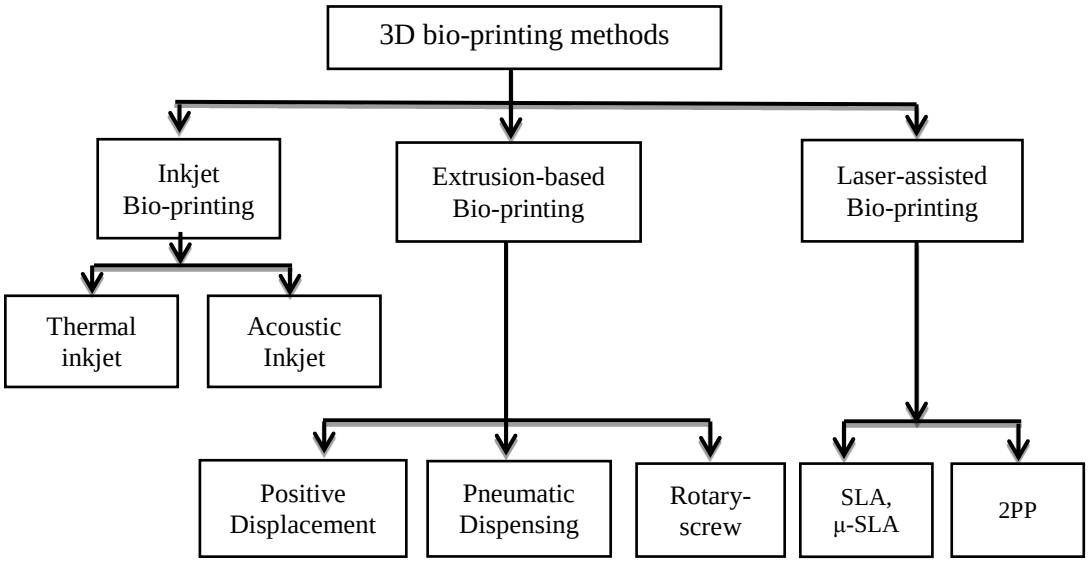

Figure 2-1. Classification of 3D bio-printing technologies in TE

2.1.1 Inkjet printing

Most inkjet bio-printers are modified based on commercial 2D inkjet printers in which an elevator stage is installed to control the movement in the vertical direction to print a 3D biological construct. Based on the ejection mechanism, it is divided into thermal inkjet (Cui, Boland, et al., 2012; Cui et al., 2010; Xu et al., 2005) and acoustic inkjet (Tekin et al., 2008; Xu et al., 2008). The thermal inkjet printers electrically heat the printer head to produce pulses of the pressure that forces droplets out of the nozzle to be deposited on the substrate (Cui et al., 2010). Although this method can achieve a high cell viability (Xu et al., 2008), there is a risk of exposing cells and materials to the thermal and mechanical stress (Cui et al., 2010). Also, the non-uniform droplet size, frequent clogging of the nozzle and unreliable cell encapsulation all affect the printing quality (Xu et al., 2005). By comparison, the acoustic inkjet printers use the acoustic force to break the liquid material into droplets at regular intervals, the material subsequently is ejected on the substrate under the pressure generated from the printer head (Xu et al., 2008). By using this method, the uniform droplets can be generated and the problem of exposure of cells to the heat and mechanical stress is avoided (Tekin 2008). Both inkjet printing methods have been successfully used to build 3D scaffolds (Zhang et al., 2008) and printing living cells (Cui et al., 2010; Saunders et al., 2014; Tekin et al., 2008; Xu et al., 2005). The main challenge of inkjet printing is that the viscosity of applicable materials is limited to 3.5-12 mPa/s due to the limitation of the ejection mechanisms (Saunders et al., 2014). The low material viscosity makes it hard to achieve biologically relevant cell densities (Saunders et al., 2008). However, inkjet printing also has many advantages, including the low cost, high resolution, high speed and ablity to print muti-materials. It also has

a high resolution that the width of a single line of cell drops can reach to 20μm (Chang et al., 2011).

2.1.2 Extrusion-based bio-printing

Extrusion-based bio-printers are usually comprised of a temperature-controlled device and a dispensing system used to extrude the material through the nozzle at an approporate temperature (Chang et al., 2011). Based on mechanisms of the material extrution, it is divided into three categories inlcuding i) the positive displacement, ii) pnueumatic dispensing, and iii) rotary-screw extrusion (Chang et al., 2011; Murphy et al., 2014). A positive displacement system uses a motor to drive a piston downwardly in the syringe to extrude the material through a nozzle. Therefore, amount of the extruded mateiral is decided by the motor displacement (Tirella et al., 2010). Similarily, the rotary-screw extrusion rotates a screw to dispense the material out of the nozzle (Visser et al., 2013). The amount of material dipensed is also dercied by the motor displacement. Differently, a pnueumatic system uses an air compressor with a dispenser that supplies the air pressure in the syringe to extrude the material through the nozzle. Many Factors are reported for the effect of the amount of materials extruded (Chang et al., 2011; Lee et al., 2015; Lee et al., 2012; Li et al., 2009b; Tirella et al., 2010; Weibin, 2014). Two advantages of the extrusion-based methods include i) they can print cell encapsulated hydrogel strands using biocompatible materials and, ii) can process high viscosity mateirals ranging from 30 mPa/s to 6×10^7 mPa/s (Chang et al., 2011; Jones, 2012), thus making it possible to print the very high cell density silimar to physiological cell densities in tissue-engineered organs, which is a major goal in the bioprinting field (Marga et al., 2012). However, a low cell viability was reported since the high pressrue and small nozzle sizes cause the high shear stress at

the entrance of the nozzle, thus causing the cells membrane disruption (Aguado et al., 2011).

2.3.3 Laser-based bio-printing

Unlike the inkjek and extrution-based bioprinting technologies that deposit materials to fabricate biological constructs, the laser-based technology uses the light energy such as UV light (Gauvin et al., 2012) and laser beam (Lee et al., 2008) on photocrosslinkable prepolymers in a specific path to form a crosslinked biolgical construct in a predifined pattern (Billiet et al., 2012). Two technologies of laser-based bio-printing are Stereolithography (SLA) (Gauvin et al., 2012; Lee et al., 2008; Schuster et al., 2009) and Two-Photon Polymerization (2PP) (Raimondi et al., 2013; Xing et al., 2007). Stereolithography (SLA) uses the light energy to crosslink an individual layer of photocrosslinkable materials reserved in a reservoir (Lee et al., 2008). As the laser scaner moves in X and Y directions, a 2D pattern of the polymerized material is built on the fabrication platform which is allowed to move in the verticle direction to form 3D constructs (Schuster et al., 2009). Based on the SLA technology, micro-stereolithography (μ-SLA) is proposed to fabricate soft scaffolds. It proves a higher resolution than normal SLA (Lee et al., 2008). Unlike the SLA techology, 2PP is a promising technology to fabricate a complex 3D microstructure with an extraordinary precision (up to 100 nm) (Xing et al., 2007). 2PP uses a photophlymerization process by moving the laser focus in the photosensitive material to absorpt two photons (Kufelt et al., 2014). Due to the extraordinary high resolution, 2PP makes it possible to select and print a single cell per laser beam (Raimondi et al., 2013). The advantage of the laser-based biopriting is that it avoids the problem of material clogging faced by the extrusion-based and inkjet bioprinting since the laser

beam replaces the nozzles to print the strands. In addition, it is reported that the laser beam has little effect on the cell viability and function, which leads to a high cell viability over 90% (Chang et al., 2008; Koch et al., 2009). Guillotin et al. (2010) reported the laser-based technology has the ability to print materials with a range of viscosities (1–300 mPa/s) and with a medium cell density up to 10^8 cells/ml, which is better than inkjet bioprinting (Guillotin et al., 2010). However, the high cost of laser-based systems is the major disadvantage compared to other technolodgies.

Based on above analysis, the key features of 3D printing technologies are summarized into Table 2-1. The laser-based bioprinting has a better printing resolution than others. Among them, the TPP (Two-Photon Polymerization) method has the highest resolution to print even an individual cell. The laser-based bioprinting is suitable to the microstructure scaffolds fabrication with or without the cell encapsulation (Billiet et al., 2012). It has been used to fabricate mutiple tissue types including cartilage(Lee et al., 2008), bone (Schuster et al., 2009), and skin (Michael et al., 2013). However, the system cost is much higher than other methods. Although the cost of inkject-based bioprinitng is low, it is limited to apply low viscosity materials with the low cell density. It is suitable to cell solution printing. Several types of the cells solution have been printed with a high cell viability, including mammalian cells (Xu et al., 2005), human fibroblast cells (Saunders et al., 2008), Chinese hamster ovary(Cui, Boland, et al., 2012). A notable application of inkjet bioprinting is to directly deposite cells into skin (Skardal et al., 2012) or cartilage (Cui, Breitenkamp, et al., 2012) wounds with fast crosslinking for direct lesions reparing. Compared to other methods, the extrusion-based bioprintings are both low cost and able to print high viscosity meterials with the high cell density encapsulaiton or without the cell encapsulaiton for the soft scaffold fabrication. Among them, the pnumatic dispensing system is used in

the research since it is flexible for adapting multiple applications with the simple operation and easy maintenance. The extrusion-based bioprinting methods have been successfully used to print the tissue engineered skin (Sharma et al., 2015), aortic valve (Duan et al., 2013), and heart valve (Duan et al., 2014).

Table 2-1. The comparison of 3D bio-printing technologies

Methods	Gelation methods	Viscosity	Advantages	Disadvantages	Cell viability	Resolution
Inkjet printing	Chemical, photo-crosslinking	3.5 – 12 mPa/s	Low cost, high speed, high resolution, print muti-material	Only low viscous material applicable, low cell density	>85%	Around 20μm
Extrusion-based bio-printing	Chemical, temperature, photo-crosslinking	30 mPa/s to > 6 × 107 mPa/s	High cell density bio-printing, simple structure,	Maintain high cell viability and high printing resolution	55%-90%	Around 50μm
Laser-based bio-printing	photo-crosslinking	1 – 300 mPa/s	High resolution, high cell viability, nozzle-free	High cost, complex structures	>90%	Around 0.1-2μm

2.2 Requirements of the soft scaffold fabrication

Fabricating soft hydrogel scaffolds for the tissue culture requires the preferable biocompatibility and printing accuracy (Weibin, 2014). Many fabrication parameters are reported to affect the cell viability and printing accuracy. In an extrusion-based bio-printing process, cells are encapsulated in a biocompatible material in the reservoir and then extruded and delivered to designated targets in a controllable manner (Chang et al., 2011). Thus, the cells are subjected to the dispensing pressure and the shear stress in the nozzle. For example, Parkkinen et al. (1995) reported that pressures lower than 5 MPa do not affect the cell viability and cell damage during dispensing, which is mainly attributed to the shear stresses in the nozzle. It is also

found that cell damage increases with the applied pressure and using larger needle diameters can reduce the cell damage (Aguado et al., 2011; Chang et al., 2008). In addition, by comparing the cell viability of porous hydrogel scaffolds with solid hydrogel structures, it is proved that the porosity of scaffolds can enhance cell's viability and the proliferation capability (Aguado et al., 2011).

Besides the preferable biocompatibility, fabricating a soft scaffold with a desired printing accuracy is also a vital criterion of a successful scaffold. In an extrusion-based system, the hydrogel strands extruded from a nozzle are deposited on the substrate to form a soft scaffold in a desired geometry. A soft scaffold is comprised of multiple hydrogel strands and its width largely affects the printing accuracy, thus it needs to be carefully controlled in the fabrication process (Chang et al., 2011; Kang et al., 2013; Weibin, 2014). The width of a strand is affected by a range of factors including material properties and operational parameters (Chang et al., 2011). The material properties include viscosity and surface wetting (Pati et al., 2014). The viscosity depends on the hydrogel, a function of factors including the mechanism of gelling, polymer solvent miscibility, polymer molecular weight, polymer concentration, temperature, cross linker activity, and humidity (Guillemot et al., 2010; Jang et al., 2009). Surface wetting is mostly determined by interfacial energies associated with the surface and substrate interfaces of the printed material (Sperling, 2015). Besides material properties, operational parameters consist of the needle diameter, applied pressure, temperature and moving speed of the printer head etc. (Chang et al., 2011; Jang et al., 2009; Kang et al., 2013; Lee et al., 2015; Li et al., 2009b). In the printing process, many of these variables affect each other. For instance, a temperature sensitive hydrogel, such as collagen, will begin to polymerize and irreversibly increase viscosity as temperature increases. The increased viscosity will

require parameters modification to maintain adequate material dispensing (Lee, Polio, et al., 2010; Park et al., 2011). In order to build a scaffold with a desired accuracy, it is therefore necessary to have a detailed understanding of how specific fabrication parameters and their interactions affect printing accuracy. Thus, a parameter investigation is another prime aspect of the scaffold research.

2.3 Methods of the parameter investigation

Different methods have been used for parameters investigations in 3D extrusion-based bio-printing. They are classified into experimental methods and mathematical modeling methods as shown in Fig. 2-2. Based on the theoretical analysis, the latter proposes a mathematical model to describe a deposition process that relates to effects of process parameters on the printing accuracy in developing predictive models (Lee et al., 2015). Experimental methods design an experiment in which certain factors are chosen and deliberately changed in a controlled manner to obtain their effects on the outcome factors using the statistical analysis (Federer, 1955).

2.3.1 Experimental design

According to the number of factors to be studied at a time, the experimental designs are grouped into one-factor-at-a-time design (single variable experiment) and factorial design (multiple variables experiment) (Federer, 1955). The factorial design is further classified to full factorial design and fractional factorial design (Kennedy et al., 1999) which also includes Taguchi design, Plakett-Burman design, central composite design and Box–Behnken design (Gunst et al., 2009).

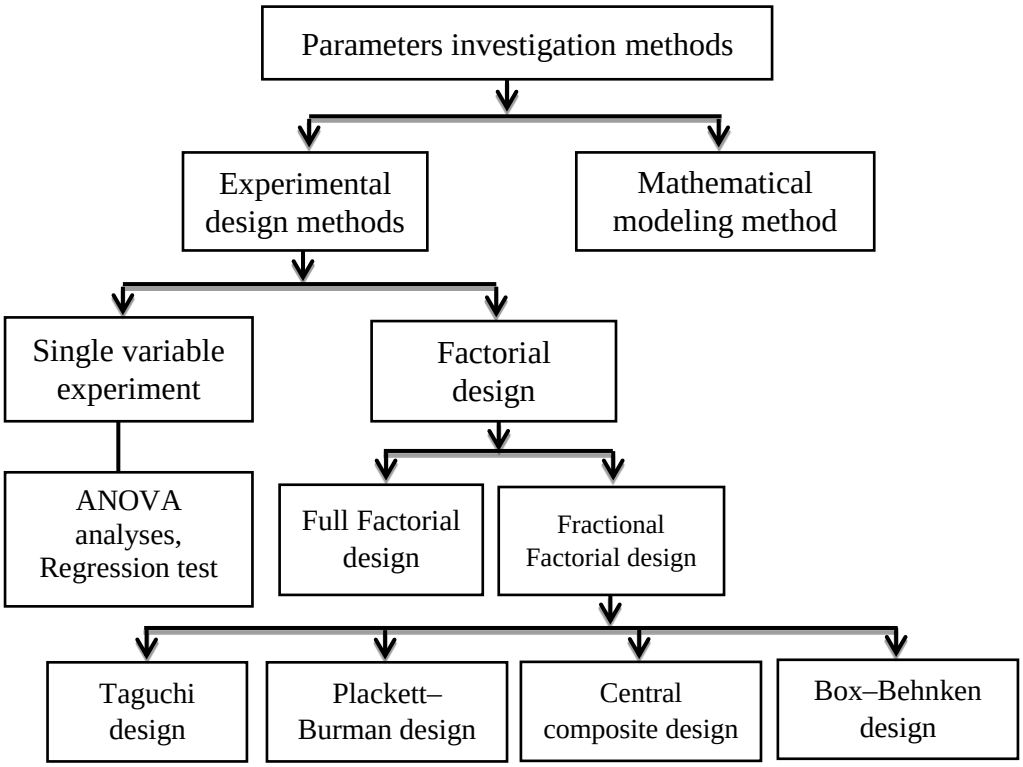

Figure 2-2 Classification of parameter investigation methods.

2.3.1.1 Single variable experiment

One-factor-at-a-time design is a traditional design, which investigates one-factor-at-a-time, while keeping levels of other factors constant. The factor to be investigated is changed over a desired range to study its effects on a response (Frey et al., 2003). When the experimental results are collected, certain graphs are created to visually display how a response is affected by the variable. Also, many statistical analysis methods, such as ANOVA analysis and regression test, are used to analyze the experimental results. Analysis of variance (ANOVA) is a collection of statistical models used to analyze differences among group means and their variation (Keselman et al., 1998). The regression test is a method that can form the statistical relationship between one or more predictors and the response variable to predict new observations (Neter et al., 1996). Since one factor-at-a-time design is easy to operate and analyze, it has been widely used to study effects of various factors on printing accuracy. Table

2-2 summarizes a number of studies using one-factor-at-a-time design to study effects of various factors on 3D bio-printing processes. For example, Kang et al. conducted single variable experiments for the pressure, path space, path height, nozzle diameter and printing speed with ANOVA analysis, it is observed that the pressure, path height and path space all significantly affect the printing accuracy, printing conditions do not affect the cell viability within the applied ranges (Kang et al., 2013). Similarly, Billiet et al. (2014) investigated effects of the printing speed, pressure, temperature and cell density on the strand width and found that they all largely influence the strand width. However, single variable experiments have two drawbacks. On the one hand, interactions among various factors are not considered, which cannot guarantee to identify the optimal conditions, especially when the interactions among different factors are significant (Czitrom, 1999). For example, Chang et al. (2011) studied effects of the needle size and pressure on the strand width using a single variable experiment but the interaction between them is ignored. On the other hand, when many factors are studied, a relatively large number of experiments is required, which is inefficient to carry out all the experiments (Czitrom, 1999). For example, five factors are investigated with each only four different levels but at least twenty runs of experiments are conducted (Kang et al., 2013). Therefore, the factorial design is introduced.

Table 2-2 One-factor-at-a-time method for the 3D bio-printing process

Material	Variables	Responds	Reference
PEG-DA, Gelatin, Alginate	Nozzle diameter, Pressure, Path height, Path space, Print speed.	Strand width	(Kang et al., 2013)
		Cell viability	
Gelatin methacrylamide	Printing speed, Pressure, Temperature, Cell density.	Strand width	(Billiet et al., 2014)

F127	Material viscosity, Needle size, Pressure, Print height.	Strand width	(Chang et al., 2011)
Gelatin	Pressure	Discharge rate	(Lee, Lee, et al., 2010)
PCL, PLLA	Pressure, Printing speed	Strand width	(Tirella et al., 2012)
Alginate	Pressure	Flow rate	(Khalil et al., 2005)
Agarose, Pluronic® F127, Alginate	Pressure	Discharge rate	(Lee et al., 2008; Park et al., 2011)
Agarose	Nozzle shapes	Discharge rate	(Weibin, 2014)
	Nozzle height, Nozzle space	Strand diameter	

2.3.1.2 Factorial design

Compared to a single variable experiment, the factorial design can study effects of more than one factor at two or more levels (Minitab). When designing an experiment, varying levels of all factors at the same time instead of one at a time can describe interactions among the factors, which is the more efficient way to deal with a large number of factors (Kennedy et al., 1999). Factorial designs are classified into two categories: full factorial design and fractional factorial design.

2.3.1.2.1 Full factorial design

In a full factorial design, every combination of each factor level is tested. For example, the number of runs for a three-factors full factorial design is $a \times b \times c$, which indicates that, the first factor is tested at level a, the second factor is tested at level b, while the third factor is tested at level c. The number of runs for a full factorial design of n factors, each at a level is a^n (Dunietz et al., 1997). Such an experiment allows the investigator to study effects of each factor on the response variable, as well as effects of interactions between factors on the response variable (Montgomery, 2008). A polynomial model is used to describe effects of factors on a response to optimize the

response if necessary (Myers et al., 2016). As all possible combinations of the factor levels are investigated in a full factorial design, many researchers use it to study effects of several factors simultaneously on a 3D bio-printing process as shown in Table 2-3. For example, Kim et al. (2009) conducted a full factorial experiment for three factors with each two levels. It confirmed that the pressure, moving speed, temperature and their interactions all largely affect the strand width. Among them, the pressure has the most significant influence on outcomes. Two empirical models based on the experimental results are generated to optimize the scaffold fabrication process (Kim & Cho, 2009). Lin et al. (2014) also carried out a 2^3 full factorial design for the solution concentration, applied pressure, and nozzle size. It concluded that the nozzle diameter influences more on the strand width than the pressure and solution concentration. The factor interaction is mainly embodied in the solution concentration and pressure. The number of runs for a full factorial design increases geometrically as the number of factors and studied levels increase. Therefore, a larger experiment is required, which is not economically and practically feasible (Luftig et al., 1998). In this case, the fractional factorial design is an alternative.

Table 2-3 A full factorial method for the 3D bio-printing process

Material	Variables	Responds	Reference
Hybrid biomaterials	Pressure, Moving speed, Temperature	Strand width, Strand height	(Kim & Cho, 2009)
Agarose	Pressure, Material concentration, Nozzle size	Strand width	(Weibin, 2014)
Hydroxyapatite (HA) powder	Material calcination time, nozzle size, deposition speed	Defined matrix for printing accuracy	(Hoelzle et al., 2008)
ABS	Air gap, Strand width	Scaffold porosity	(Chin Ang et al., 2006)

2.3.1.2.2 Fractional factorial design

In a fractional factorial design, the desired result is obtained by performing only a fraction of a full factorial design (Lundstedt et al., 1998). It is an alternative when the experimental size of a full factorial design is too large to be practicable (Underwood, 1997). By doing a fractional factorial design, effects of certain factors on a response can be studied under an economical and practical condition due to the reduced experimental size (Luftig et al., 1998). The fractional factorial design includes many methods, such as Taguchi design (Roy, 2001), Plackett–Burman design (Tyssedal, 2008), central composite design and Box–Behnken design (Anderson et al., 2000). Table 2-4 summarizes some studies using the fractional factorial design to study effects of various factors on the scaffold fabrication processes. The fractional factorial methods are detailed in the following part.

Table 2-4 A fractional factorial method for the scaffold fabrication process

Material	Variables	Responds	Reference
ABS	air gap, strand width, build orientation, build layer, and build profile	Scaffold porosity	(Chin Ang et al., 2006)
Composite material	Pressure, Material concentration, Nozzle size	ECM production	(Chen et al., 2007; Weibin, 2014)

Taguchi design

In a Taguchi design, an orthogonal array is used to study effects of many factors with two or more levels on a response with a small number of runs. The orthogonal array can facilitate the analysis of the design (Roy, 2001). Taguchi design is an efficient method to search an optimal combination of factor levels for optimum results when used properly. By using the range analysis, analysis of variance or analysis of signal-to-noise ratio, the key factors that have significant effects on a response can be

identified and the optimal factor levels for a given process can be determined from the pre-determined factor levels (Koschan et al., 2006). However, since the true optimal factor levels may not be covered by predetermined factors levels, the true optimal factors levels are not guaranteed using the Taguchi design (Koschan et al., 2006).

Plackett–Burman design

Plackett and Burman (1985) developed a Plackett–Burman design method which is a two-level fractional factorial design. It has been widely employed to screen important factors from a range of process parameters for further analysis (Kennedy et al., 1999). In this design, the number of experiment runs (N) is equal to a multiple of 4. It can examine up to n = N – 1 factors in an experiment with N runs and works for all such N up to 100, except for 92 (Anderson et al., 2001). If the number of factors to be examined is less than n = N – 1, a subset of Plackett–Burman design for N runs are used. The replications are sometimes performed to estimate the experimental errors. In order to depict the influence of various factors on a response based on the experimental results, a first-order polynomial model is used in the design as follows (Tyssedal, 2008).

$$y = \beta_0 + \sum_{i=1}^{k} \beta_i x_i \qquad (2\text{-}1)$$

Where y is the response, β_0 is a constant and β_i is the linear coefficient, and x_i is the coded factor levels. For example, Chin et al. (2006) used the Plackett–Burman design to study effects of the air gap, strand width, build orientation, build layer, and to build a profile on the scaffold porosity. The screened air gap and strand width largely affect the scaffold porosity.

Central composite design

The initial estimate of the optimal conditions for a process is usually far from the actual optimum. It is therefore necessary to locate a specific region of optimum factor

levels for the desired response. Central composite design is widely used in experimental designs based on the response surface methodology to estimate a second-order polynomial approximation to a response in a specific region (Myers et al., 2016). The Central composite design is a five-level fractional factorial design developed by Box and Wilson (Box et al., 1951). The design usually contains an imbedded factorial or a fractional factorial design with center points that are augmented with a group of 'star points' that allows the estimation of curvature. Take a two-factors of the central composite design as an example as shown in Fig. 2-3. If the distance from the center of the design space to a factorial point is ± 1 unit for each factor, the distance from the center of the design space to a star point is $|\alpha| > 1$. The precise value of α depends on certain properties desired for the design and on the number of factors involved (Anderson et al., 2001). For example, Chen et al. (2009) investigated the effects of the addition of chondroitin-6-sulfate (CSC) and dermatan sulfate (DS) Central Composite Design on the 3D chitosan scaffolds fabrication. They found that a combination of 2.8 mg CSC and 0.01 mg DS is optimal for the ECM production in a scaffold.

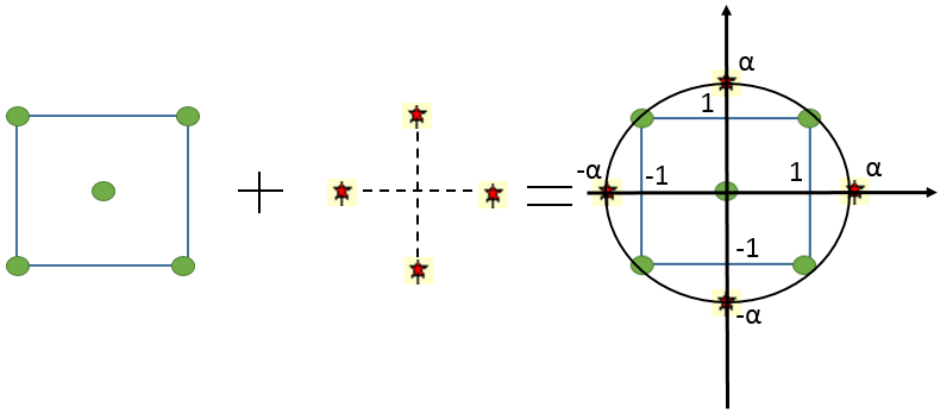

Figure 2-3 Generation of a Central Composite Design for two factors (Pham, 2006)

Box–Behnken design

Similarly, Box–Behnken design is also based on a response surface method to further search the optimum experimental conditions. Box and Behnken (1960) developed the Box–Behnken design which is a three-level fractional factorial design. The design is a combination of a two-level factorial design with an incomplete block design. Some factors are put through all combinations for a factorial design in each block, while other factors are kept at the central levels. Thus, it usually includes some central designs (Ferreira et al., 2007). Box–Behnken design is an effective alternative to the central composite design since it involves less factor levels than the central composite design and does not contain extreme high or extreme low levels.

2.3.2 Mathematical modeling methods

In addition to experimental design methods, mathematical modeling methods are widely used for parameters investigation. Based on the theoretical analysis, many mathematical models have been proposed to describe a deposition process to analyze effects of process parameters on the printing accuracy. In extrusion-based scaffold fabrication processes, the speed of a dispensing head has to be matched to the flow rate to produce continuous strands without material stacking or strands breakage (Li et al., 2009b). For example, by assuming that the diameter of strands formed is equal to the internal diameter of the needle by ignoring material swelling, the speed (v) of the dispensing head can be determined by

$$\mathrm{v} = \frac{4\mathrm{Q}}{\pi D^2} \tag{2-2}$$

Where Q is the volumetric flow rate and D is the diameter of strands. The appropriate dispensing head speed is dependent on the flow rate in the dispensing process (Li et al., 2009b; Ren et al., 2014). Therefore, numerous efforts have been made to find the flow rate function to predict the strand width with desired process parameters. At first,

flow rates in most studies were determined by the trial and errors (Ang et al., 2002; Landers et al., 2002). The approach is first improved when the Hagen–Poiseuille law is applied to develop models of the flow rate by assuming Newtonian material flow in the needle (Vozzi et al., 2002; Weibin, 2014; Woodfield et al., 2004). Based on the model, the flow rate is related to operational parameters, material viscosity and geometry parameters as follows:

$$Q = \frac{\pi D^4 P}{128 \mu L} \tag{2-3}$$

Where D and L are the nozzle diameter and length, respectively, μ is the viscosity of the material and P is the pressure drop applied in the needle. However, the limitation of this model is the assumption of Newtonian flow in the nozzle since most materials used for the scaffold fabrication are high-molecular-weight polymer solutions and colloid gels that are non-Newtonian fluids (Smay et al., 2002). In order to improve the model, non-Newtonian properties of materials are therefore considered and the flow rate is represented as follows (Khalil et al., 2007; Ren et al., 2014),

$$Q = \left(\frac{n}{3n+1}\right) \pi \Upsilon_0^{\frac{n-1}{n}} \left(\frac{P}{2\eta_0}\right)^{\frac{1}{n}} R^{\frac{3n+1}{n}} \tag{2-4}$$

Where η_0 is the limited viscosity at low shear rates and the constant γ_0 is the corresponding shear rate, and n is decided by material properties. It is proved that this model has a better accuracy than the previous one (Li et al., 2009a). Due to the utilization of small nozzle diameters, the surface tension of materials being dispensed becomes significant to affect the dispensing process. The pressure difference between the inside and outside of the material is given by

$$P = \frac{2\sigma}{D} \tag{2-5}$$

Where σ is the surface tension of the material and D is the diameter of the dispensing nozzle. For this reason, this effect is considered to improve the model of flow rates

(Chen et al., 2008). In addition, the slip between the shear flow and needle wall also needs to be taken in account when materials, such as colloidal gels that are mixtures of fine particles and high-molecular-weight polymers, are used for the scaffolds fabrication due to interactions of the solid fine particles and high-molecular weight polymer solution. For instance, Li's team reported a better estimation by considering wall slip factors (Li et al., 2009b). Furthermore, the fluid flow behavior also changes with temperature that needs to be taken into account, as it can greatly affect the flow rate (Chen et al., 2006) or the strand width and height (Kim, Yoon, et al., 2009) during dispensing. Although many models are developed to describe the deposition process to predict the printing accuracy, more factors need to be considered and quantified for a better estimation, which is a complex process (Lee et al., 2015).

In summary, the laser-based bio-printing has the highest printing accuracy but the cost is high while the inkjet bio-printing is more suitable for cells solution printing due to the limitation of applications of low viscosity materials. By comparison, the extrusion-based methods are both low cost and flexible for adapting to multiple application situations with the simple operation and easy maintenance. It is therefore used in this research. The biocompatibility and printing accuracy are two prime criteria to build a scaffold successfully. Many process parameters are studied to affect the printing accuracy in an extrusion-based system. Parameter investigations is an important aspect for the scaffolds fabrication. Both experimental design methods and mathematical modeling methods have been widely used to investigate parameters' effects on the printing accuracy. However, most studies used for the customized biomaterials in the experiments cannot be expanded to other materials. There is not an efficient and scientific method for researchers to select process parameters for a desired strand width for the scaffold fabrication using customized materials in various

viscosities. By using a pneumatic dispensing system for 3D bio-printing, this research carries out a series of experiments based on the theoretical analysis and experimental design methods to investigate parameters effects on strand widths. Thus, a parameter selection method is proposed for users to efficiently and systematically set appropriate parameters to print a strand with the required accuracy using customized materials in the various viscosity. Next chapter investigates relationships of the process parameters with the strand width.

Chapter 3
Parameter Investigation

As a scaffold is fabricated by multi-strands of the hydrogel material, the width of a single strand is used to evaluate the printing accuracy of a scaffold in this research. In order to investigate effects of process parameters on the strand width, a systematic parameter investigation is proposed as shown in Fig. 3-1. Process parameters that have potential effects on the strand width are first classified based on the type of parameters. In order to screen the significant factors, a simplified mathematical model is built to describe the deposition process under the assumption of Newtonian fluid behavior using the Hagen-Poiseuille equation. Based on the mathematical model, a 2^3 full factorial experiment is designed and implemented to identify effects of the selected parameters and their interactions on the strand width. Based on the experimental results, a parameter selection method is proposed in the next chapter.

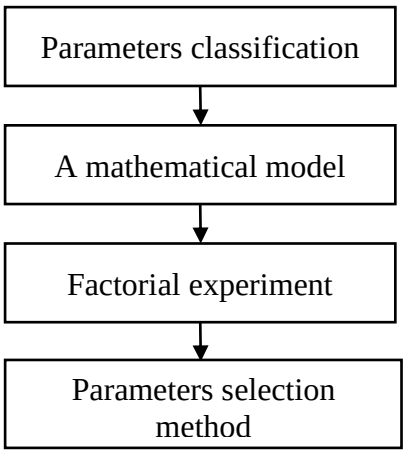

Figure 3-1. The process of parameter investigation

3.1 Parameters classification

Using a pneumatic dispensing system for the soft scaffolds fabrication, many factors and their interactions have been reported to affect printing quality of a scaffold. They are classified into three categories based on the type of parameters including material parameters, experimental parameters, and printer parameters as shown in Fig. 3-2 (Weibin, 2014). The material parameters include two main factors, viscosity and surface wetting (Chang et al., 2011). The viscosity depends on the hydrogel, a function of factors including mechanism of gelling, polymersolvent miscibility, polymer molecular weight, polymer concentration, temperature, crosslinker activity, and humidity (Guillemot et al., 2010; Jang et al., 2009). Surface wetting will be mostly determined by the interfacial energies associated with the surface and substrate interfaces of the printed material (Sperling, 2015). The experimental parameters consist of the nozzle size, nozzle shape, dispensing pressure, and temperature (Billiet et al., 2014; Park et al., 2011). Two types of nozzles, i.e., cone-tips and needle-tips, are widely used in the experiments. Using cone-tips in an experiment produces a higher flow rate than that using needle-tips under a same pressure because the friction inside the needle-tip is much higher than that in cone-tip (Weibin, 2014). Printer parameters are comprised of the printing height, printing space and moving speed of the printer head. A printing height refers to the distance between the bottom of nozzle and substrate. The printing space is the distance between adjacent centerlines of pattern lines. They are all considered affecting the strand width (Chang et al., 2011; Kang et al., 2013; Weibin, 2014). These parameters may also affect each other. For instance, as the hydrogel is a non-Newtonian fluid, the viscosity is decided not only by materials properties, but also the flow rate of materials influenced by the pressure and nozzle pattern. The identification of parameters effects is a cyclical and complex

process (Weibin, 2014). It is therefore necessary to screen the significant parameters for a practical factorial experimental design.

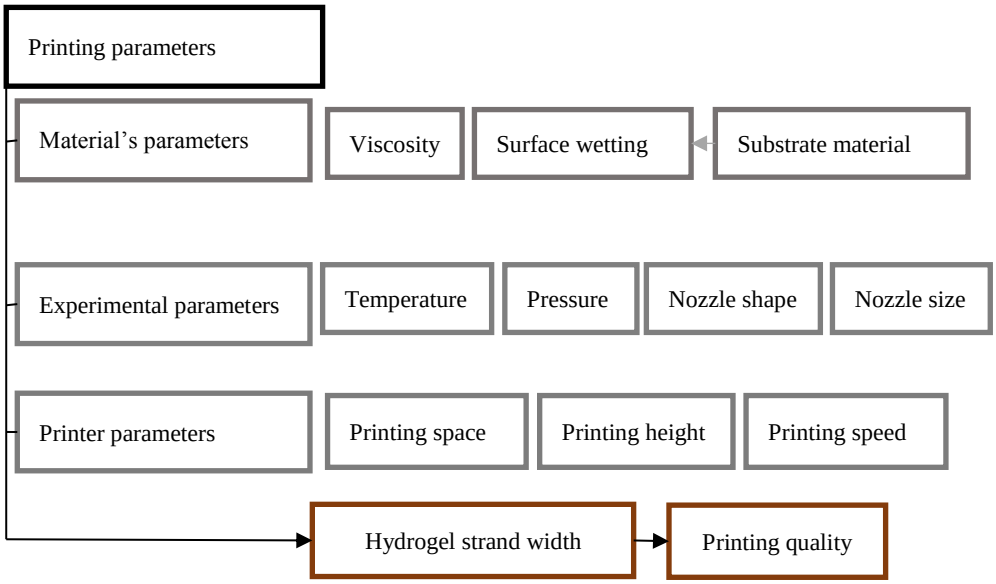

Figure 3-2 Parameters classifications

3.2 A mathematical deposition model

Many factors influence the strand width. If a full factorial experiment is conducted to investigate relationships of all the factors, it would be a huge experimental size to accomplish. For this reason, a simplified mathematical model is developed to relate significant operational parameters and material properties. It is to design a factorial experiment for the investigation of relationships of main parameters that affect strand widths. In this research, the model focuses on the tip of the needle where the hydrogel exits. It is assumed that the shape of the nozzle is cylindrical, and properties of the hydrogel are not sensibly affected by the solution evaporation soon after its extrusion. As shown in Fig. 3-3, forces acting at the tip are as follows:

- the weight of the hydrogel in the syringe (mg);
- the applied pressure of the dispensing system, P;
- the surface tension at the interface between the polymer solution and air, γ

• the dynamic friction between the fluid and wall of syringe, which is a function of the viscosity of the solution, μ.

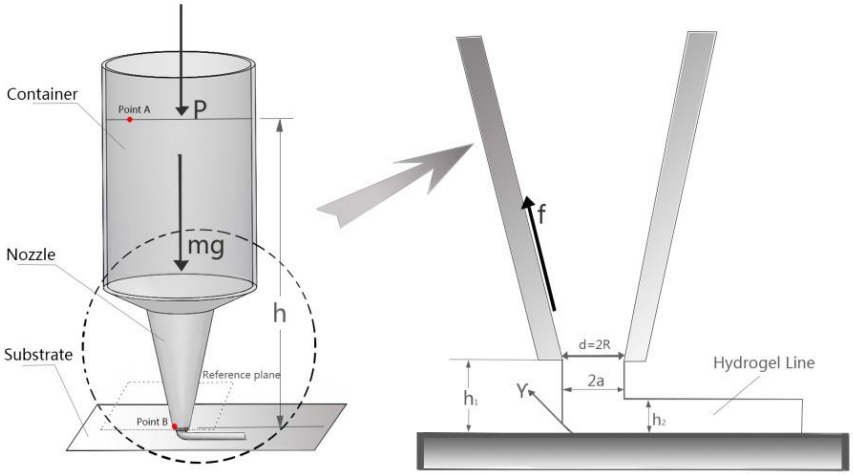

Figure 3-3. A mathematical model for the parameter investigation(Weibin, 2014)

If all the forces and energy are considered, it would be a multivariable system with an infinite equation to be solved. To simplify the model, we assume that the driving pressure P is the dominant force, while the other forces can be neglected. Hence, the flow of the hydrogel from the needle Q_1 is as follows.

$$Q_1 = \frac{\mathrm{dV}}{\mathrm{dt}} \tag{3-1}$$

Where V is the volume of hydrogel deposited and t is the time.

With the assumption of Newtonian flow in the needle, Hagen–Poiseuille law is used to describe the flow process of hydrogels. (Tartarisco et al., 2009; Weibin, 2014; Woodfield et al., 2004). According to Hagen-Poiseuille's Equation,

$$Q_1 = \frac{\pi \mathrm{R}^4 \mathrm{P}}{8\mu \mathrm{L}} \tag{3-2}$$

Where R is the internal radius of the needle tip, P the total applied pressure and μ the viscosity of the hydrogel.

Many studies assumed that the strand profiles deposited are approximate to elliptical segments (Li et al., 2009b; Melchels et al., 2009; Weibin, 2014). Here, it is considered that the volume of the hydrogel (Q_1) extruded from a syringe is equal to the hydrogel

(Q_2) deposited on the substrate under the assumption that the deposited hydrogel strand is continuous and uniform. Therefore, we can approximate the volume of the hydrogel deposited on the substrate as a function of time t:

$$Q_2 = S_{ellips} v_p = \pi a b v_p \quad (3\text{-}3)$$

Where v_p is the moving speed of the printer head, while a and b are the semi-major and semi-minor axes, respectively. As Q_1=Q_2, the strand width can be described as follows,

$$a = \frac{PR^4}{8\mu h b v_p} \quad (3\text{-}4)$$

Where v_p is the moving speed of the printer head, h is the distance from the material surface in the material container to the nozzle exit, R is the internal radius of the nozzle, μ the viscosity of the hydrogel, a and b are the semi-major and semi-minor axes, respectively.

3.3 Design of Experiment

3.3.1 Experimental design

A full factorial experiment is chosen for parameters investigation since all levels of factors combinations are investigated. Based on the ANOVA analysis, the statistical significance is determined at a level of less than 5% using Minitab 17 software to investigate relationships of the selected factors. By using graphs in the factorial design, the influence degree of variables and their interactions are compared and visually presented using bars in descending order on a Pareto chart to identify the most significant parameters. Moreover, normal effects plots and interaction plots can

intuitively indicate relationships between factors and responds, their interactions and responds. Based on the mathematical model, three operational parameters are considered to have effects on strand widths, including v_p, moving speed of the printer head; applied pressure P and nozzle diameter R. Therefore, a full factorial experiment of three factors with each two levels is conducted to identify significant factors and their interactions.

In order to select proper levels of factors, the experimental results from Billiet et al. are used as references (Billiet et al., 2012). Billiet et al. reported that the high inlet pressures resulted in the decreased cell survival using G27 (interior diameter 210μm) and G30 (interior diameter 160μm) nozzle sizes, especially when it is over 30 psi. G27 nozzle has a higher cell viability than G30 using 15 psi to 75 psi pressures (Billiet et al., 2014). Therefore, G27 and G23 (interior diameter 340μm) nozzles are chosen for a high cell survival. Also, the low pressure is preferable in the experiment. In addition, it is reported the most commonly used strands are 200 to 1500μm in the pneumatic dispensing system (Chang et al., 2011). Based on the above analysis, a series of the strands with widths ranging from 200 to 1500μm are printed using parameters combinations of pressures 10psi and 20psi, speeds 500mm/min and 1500mm/min, and nozzles G30 and G27. The printed strands are trim and uniform without material staking and strand breakage because strands with material stacking and breakages cannot be used for the scaffold fabrication. Therefore, two levels of each factor are chosen for the factorial experiment. By using each parameter set, a 25mm-long strand is printed on the glass substrate as the experimental sample as shown in Fig. 3-4. The hydrogel strand is observed using a microscope and measured using the Clemex vision PE software as shown in Fig. 3-5. Five replicates of the 2^3 full factorial experiment are conducted to investigate relations of operational

parameters and their interactions. Results are shown in Table 3-1 and analyzed using Minitab 17 software.

Table 3-1. 2^3 full factorial experiments design and data

a-Speed(mm/min)	b-Pressure(psi)	c-Nozzle diameter(µm)	Treatment Combination	Replicates(µm)						
				1	2	3	4	5	Sum	Average
500	10	210	(1)	418.04	424.52	421.27	430.90	411.85	2106.58	421.316
1500	10	210	a	222.96	223.47	226.66	223.40	226.66	1130.15	226.03
500	20	210	b	600.06	609.51	590.36	583.98	590.43	2974.34	594.868
1500	20	210	ab	363.91	354.44	341.46	341.58	351.15	1752.54	350.508
500	10	340	c	1049.89	1053.13	1034.03	1040.41	1056.33	5233.79	1046.758
1500	10	340	ac	545.76	564.86	539.38	545.91	568.02	2763.93	552.786
500	20	340	bc	1567.29	1570.34	1589.21	1586.00	1582.81	7895.65	1579.13
1500	20	340	abc	1005.44	982.87	995.70	1021.23	1017.96	5023.2	1004.64

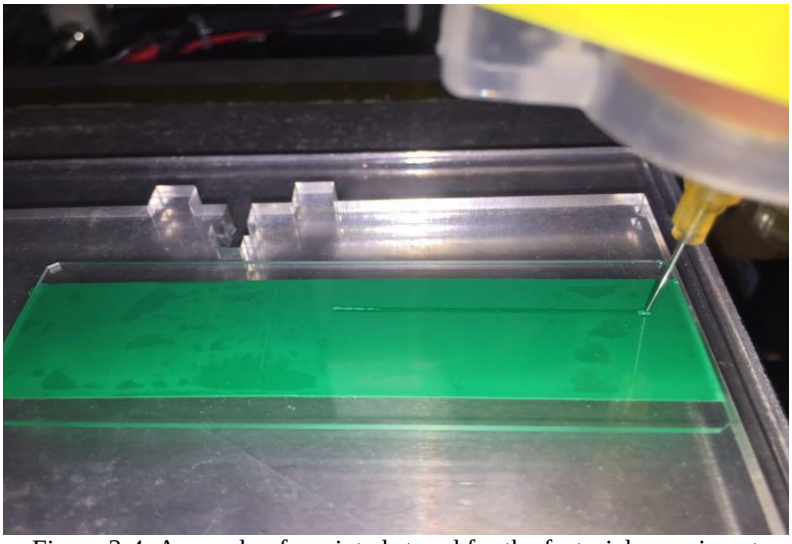

Figure 3-4. A sample of a printed strand for the factorial experiment

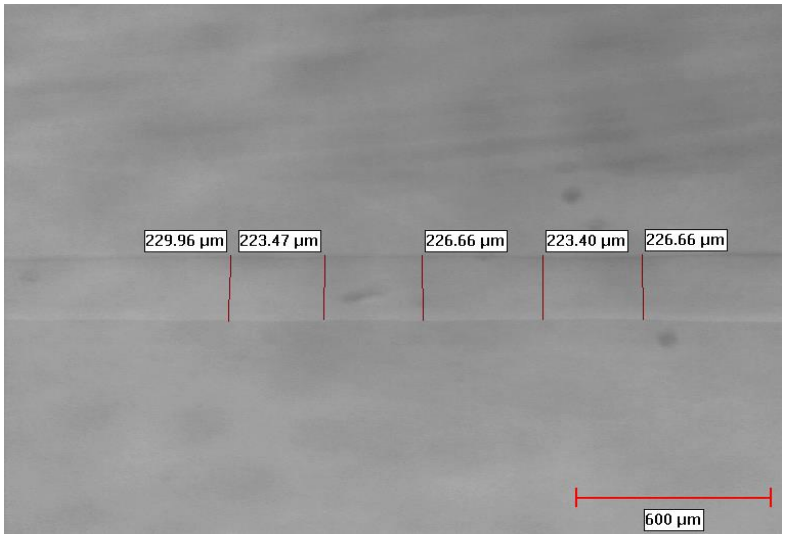

Figure 3-5. The measurement of a strand width using a microscope.

3.3.2 Results analysis

The factorial experiment analysis is based on the residual analysis. There are three requirements of a valid experimental model of the residuals including 1) the residual of each variable fits the normal distribution, 2) The sum of these residuals is zero, and 3) There is no obviously tendency in these residuals of the data (Weibin, 2014). Therefore, a normal probability plot is used to determine whether the group of data belongs to a normal distribution. If a group of data is normally distributed, the residual points would have the appearance of a line. Obviously, residuals of these experiment data obey the normal distribution well as shown in Fig. 3-6. Similarly, the histogram is close to symmetrical, which equally illustrates the normal distribution of residuals. Versus fits are evenly distributed across the zero, which means the sum of these residuals is zero. Versus order in Fig. 3-6 shows that there is no relation between residues and experiment sequences, these data are also evenly distributed across two sides of the mean. Therefore, these data are validated for the factorial experiment.

The normal probability plot displays statistical significant factors that have negative effects on the left side of the line and positive effects on the right side of the line. Fig. 3-7 therefore indicates that the factors, including A-speed, B-pressure, C-nozzle diameter, and interactions AC, BC, AB, and ABC, all have statistical significant effects on the width of hydrogel strands. Among them, the factors of C-nozzle diameter, B-pressure and interaction BC have positive effects, and C nozzle diameter has the largest positive effect. On the contrary, the factor of A-speed and interactions of AC, AB, and ABC have negative effects on the strand width, and factor A-speed has the largest negative influence. However, it is difficult to compare the magnitude of positive and negative effects. For this reason, the Pareto chart is used to display that the nozzle diameter (factor C) has the most significant influence on output results than

other factors while the second factor is the speed that influences a little more on the width of strands than pressure. By comparison, the standardized effect of interactions of ABC and AB have the least influence as shown in Fig. 3-8. Therefore, the nozzle diameter should be carefully controlled in the experiment as it dramatically affects the strand width.

The results can also be found in Fig. 3-9. It confirms that the nozzle diameter affects more on the strand width than the speed and pressure as the slope of the nozzle diameter line is larger than the slope of speed and pressure lines. In addition, it intuitively shows that the strand width is directly proportional to the pressure and nozzle diameter, and inversely proportional to the moving speed of the printer head. Therefore, the pressure and speed should be adjusted in the experiment to fine tune a strand width.

An interaction occurs when two lines are nonparallel. The more nonparallel the lines are, the greater the strength of the interaction. Therefore, the interaction is mainly embodied in the relation between factors A (speed) and C (nozzle diameter), B (pressure) and C (nozzle diameter), both of which have a larger angle formed by two lines than the angle of lines of A (speed) and B (pressure) as shown in Fig. 3-10. It means that relationships between A (speed) and width, B (pressure) and width, largely depend on the value of factor C (nozzle diameter) whereas the relation between B (pressure) and width is not obvious influenced by factor A (speed). In other words, the magnitude of a strand width will change a lot when the pressure or speed is adjusted in a same unit using different sizes of nozzles. On the contrary, the speed-width relation is not largely influenced by the change of pressure. Therefore, only by deciding a nozzle size first can the relation of speed-width or pressure-width be initialized. Moreover, Fig. 3-10 displays that interactions between A (speed) and C

(nozzle diameter), A (speed) and B (pressure), have a certain negative correlation while B (pressure) and C (nozzle diameter) have a certain positive correlation.

In addition, the two-levels factorial experiment assumes effects of factors are linear (Box et al., 2005). Results of ANOVA are shown in Table 3-2. The p-value tests the null hypothesis that the coefficient is equal to zero (variable has no linear effect on respond). A low p-value (< 0.05) indicates that the null hypothesis can be rejected (significant). In other words, a statistically linear relationship exists between variable and responds. Conversely, a larger p-value (≥0.05) suggests that the null hypothesis cannot be rejected (no linear relationship). It means that changes in the predictor are not associated with changes in the response. Based on the ANOVA analysis, it indicates that a linear relationship statistically exits between speed-strand width and pressure-strand width. Therefore, the strand width can be accurately predicted by using the single factor experiment to build a statistical linear relationship of the speed and strand width.

Table 3-2 The results of Analysis of Variance.

Source	DF	Adj SS	Adj MS	F-value	P-Value
Model	7	7173619	1024803	10697.45	0.000
Linear	3	6630583	2210194	23071.22	0.000
Concentration	1	1415140	1415140	14772.01	0.000
Dispensing Pressure	1	1025412	1025412	10703.81	0.000
Diameter of Nozzle	1	4190031	4190031	43737.84	0.000
2-Way Interactions	3	542543	180848	1887.79	0.000
Speed*Pressure	1	9520	9520	99.37	0.000
Speed*Diameter of Nozzle	1	242302	242302	2529.28	0.000
Pressure *Diameter of Nozzle	1	290721	290721	3034.71	0.000
3-Way Interactions	1	492	492	5.14	0.030
Speed*Pressure*Nozzle diameter	1	492	492	5.14	0.030
Error	32	3066	96		
Total	39	790321			

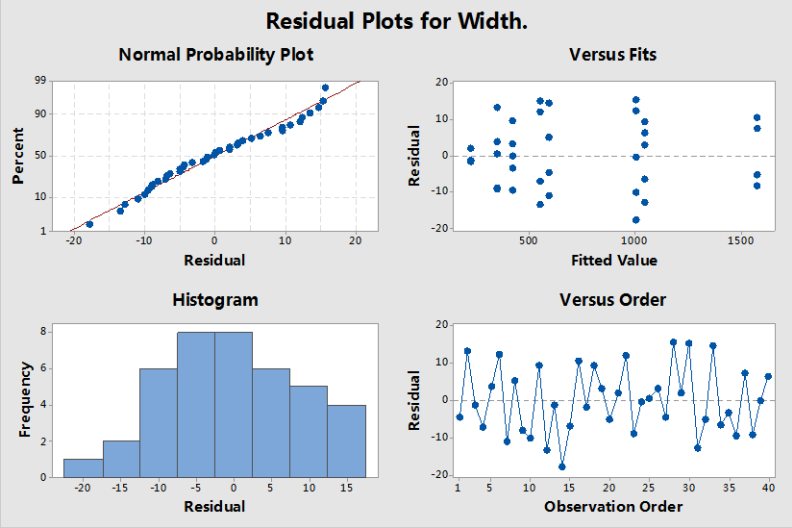

Figure 3-6. Residual plots for the strand width

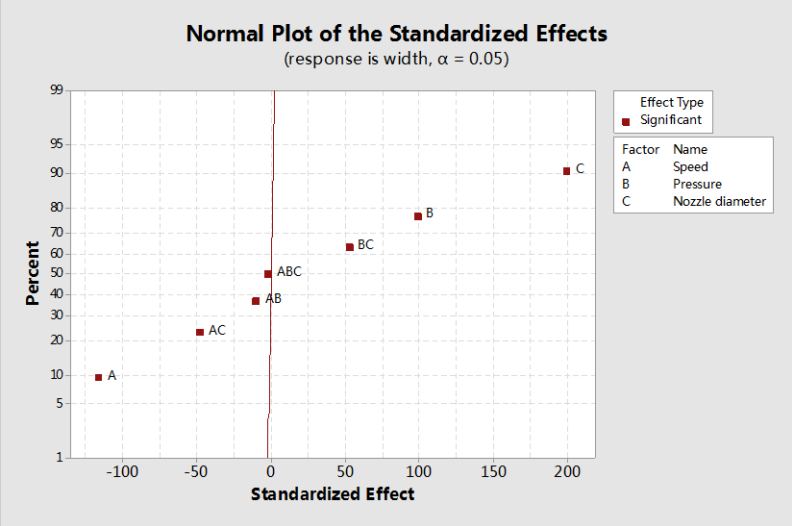

Figure 3-7. Normal plot of the standardized effects

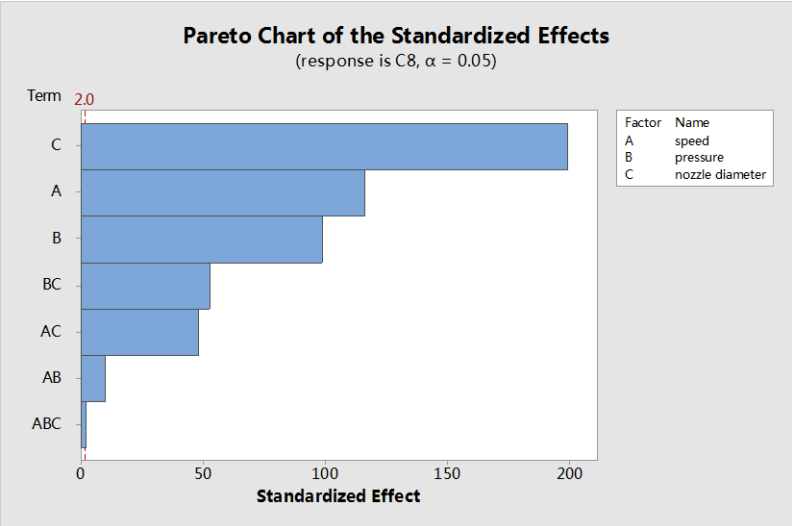

Figure 3-8. Pareto chart of standardized effects

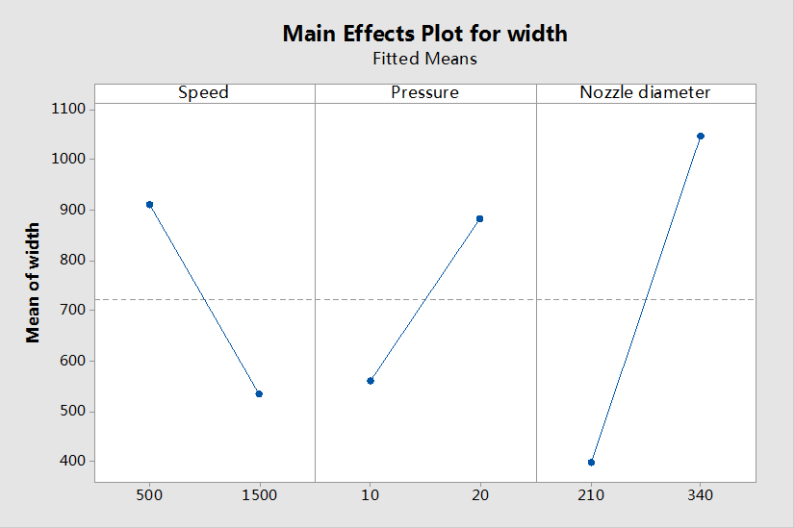

Figure 3-9. Main effects plot for widths

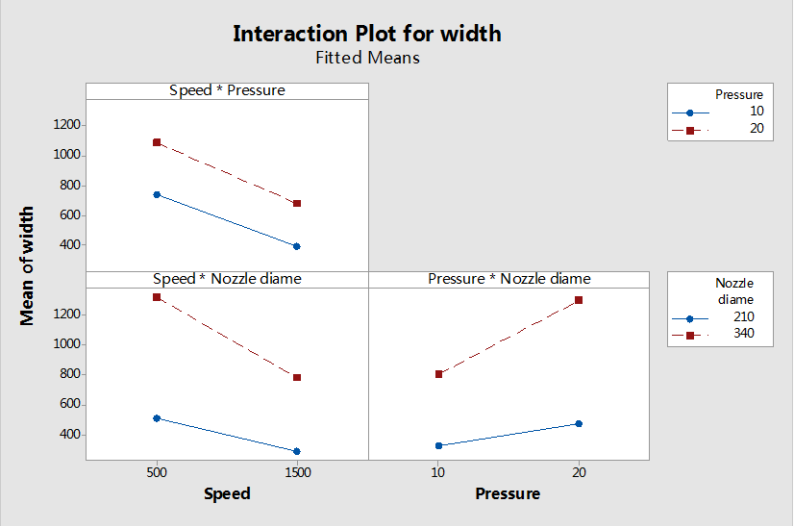

Figure 3-10. Interaction plot for strand widths

In summary, the factorial experiment indicates that the nozzle diameter not only dramatically affects the strand width directly but also significantly influences the relationship of pressure and strand width, speed and strand width. For this reason, it needs to be carefully selected first in the experiment so that the pressure-width and speed-width relationship can be decided, hence the strand width can be predicted. To fine tune a strand width, the pressure and speed should be adjusted instead of the nozzle diameter as they have less influence on the strand width than the nozzle diameter, and they are independent from each other. Besides, it also indicates that a statistical linear relationship exists between speed-width and pressure-width.

Therefore, by carrying out a single factor experiment to build a statistical linear relationship of speed-width, the strand width can be predicted. As a result, a data table is required to help users to make initial parameters selection to build regression model for speed width. The next chapter will propose a parameter selection method based on the data table and experiment results.

Chapter 4

A proposed method for the parameter selection with verification tests

4.1 A method for the parameter selection

Based on the mathematical model, a 2^3 full factorial experiment for three main operational parameters is conducted to identify the significant factors and their interactions. The important findings are summarized as follows:

(1) Factors of A (speed), B (pressure), C (nozzle diameter), and interactions of AC, BC, AB, ABC all have significant effects on the strands width.

(2) Among the factors, the nozzle diameter has the most significant influences on the strand width.

(3) The nozzle diameter also significantly affects relationships between A (speed) and strand width, B (pressure) and strand width.

(4) A statistical linear relationships of speed-width and pressure-width exist.

Therefore, by carrying out a single factor experiment of speed-width, a linear regression model of speed-width can be built to predict strand width. In order to make initial parameter selection to build a regression model for speed-width, a data table that includes a series of experimental results using the alginate material is built. Specifically, the experimental results are classified based on material viscosities as shown in Table 4-1. The proposed simplified mathematical model indicates the

material viscosity is the only material property affecting the strand width. This solution is tested for other materials in various viscosities that would be used by different research groups. Based on the data table and parameters relationships, a five-step parameters selection method is proposed to effectively and systematically set appropriate parameters for desired strand widths using customized materials. It is summarized in five steps as shown in Fig. 4-1 and the process is introduced in detail as follows.

(1) Measure the viscosity of customized materials to fit the material into the low viscosity, medium viscosity, and high and very high viscosity classifications.

(2) Search the data table to find the desired width of hydrogel strands and select an initial parameter set.

(3) Use the selected nozzle and check whether the pressure is strong enough to dispense the material out of the syringe.

(4) Based on the selected parameter set, set up a single variable experiment for the speed-strand width to build a linear regression model for them.

(5) Based on the regression model, find the desired parameter set with the targeted strand width.

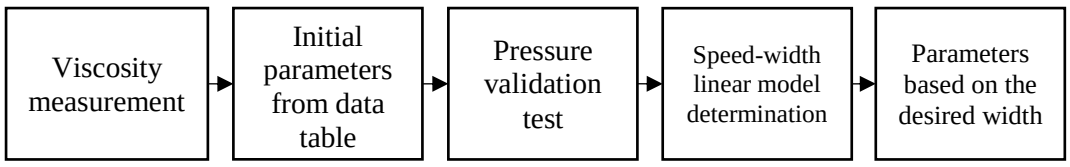

Figure 4-1. Five steps for the method of parameters selection

Table 4-1. Data table for the initial parameters selection

	Viscosity(Pa ·s)	Nozzle diameter(μm)	Pressure(psi)	Speed(mm/min)	Width(μm)
Customized material	Low viscosity ≈10	30g(160)	20	240	159.626
				60	320.470
		27g(210)	10	240	233.102
				60	477.578
		25g(250)	3	240	319.124
				60	580.948
		27g(210)	20	240	205.154

	Medium viscosity ≈90			60	328.102
		25g(250)	10	240	250.144
				60	392.886
		23g(340)	5	240	340.545
				60	421.436
	High viscosity ≈400	25g(250)	30	240	245.546
				60	393.860
		23g(340)	20	240	329.541
				60	526.828
		21g(510)	15	240	510.548
				60	751.154
	Very high viscosity ≈1300	23g(340)	30	240	330.215
				60	521.568
		22g(410)	25	240	390.456
				60	518.112
		21g(510)	20	240	489.514
				60	641.476

4.2 A verification test for targeted width 300μm

To evaluate performance of the proposed parameters selection method, a 9% concentration of the alginate solution is prepared to print strands with targeted widths 300μm and 600μm, respectively. Based on the proposed method, the viscosity of the alginate solution (around 500 Pa s) is first measured using TA Instruments Trios V3.3 machine. By searching the data table, the viscosity of the 9% alginate solution (around 500 Pa s) is the closest one to the high viscosity material (around 400 Pa s), which fits to the high viscosity material classification. Therefore, the experimental results in this classification can be used as the best reference to make an initial parameter selection for this test. Specifically, the parameter set in the first row of the high viscosity classification in Table 4-1, including the nozzle (25G), pressure (30 psi) and speed 60-240 mm/min, can be used to construct a strand with the width ranging from 245.546μm to 393.86μm using a material with the viscosity around 400 Pa·s. This range covers the targeted strand width, 300μm. Therefore, this parameter set is most likely to achieve the targeted width using 9% alginate solution due to the similar material viscosity to materials used in the data table. Therefore, the parameter set is

chosen as an initial parameter set. The next step is to build the speed-width linear regression model that requires at least three pairs of experimental data of the speed-strand width. Based on the speed range of initial parameters (60mm/min-240mm/min), three speeds, 80mm/min, 110 mm/min, and 140 mm/min, are selected to print a 25mm long hydrogel strand on the glass slices and measured using a microscope as shown in Fig.4-3 and Fig. 4-4, respectively. The same experimental process and measurement method as the factorial experiment are also used for two verification tests. The experimental results are shown in Table 4-2. Hence, a fitted linear plot is built using these data, its regression model strand width = 454.1 - 1.22 speed is shown in Fig. 4-2. By taking the advantage of the linear regression model, the targeted strand width (300μm) is predicted when the speed is set at 126 mm/min. By using the predicted parameter set, a strand is printed on the glass slice to verify the predicted parameter set. It is found that the width is 306.32μm as shown in Fig.4.5 which is 2 % error relative to the target width. It is acceptable compared to the predictive model proposed by Lee group that has an average error 57 % (Lee, et.al., 2015). Therefore, the parameter set is correctly selected for the targeted width, including nozzle 25g, pressure 30 psi, and speed 126mm/min.

Table 4-2. Experimental data for the targeted width 300μm

Speed (mm/s)	80	110	140
Strand width(μm)	360.62	311.72	287.44

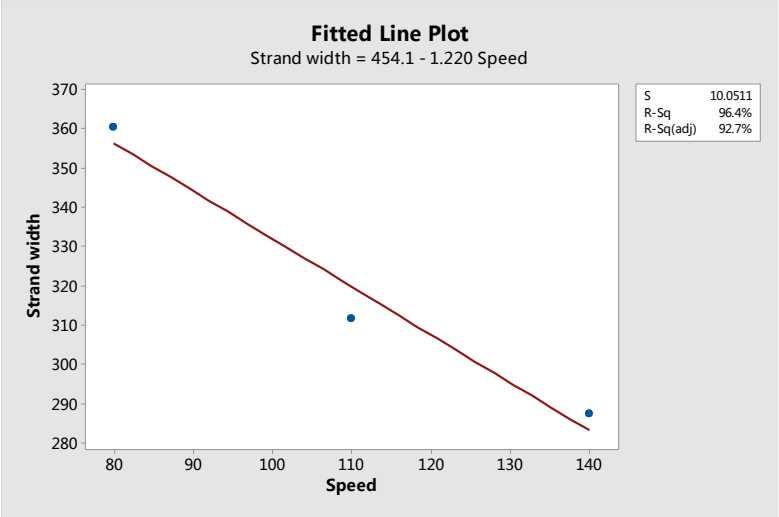

Figure 4-2. A fitted line plot of speed and strand width

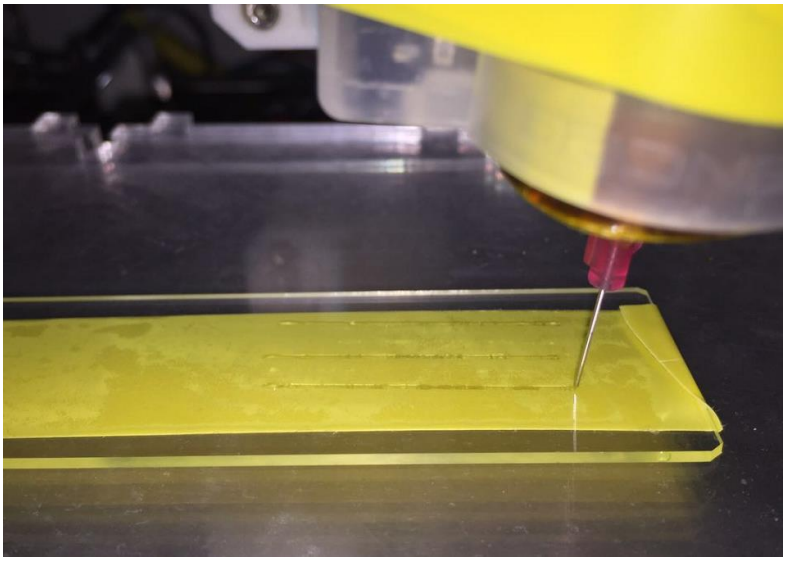

Figure 4-3. Three strands are printed on the glass substrate

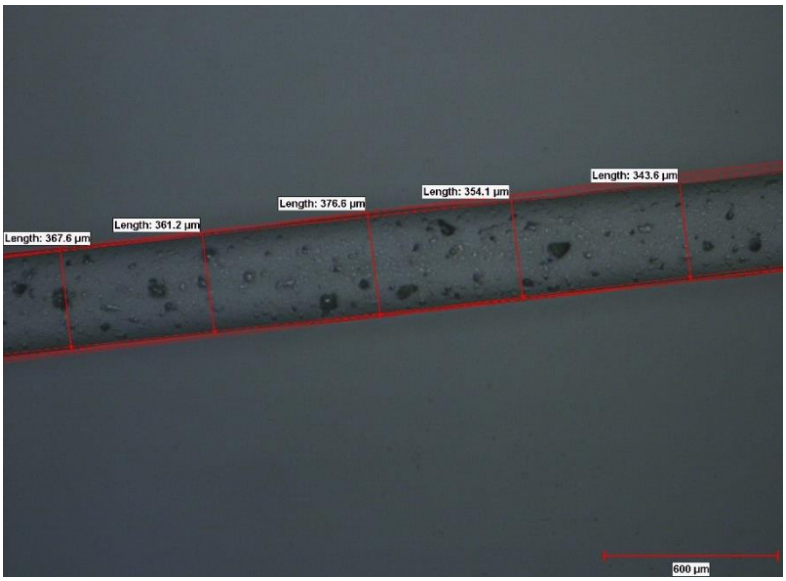

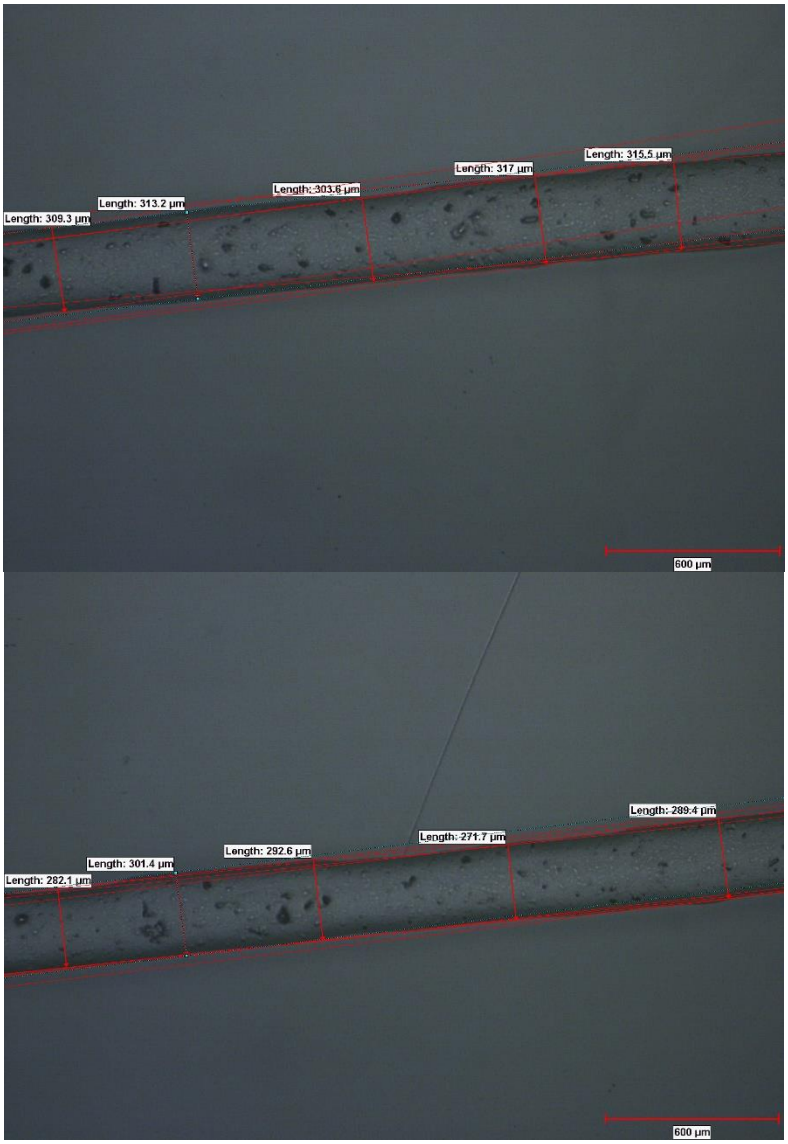

Figure 4-4. The measurement images of three strands using a microscope

Figure 4-5. The measurement image of the strand using predicted parameter set

4.3 A verification test for targeted width 600μm

Another experiment using the same material is carried to print a strand with the targeted width 600μm. It is known that the material is fitted to the high viscosity material classification, therefore the corresponding experimental results are used as references to make an initial parameter selection. By checking Table 4-1, it is found that the range of strand widths (510.54μm -751.15μm) using a 21g nozzle covers the targeted strand width 600μm and the range of strand widths (339.54μm- 556.82μm) using a 23g nozzle is close to the targeted strand width. Therefore, there are two possible choices for an initial parameter selection. The first one is to use 21g nozzle along with corresponding pressures and speeds. The second one is to use 23g nozzle with corresponding speeds while the pressure needs to be slightly increased to make adjustment to the targeted width. At this time, the latter one is selected as an example. The pressure is adjusted to 30 psi in the test. To build a linear regression model, three speeds including 60mm/min, 120 mm/min, and 180 mm/min, along with 30 psi pressure and 23g nozzle, are used to print three strand samples on the glass slice as shown in Fig. 4-7 and measured by a microscope as shown in Fig. 4-8. Based on the results as shown in Table 4-3, a fitted line plot is built as shown in Fig. 4-6. The regression model, strand width = 768.3 – 1.917speed statistically predicts that a speed of 87 mm/min can print a strand with the targeted width 600μm. Hence, a strand is printed on the substrate using the predicted parameter set and measured by a microscope as shown in Fig.4-9. It is found that the width is 600.4μm which is 0.06 % relative to the targeted width. It is acceptable compared to the predictive model proposed by Lee group that has an average error 57 % (Lee et.al., 2015). Therefore, the desired parameter set is found, i.e. 23g nozzle, 87 mm/min speed, and 30 psi pressure with a desired printing accuracy.

Table 4-3. Experimental data for targeted width 600μm

Speed (mm/s)	60	120	180
Strand width(μm)	636.86	556.32	425.96

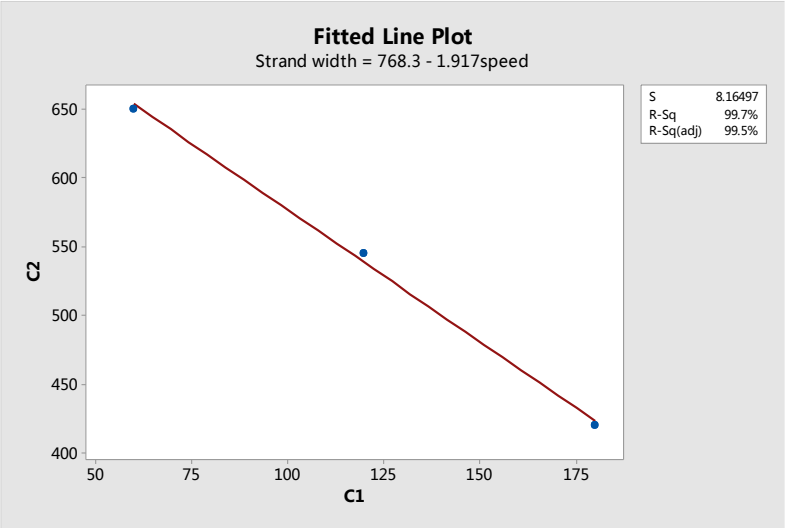

Figure 4-6. Fitted line plot of speed and strand width

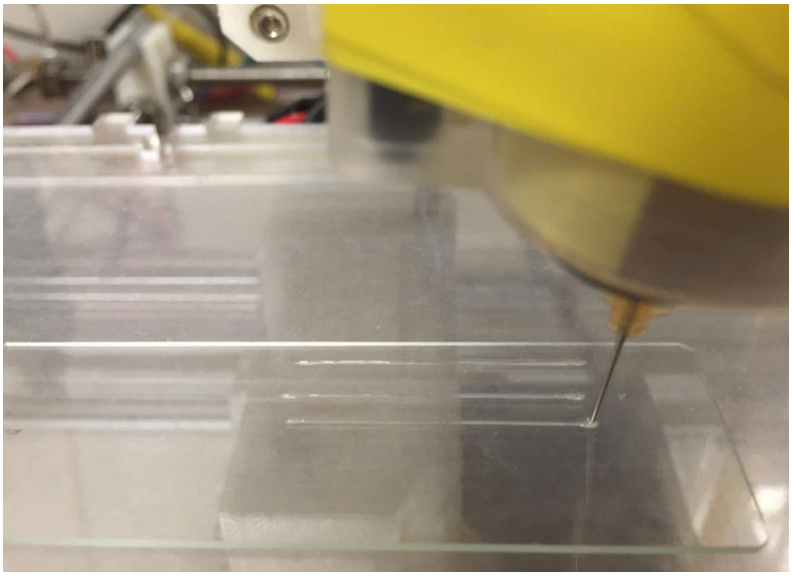

Figure 4-7. Three strands are printed on the glasses substrate

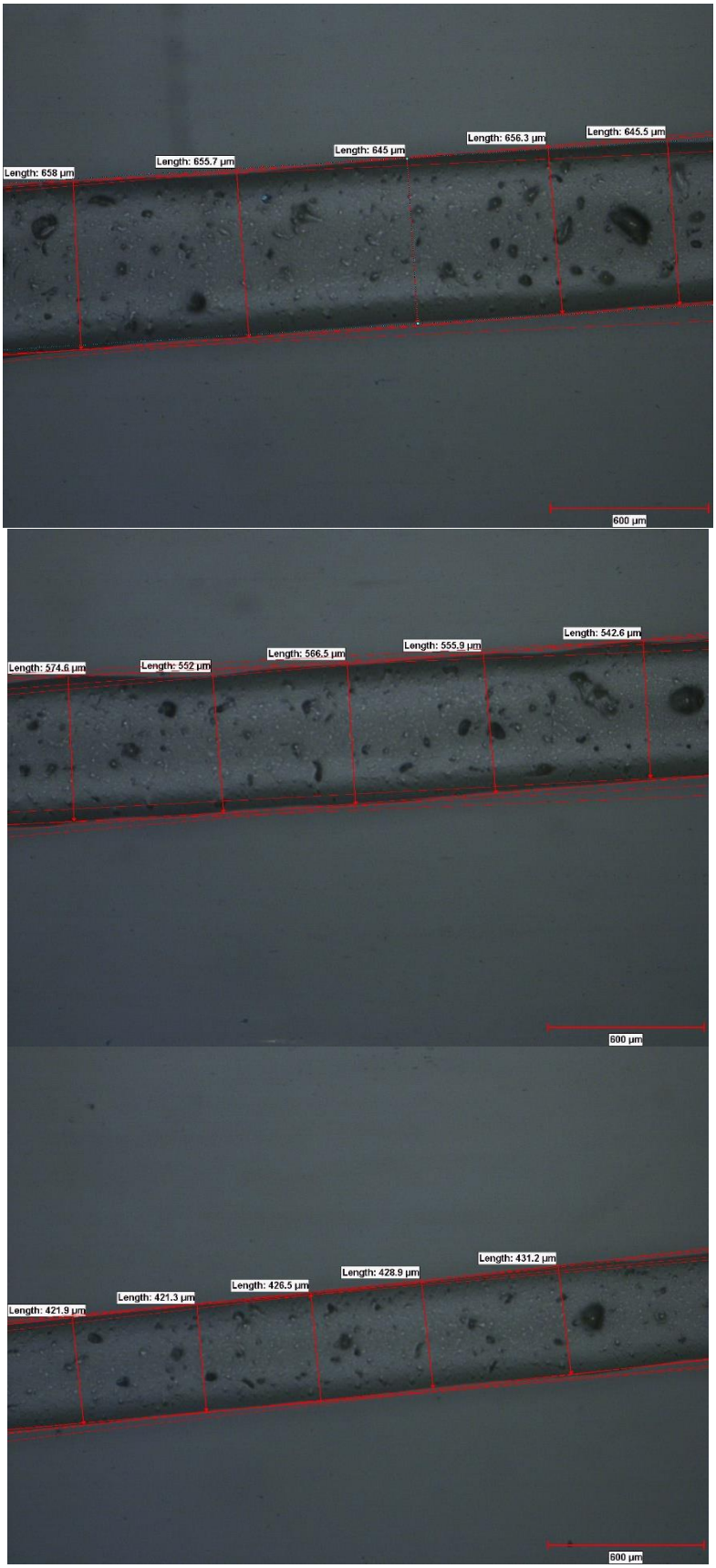

Figure 4-8. The measurement images of the strands using a microscope

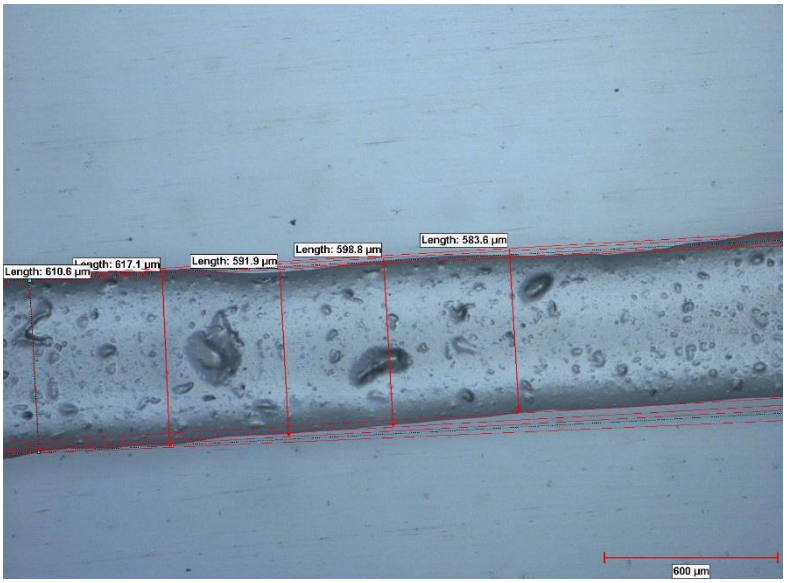

Figure 4-9. The measurement image of the strand using a predicted parameter set

In summary, in order to propose the parameter selection method, a simplified mathematical model is first proposed to identify the significant factors that affect the strand width. Then, a factorial experiment is carried out based on a mathematical model to investigate relationships of operational parameters and their interactions. It is found that the nozzle size has the most significant influence on the strand width that should be selected first and carefully controlled in the experiment.

Compared to the nozzle size, the pressure is directly proportion to a strand width, and the speed is inversely proportion to a strand width. They affect less on the strand width than the nozzle size, therefore, they are used to fine-tune a strand width. A statistical significant linear relationship is also found between the speed-width and pressure-width.

Therefore, the strand width can be accurately predicted by building a statistical linear relationship of the speed-width. Based on the experimental results, a method is proposed for users systematically select parameters for the desired strand widths using customized materials. This method uses the material viscosity as a bridge to expand experimental results listed in the data table to the customized materials. It guides users

to match a customized material to a material classification using the material viscosity in which the related experimental results are used as references. It can significantly save users' time to decide initial parameters and to narrow down the selection range to improve the printing accuracy.

By using the proposed method, two appropriate parameter sets are found using a customized material to print the strands with widths 306.32μm and 600.4μm which are very close to the targeted widths 300μm and 600μm, respectively. Although there is still a small variance of experimental results from the targeted width, its prediction accuracy is better than some previous prediction models. For example, Lee proposed a prediction model for the speed-strand width (Lee et al., 2015). To verify the model, four hydrogel strands were printed using different speeds. The printed widths were around 1700μm, 1400μm, 1200μm, 1050μm, respectively. While the corresponding predicted hydrogel widths using the prediction model were 700μm, 550μm, 450μm, 350μm, respectively, which are far from the expected results.

Therefore, it is possible to rationally and systematically determine the operational parameters for the scaffolds fabrication using the proposed method in this research, instead of using a trial and error process reported previously. In order to further evaluate the proposed method and to verify the effects of printing parameters on the printing quality of scaffolds, a series of scaffolds comparison tests are described in next chapter.

Chapter 5
Experiments of the scaffolds fabrication

In this chapter, a scaffold model is first designed using CATIA to generate printing paths in a G-code file to drive the 3D printer. The material preparation process and machine operation procedures are introduced. The parameters selection method is conducted to chosen optimum printing parameters for desired strand widths. A series of comparison tests are implanted to verify effects of printing parameters on the printing quality of scaffolds.

5.1 Experimental design

5.1.1 Model design

A scaffold model shown in Fig. 5-1 is used in the case study. Geometrical dimensions of the scaffold model are 9.6mm×9.6mm×0.4mm. The width of each strand of the pattern is 0.6mm. There are 64 square holes in the model. The side length of the hole is 0.6 mm. The model is designed using CATIA which can be saved as a ".stl" format file for printing path planning. A G-code file of the printing path is created to control the 3D printing process.

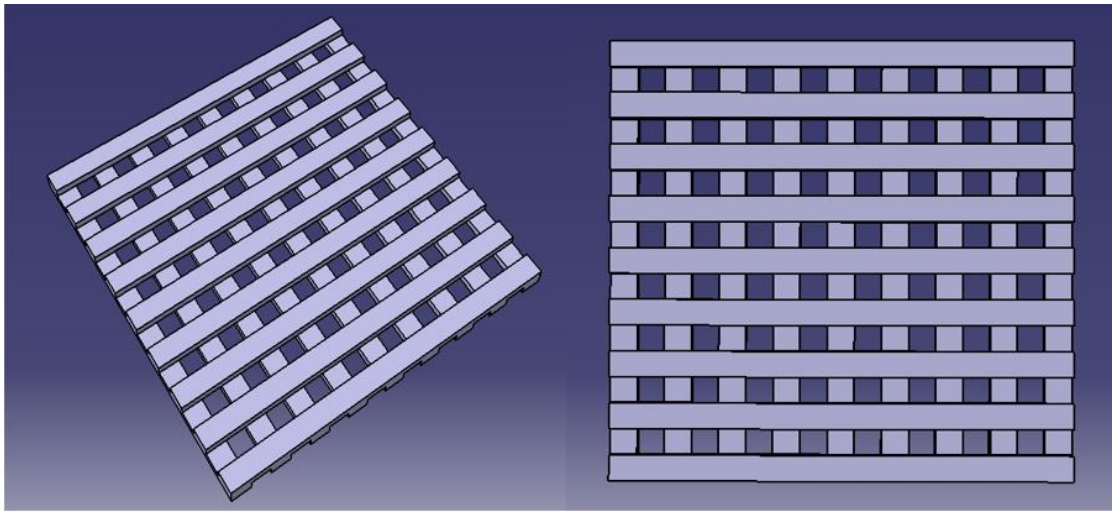

Figure 5-1. A two layers scaffold designed in CATIA software

5.1.2 Material and substrate design

There are two basic requirements for materials in the soft scaffolds fabrication including i) it is biocompatible, and ii) it can first be gelled in situ during the fabrication process and then supported so that it does not collapse or deform under its own weight (Hinton et al., 2015). The alginate, a kind of biocompatible material, is chosen in this research to fabricate soft scaffolds because it remains stability at the room temperature and is easy to control in a lab without a temperature control system. However, it cannot be gelled or solidified in situ soon after printed without the crosslinking, causing the strands to deform and merge together. Therefore, in order to form a gel, the sodium alginate needs to contact with divalent ions such as calcium (Ca2+). As soon as the sodium alginate is added to a solution of the calcium chloride, the sodium ions (Na+) are exchanged with calcium ions (Ca2+). As a result, the alginate is crosslinked to form a gel to stay in situ without diffusion to form a trim strand during the scaffold fabrication process (Pignolet et al., 1998). In order to construct a scaffold in the desired geometry using alginate, a piece of paper wetted with the calcium ions solution is covered on the glass slice substrate to crosslink the alginate with the calcium ions to avoid adjacent strands diffusion in this research.

Although the crosslinking reaction of alginate and calcium ions is used to improve printing quality, a scaffold can only be printed with two layers in the experiment. It is because the first two layers cannot provide enough support for subsequent layers. Specifically, the bottom of semi-ellipse strands contacting with the calcium ions solution can be gelled right away, while the upper part of the strands, which do not directly touch the calcium solution paper, cannot be crosslinked to gel in situ to support the subsequent layers. Therefore, the pure alginate solution is not suitable for a scaffold fabrication with multi-layers.

The alginate has been widely used as a natural biomaterial for tissue engineering and 3D cells cultivation with the good cytocytology compatibility (Park et al., 2011). Normally, the alginate is often used as an additive mixed with other bio-materials to synthesis a new material with more preferred properties. For example, to fabricate a scaffold for the skin regeneration, the alginate was added with chitosan, gelatin and silk to improve mechanical strength and transmit preliminary mechanical signals to the cells for developing tissues (Sharma et al., 2015).

Due to the limitation of materials and experimental devices, the pure alginate solution is used for the soft scaffold fabrication in the research. Although the pure alginate solution is only capable of fabricating a scaffold with two layers without the obvious deformation, the objective of this study is to select optimum printing parameters using the proposed method for the scaffolds fabrication and to verify the parameters' influence on the quality of printed scaffolds.

5.1.3 Experiment design

To fabricate a scaffold with the desired printing accuracy, a strand with a desired width and the corresponding printing parameters should be decided first. In this case,

the targeted strand width is 0.6mm and the corresponding parameter set is decided using the proposed parameter selection method. In the comparison test, a group of scaffolds are fabricated using the optimized parameters set as the control group. The scaffolds in the control group are used as references to compare the models in the experimental group printed using different parameters. Experimental group is matched as closely as possible to the control group, but a factor is changed in each experiment to verify the variable influence on the printing quality. The number of pores and pores' size in the scaffolds are measured to evaluate the printing quality.

According to the results of the factorial experiments, the speed is inversely proportion to a strand width while the pressure and the nozzle size are directly proportion to a strand width. Among them, the nozzle diameter has the largest influence on the strand width while the speed affects a little more on the width than the pressure. In order to intuitively verify the conclusion, the variables are changed at a same level to print scaffolds with a larger size. Therefore, the nozzle diameter and the pressure are doubled while the speed is reduced by a half based on the optimized parameter.

These comparison tests are conducted using a substrate covered by a piece of paper wetted with the calcium ions solution to gel the alginate in situ by crosslinking to fabricate scaffolds with a better quality. In addition, another experiment is also implemented to fabricate a same scaffold on a glass slice substrate to verify the phenomenon of strands deformation by comparing the printing quality of the scaffold printed on the glass substrate with the scaffold printed on the calcium paper.

5.2 Printing preparation

5.2.1 Material preparation

As shown in Fig. 5-2, 0.6 g alginate powder is first prepared using an electronic scale and then dissolved in 10 ml water in the beaker. As the powder is hard to be dissolved in water at the room temperature, the solution has to be heated up to 40~50℃ with stirring on a heating stage for around 4 hours to totally dissolve the powder. When the solution in the breaker is homogeneous without apparent clots, it is then loaded into a syringe which is then attached on the printer head.

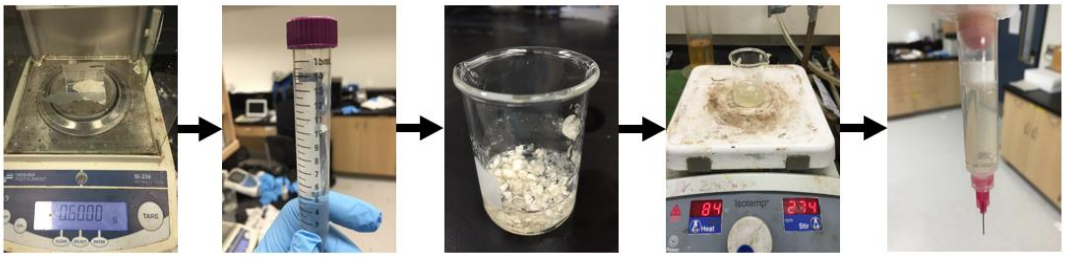

Figure 5-2 Alginate solution preparation process

5.2.2 Equipment setup and operation

There are four devices in a pneumatic dispensing system including a computer, a 3D printer, a dispenser and an air compressor. The 3D operation procedures are shown in Fig. 5-3. Firstly, the operator physically presses the toggle switch that is actuated by a lever angled in one of two positions on the air compressor to compress the air in the air tank to 60 psi. Then the rotary spin is switched on for the dispenser to prepare an appropriate pressure for printing the scaffold. After that, The ‘Connect’ button in the software interface is clicked on to connect the computer with the 3D printer, and ‘Load’ button is to load a g-code file for generating printing paths. The printing process of a 3D model can be monitored on the interface window of software. A glass

substrate is put on the center of the work platform, a paper wetted with the calcium solution covers the glass substrate if necessary. When all the above processes are completed, the ‘Start’ button on the computer is clicked and the pushbutton on the dispenser is pressed to start printing scaffolds. When the printer head stops moving, the pushbutton is pressed again on the dispenser to stop the outputting pressure to the printer head. The printing process is then completed.

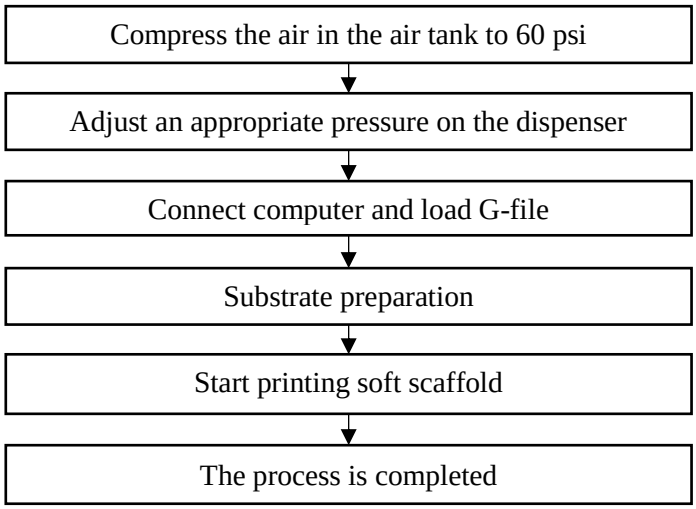

Figure 5-3. A flowchart of the equipment setup and operations

5.3 Parameters selection for the scaffolds fabrication

6% concentration of the alginate solution is used to fabricate a designed scaffold which is comprised of multiple strands with a 0.6 mm width as shown in Fig. 5.1. Therefore, the target strand width for the scaffold fabrication is 0.6mm. Two kinds of substrates are used in the experiment, including the paper wetted with the calcium chloride and the glass slices. The former substrate is not a glass slice so experimental results in the data table obtained from the experiments using the glass slices substrate cannot be utilized to make an initial parameter selection for the desired strand width. Therefore, only a speed-strand width regression model in the proposed method is used

to predict the targeted width for the scaffolds fabrication while the parameter selection method is used in the parameters selection for the glass substrate.

5.3.1 Parameters selection for the scaffold fabrication on the glass slices

Firstly, the viscosity of 6% alginate solution (around 100 Pa • s) is measured using a TA Instruments Trios V3.3 machine. By searching the data table, the viscosity of the alginate solution (around 100 Pa • s) is closest to the medium viscosity material (around 90 Pa • s). Therefore it fits to the classification of the medium viscosity material and the experimental results in this classification are used as references to make an initial parameter selection. Among them, the parameter set in the third row of the classification in Table 4-1, including the nozzle (23G), pressure (5 psi) and speed 60-240 mm/min, can construct a strand with the width ranging from 340.545μm to 421.436μm using a material with the viscosity around 90 Pa • s. Since the range does not cover the targeted width, 600μm, the pressure is increased to 10 psi with an adjustment for a larger strand width. Thus, an initial parameter set is decided, including 23g nozzle under 10 psi with a speed range 60mm/min-240mm/min. To build a speed-strand width regression model, three speeds; 60mm/min, 180 mm/min, and 240mm/min, are selected to print a 25mm long hydrogel strand on the glass slice, respectively, as shown in Fig. 5-4. The samples are measured five times by a microscope and mean values of experimental results are shown in Table 5-1. Hence, a fitted line plot is built using these data. The regression model, strand width = 425.0 + 0.9118 speed, is shown in Fig. 5-5. By taking the advantage of the linear regression model, the targeted strand width (600μm) is predicted when the speed is set at 191mm/min. By using the predicted parameter set, a strand is printed on the glass slice to verify the parameter set. It is found that the width is 589.15μm which is very

close to the targeted width (600μm). Therefore, the desired parameter set for the scaffolds fabrication on the glass substrate is decided, including nozzle 23g, pressure 10psi and speed 191mm/min.

Table 5-1 Experimental data for the targeted strand width 600μm on a glass substrate

Speed (mm/s)	60	150	240
Strand width(μm)	476.38	568.54	640.51

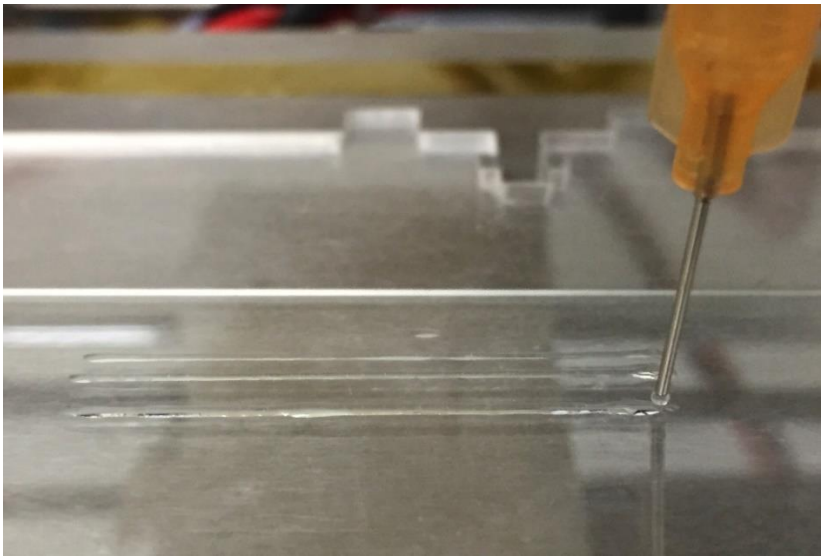

Figure 5-4 A hydrogel strand printed on a glass substrate

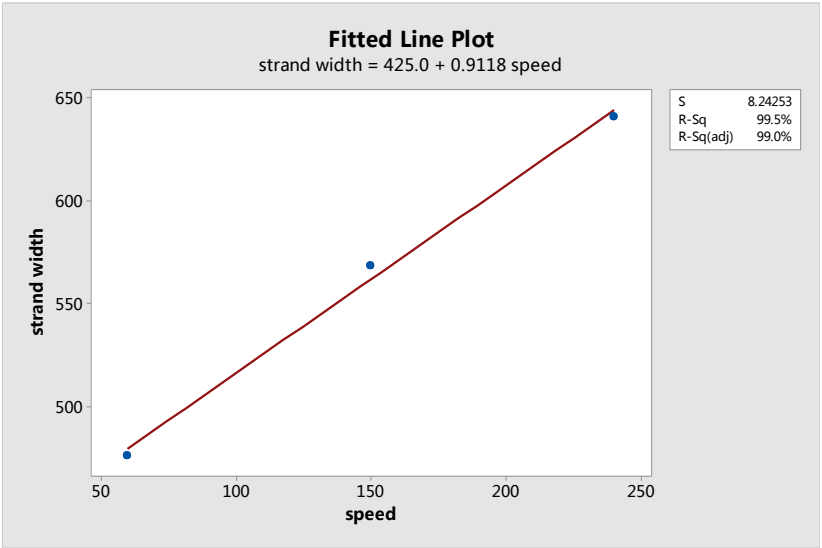

Figure 5-5 A linear regression model of the speed and strand width

5.3.2 Parameter selection for scaffolds fabrication on the paper wetted with the calcium chloride solution

It is found that once the strand is printed on the paper to crosslink with the calcium ion, the hydrogel strands would shrink. Therefore, the strand width should be increased based on printing conditions of the glass substrate. Based on parameters for the glass substrate, the nozzle size is unchanged as it dramatically affects a strand width. The pressure is increased to 20 psi to fine tune the strand width to compensate for the shrink phenomenon. By using a 23G nozzle under 20psi pressure, three speeds including 100mm/min, 200 mm/min, and 300 mm/min, are chosen to print a 25mm long strand sample on the calcium solution paper, respectively as shown in Fig. 5-6. Each sample is measured by a microscope for five times, the mean values of experimental results are shown in Table 5-2. Hence, a fitted line plot is built using these data, its regression model is C2 (strand width) = 766.2 - 1.825 C1 (speed) as shown in Fig. 5-7. By taking the advantage of the linear regression model, the targeted stand width (600μm) is predicted when the speed is set at 91 mm/min. By using the predicted parameter set, a strand is printed on the substrate to verify the predicted parameters set. It is found that the strand width is 609.2μm which is very close to the targeted width (600μm). Therefore, the optimum parameter set is decided, including nozzle 23g, pressure 20 psi and speed 91mm/min.

Table 5-2 Experimental data for the targeted width 600μm on a paper substrate with crosslinking

Speed (mm/s)	100	200	300
Strand width(μm)	579.52	409.51	214.51

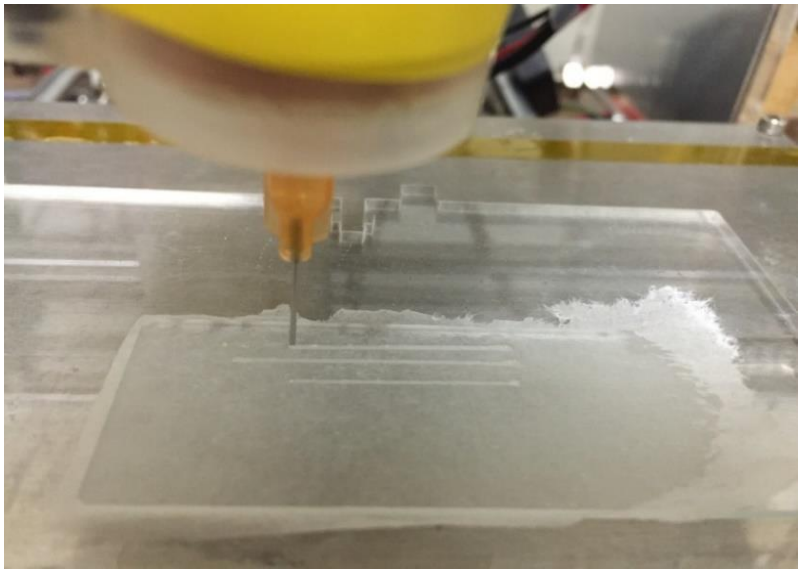

Figure 5-6 A hydrogel strand printed on a paper wetted with the calcium ion solution

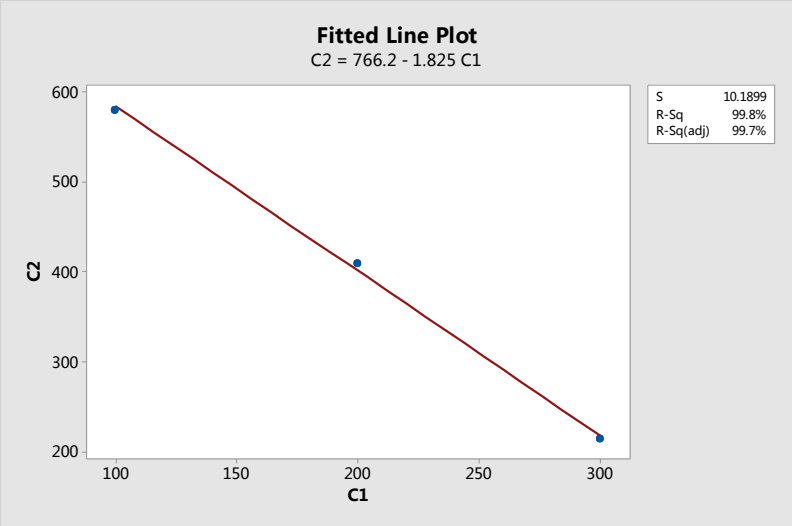

Figure 5-7 A linear regression model of the speed and strand width

5.4 Printing results and discussions

The optimized parameter set, including nozzle 21g, pressure 20 psi and speed 91mm/min, is used to fabricate scaffolds on the paper substrate in the control group. The scaffolds are measured using a microscope as shown in Fig. 5-8. It shows that the scaffolds have two layers without the obvious diffusion of the strands. The shape is uniform and the pores size are consistent. Moreover, lengths of five different pores are measured and the results are very close to the predicted pores size 0.6mm ×0.6mm. Therefore, the printing quality of the scaffold using the optimized parameters is

relatively good. The scaffolds in the control group are used as a reference to compare the scaffolds fabricated using different parameters to evaluate the influence degree of the variables. As shown in Fig. 5-8, the experimental groups are listed as a) the pressure is changed to 40 Psi to verify the influence of pressure on the scaffold quality, b) the speed is changed to 45mm/min from 91mm/min to verify the influence of the speed on the scaffold quality, c) the nozzle diameter is changed to 0.34 mm from 0.51mm to verify the influence of nozzle diameter on the scaffold quality, and d) the calcium paper substrate is changed by a glass substrate.

Fig. 5-8 a) displays that many adjacent strands fused together and only roughly 17 pores still exist. Lengths of six pores are measured and the mean value is 245.98μm. It is because the strand width increases when the pressure goes up, causing strands bind together and the disappearance of the pores. Through this experiment, it is verified that the pressure is proportion to the strand width.

In addition, the factorial experiment concludes that the strand width is inversely proportional to the speed. It is verified by the comparison test b as shown in Fig. 5-8 b). It displays that many pores disappear and only roughly 11 pores can be seen. Lengths of six pores are measured and the mean value is 163.46μm. It is because the strands become wider and bind together as the speed is decreased to a half from 91mm/min. By comparing two experimental tests, it is found that the scaffold fabricated using a higher pressure has more pores with a larger mean length than the scaffold fabricated using a lower printing speed. It is because the strands printed using a lower speed are wider than the strands using a higher pressure, causing more adjacent strands bind together and more pores disappear. It means the former scaffold has a better printing quality than the latter one. It is verified in the results of the

factorial experiment that the speed influences a little more on the strand width for printing quality than the pressure.

When it comes to the experimental group c), the nozzle diameter is changed from 340μm to 510μm, which is almost doubled. It is because there is not an available nozzle size of 640μm from the manufacturer. It is obvious that the scaffold forms a cuboid and all the pores disappear as the strand width dramatically increases when using a larger nozzle size. It is therefore verified that the nozzle diameter is proportional to the strand width, which has the most significant influence on the printing quality.

In the experimental test d) shown in Fig. 5-8, the alginate printed on the paper wetted with the calcium chloride solution can be gelled in situ to fabricate a scaffold with a uniform shape while the strands printed on the glass slice diffuse and bind together, causing the scaffold deformation. It is observed that shapes of the pores in the scaffold are round holes as shown in the experimental group, while shapes of the pores in the control group are square orifices. It means the scaffold in the control group has a better printing quality than the one in the experimental group due to the preferable geometry. This phenomenon can be explained by the elastic stress limit of a material. It is found that the material with a higher elastic stress limit can form a 3D scaffold with a better quality (Li et al., 2009b). Here, the hydrogel strands printed on the paper crosslinked with the calcium ion produce a polymer with a higher elastic stress than the pure alginate solution printed on the glass. It explains that the printing quality of the scaffolds in the control group have a better printing quality than the ones in the experimental group. Therefore, using a material with a higher elastic stress is preferable for a soft scaffold fabrication. Through the comparison tests, it proves the conclusions of the experiments and theoretical analyses.

Control group Experimental group

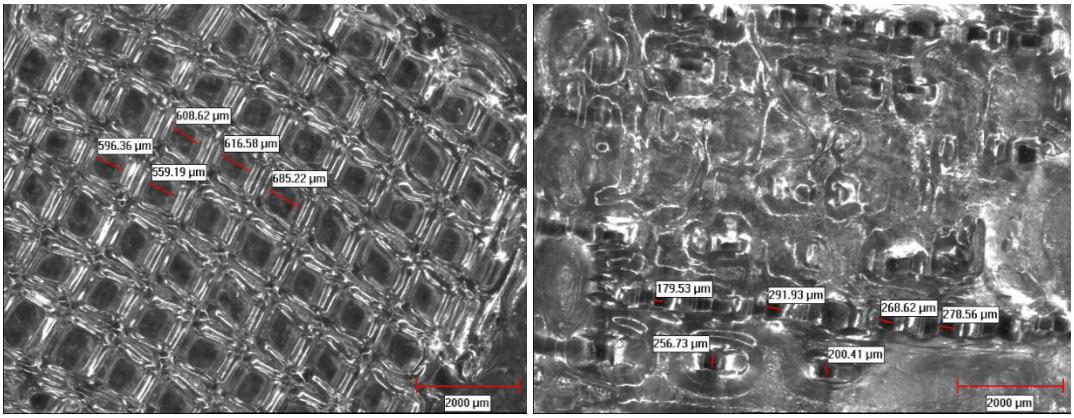

a) Nozzle 23g, pressure 20psi and speed 91mm/min. Nozzle 23g, pressure 40psi and speed 91mm/min

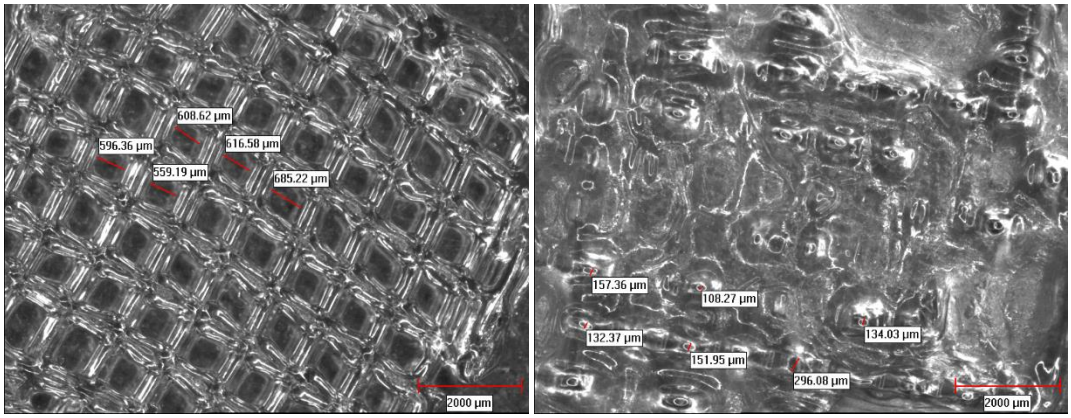

b) Nozzle 23g, pressure 20psi and speed 91mm/min. Nozzle 23g, pressure 20psi and speed 45mm/min

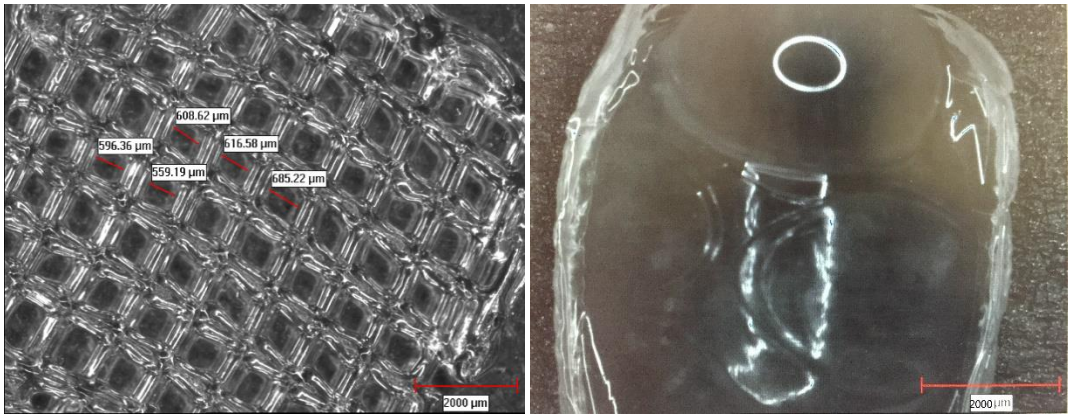

c) Nozzle 23g, pressure 20psi and speed 91mm/min. Nozzle 21g, pressure 20psi and speed 91mm/min

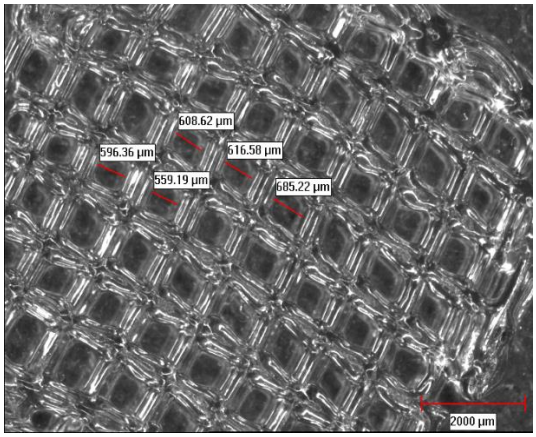

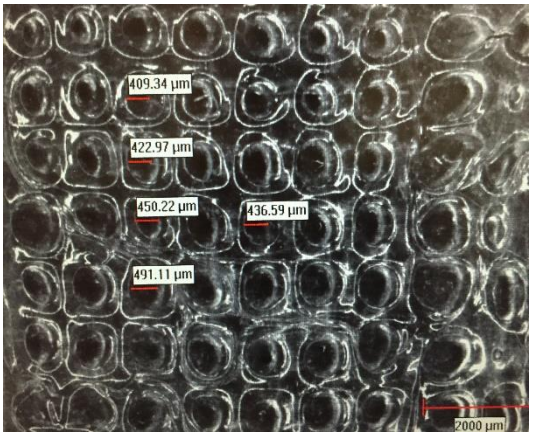

d) Nozzle 23g, pressure 20psi and speed 91mm/min Nozzle 23g, pressure 10psi and speed 120mm/min on glass

Figure 5-8 Examples of soft scaffolds: a) Comparison of pressures, b) Comparison of nozzle speeds, c) Comparison of nozzle diameters, d) Comparison of substrates.

Chapter 6

Modeling and simulation of a 3D bio-printing system for training

6.1 Introduction

6.1.1 Importance of a training system for 3D bio-printing

The pneumatic dispensing system has been widely used in 3D bio-printing technologies. Although there are commercially available extrusion-based bio-printers such as Organovo and EnvisionTEC (Hinton et al., 2015), using these printers are not only expensive, but also may not meet users' individual requirements. Most research groups build their pnumatic dispensing systems for bio-printing (Li et.al 2009., Lee et.al 2014., Chang et.al 2011., Kang et.al 2013). The bio-printing process using a punumatic dispensing system is challengable as the variable biomaterials, especially cells materials. There is a need to develop a cost-effective method to best use of these materials (Weibin, 2014). The system uses an air compressor that would be dangerous if the air pressure is over the limit. Any faults in the operation of machines may cause the material loss or even hazard to operators. Therefore, it is necessary to develop a simulation system of 3D bio-printing to demonstrate the system configuration and operation procedures to help users avoiding operation mistakes in the real world. In conventional training workshops, trainees mainly acquire skills through apprenticeship. Repetitive physical training is important to gain the practical

skill to enhance the sensory feedback. However, there are many limitations in the conventional training process such as the low safety, high training cost, limited availability of training machines and personnel (Sun et al., 2012). The virtual reality (VR) technology is a cost-effective tool to overcome the drawbacks of the physical training mode. Therefore, this research uses the VR technology to develop a simulation system of 3D bio-printing for the operation demonstration and user training purpose.

6.1.2 Virtual Reality

VR technology can replicate a real or imagined environment to simulate a user's physical presence in the environment that allows the user to interact with it. VR can create the sensory experience, including sight, touch, hearing, and even smell (Wei, 2016). As shown in Figure 6.1, a VR system consists of hardware and software. The hardware includes a VR engine, input devices and output devices while the software has modeling tools, VR development toolkits etc. (Bamodu et al., 2013).

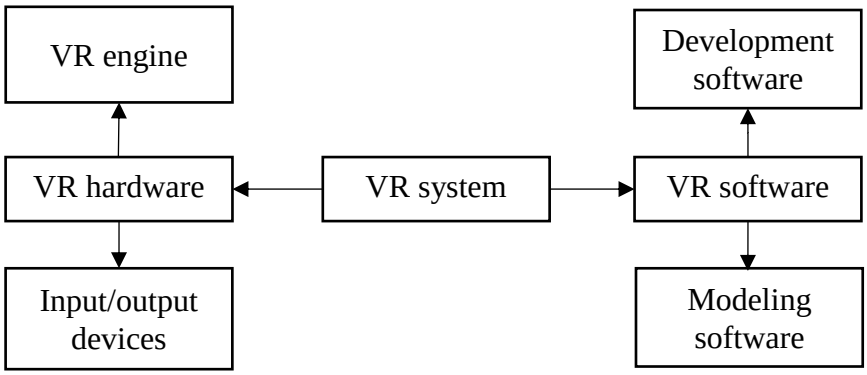

Figure 6.1 Components of a VR system

As shown in Figure 6.2, the input and output devices are the means by which the user interacts with the virtual world. The input devices, such as haptic devices, tracking devices (Kumar et al., 2012), data gloves, keyboards and mouse, are used to send

signals for actions of the user to provide appropriate responds through the output devices, such as head mounted displays (HMD) (Li et al., 2007), surround screens (Cruz-Neira et al., 1993), computer monitors and haptic devices in the real time. The VR engine could be a computer with a powerful CPU and a graphics accelerator or distributed computer systems interconnected through the high speed communication network. It processes the input data from users to determine actions that will take place in the virtual world and serves as an interface between input and output devices (Bamodu et al., 2013).

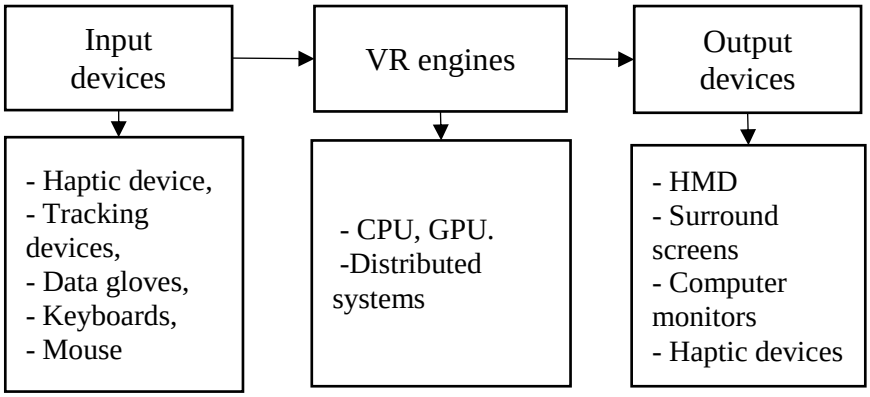

Figure 6.2 Hardware of a VR system

As shown in Figure 6.3, the VR software is classified into modeling and development tools. The modeling tools such as 3Ds Max, Maya, Creator, CATIA, Pro/E, and SolidWorks are used to design the virtual objects. The VR development software such as the Worldviz, EON, Virtual Reality studio and VR juggler are used for interfaces with the hardware, to build the virtual world and to deliver simulation contents to users.

In this study, the phantom omni® haptic device is used to enable users to operate the 3D printing system with the force feedback to enhance the reality of simulation. A computer and a conventional monitor are used for data processing and graphic display. SolidWorks software is used to model the virtual machines. Also, a VR

development software, Worldviz, is selected to build the 3D printing simulation system.

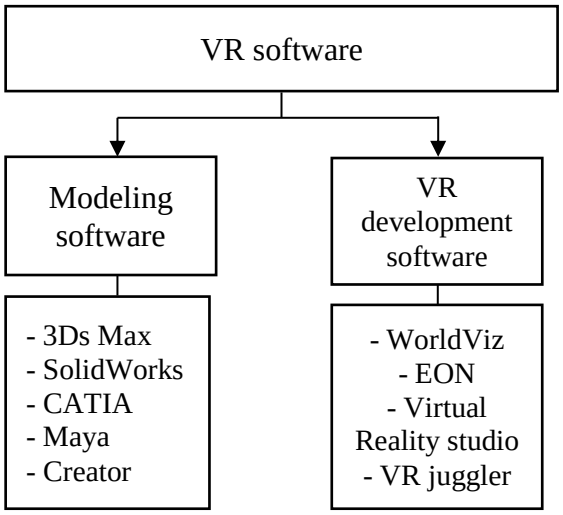

Figure 6.3 Software of a VR system

6.1.2 Haptic technology

Haptic devices provide the tactile sensation to human interactions through computers. By using the phantom omni® haptic device, users can manipulate objects with six degrees of freedom movements in a virtual world with the force feedback (Center, 2012). As shown in Table 6.1, there are three core functions of haptic devices. Firstly, when an object is linked with a haptic device by using OpenHaptics toolkits, users can manipulate objects in the virtual world by moving the stylus on the haptic device that senses the human body's movements, achieving virtual reality interactions. Compared to traditional methods that only use a computer keyboard and a mouse to interact with the virtual world, this function largely enhances the reality of a simulation (Arbabtafti et al., 2011). Secondly, by using the predefined functions of the OpenHaptics Toolkit, the contacting time of the stylus and objects, the stylus velocity and force feedback can be accurately recorded to overcome the difficulty of data recording in the virtual world. For example, Aras et al. designed an experiment for subjects to perform point-

to-point transfer tasks using a haptic device with two different display techniques to evaluate the performance of the subjects' flexibility (Aras et al., 2014). Karadogan et al. also used a method to record velocity vectors of the stylus and forces exerted by users (Karadogan et al., 2010). The third core function is that users can get the accurate force feedback based on requirements using various haptic modeling algorithms. As shown in Table 6.2, the modeling algorithms can be grouped into three categories, including the single point-based algorithm, surface-based algorithm (Pflesser et al., 2002; Wang et al., 2012), and voxel-based algorithm (Arbabtafti et al., 2011). Specifically, i) the single point-based algorithm calculates the feedback force based on two points and constants defined by users. The advantage of this method is that it can provide users the stable and fast force feedback but it is only suitable for the simple force feedback rendering (Lee et al., 2014). For example, Kagawa et al. (2010) proposed an advanced image edition tool with the force feedback interface. A virtual spring-damper model was used to calculate the reactive force based on the distance between the actual position of the stylus point and the surface contact point (SCP). ii) For the surface-based algorithm, the sample points covering on the surface of models are used to detect collisions of virtual objects for the force feedback computation. For example, Pflesser et al. calculates the collision force by adding the individual force vectors applied on all points of the spherical tool surface penetrated inside the bone volumetric pixels (Pflesser et al., 2002). Compared to the single point-based algorithm, it can provide a more accurate force feedback (Pflesser et al., 2002; Wang et al., 2012). However, the calculation of interior structure of virtual objects was not considered (Arbabtafti et al., 2011). iii) The voxel-based method uses volume voxels to represent objects for the collision detection and force feedback calculation. A collision detection algorithm is used to detect voxels in a sharing space of two

models in the real time, and feedback forces created by each voxel are summed and output to haptic devices (Arbabtafti et al., 2011). For example, in order to get the more realistic force feedback, the tool tip and bone volume are represented as multiple voxels and the force vectors related to each penetrated voxel of the tool volume inside the bone were calculated based on the location inside the tool head and summed, then output with a haptic device (Blevins et al., 2006). Compared to the other two haptic rendering methods, it provides more reliable and realistic force feedback since the force feedback is calculated by defining the detection model as many 3D units instead of a surface or a point but the rendering speed is lower than other two methods.

Table 6.1. Core functions of the haptic technology.

	Core functions	Methods
Haptic technology	Virtual objects manipulation	OpenHaptic Toolkit (Version, 2009)
	Contacting time and stylus velocity recording	OpenHaptic Toolkit (Version, 2009)
	Force feedback	Haptic modeling algorithms

Table. 6.2 Methods of haptic modeling

	Methods	Advantages and disadvantages
Haptic modeling algorithm	Single point-based method (Lee et al., 2014)	Only suitable for simple force feedback
	Surface-based method (Pflesser et al., 2002)	More accurate than point-based method
	Voxel-based method (Arbabtafti et al., 2011)	Most accurate force feedback but low rendering speed

In this study, a phantom omni® haptic device is linked with a cursor which is defined as a single point object for haptic interactions with switches on the virtual machines. A spring-damper model is used to calculate the force feedback based on the distance

between the surface contact point (SCP) and the actual positon of stylus. Therefore, users can get the force feedback when using the virtual cursor to touch the switches on the machines by manipulating the stylus of the haptic device. It achieves to operate the 3D bio-printing system with the force feedback, which largely enhances the reality of a simulation.

6.2 The proposed System structure

Figure 6.4 shows the system structure of the proposed VR-based 3D bio-printing system. When a user manipulates the haptic device to interact with the virtual machine models that are defined as haptic objects, the stylus position is read by a computer to compute the reactive force based on the force computing system. Then the reactive force is output to the user through the haptic device. Meanwhile, the visual system uses the geometrical information of virtual machine models that include dynamic models, static models and haptic models to provide users the visual feedback through the computer monitor. In addition, basic attributes such as light, sound, and viewpoints are also added in the virtual environment.

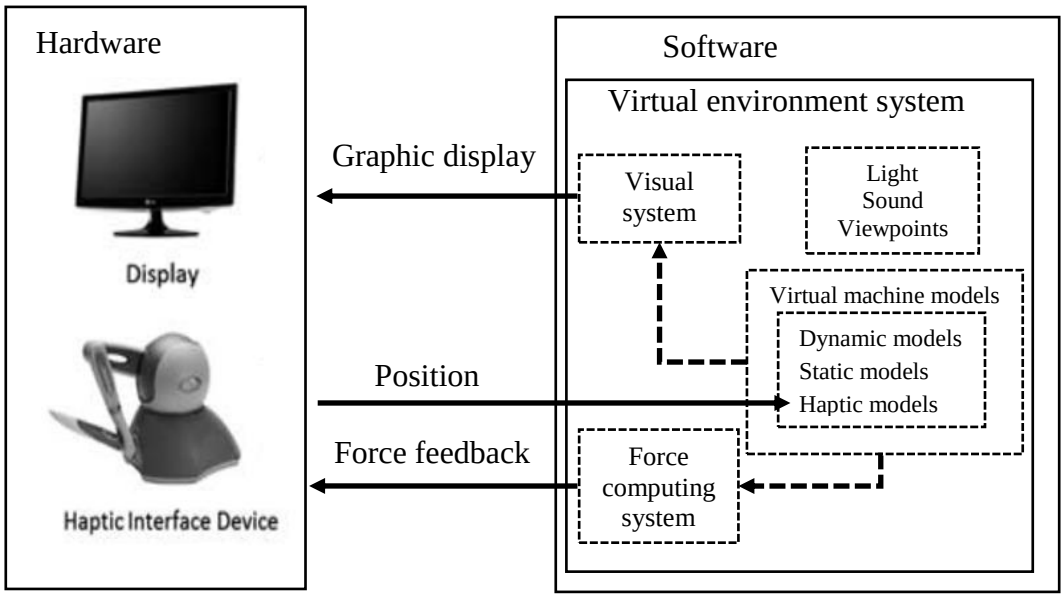

Figure 6.4. System structure of the 3D printing simulation system.

6.3 Model visualization

6.3.1 Objects modeling

The 3D printing simulation system consists of a set of virtual machine objects, including a 3D printer, an air compressor, a dispenser and a computer. As shown in Figure 6.5, virtual machines are first modeled using the SolidWorks software based on real machines. The models are exported as .SAT data format to save the model geometry with polygon meshes. Then, the 3Ds Max software is used to assign texture coordinates on vertices of polygons of the models. Based on the texture coordinates, 2D images are attached on the machine models which are exported as the osgb. binary format to be loaded in the Worldviz software to support embedded image data within the files (VIZARD, 2015). At last, the Worldviz software utilizes OpenGL graphic API to obtain high performance graphic rendering.

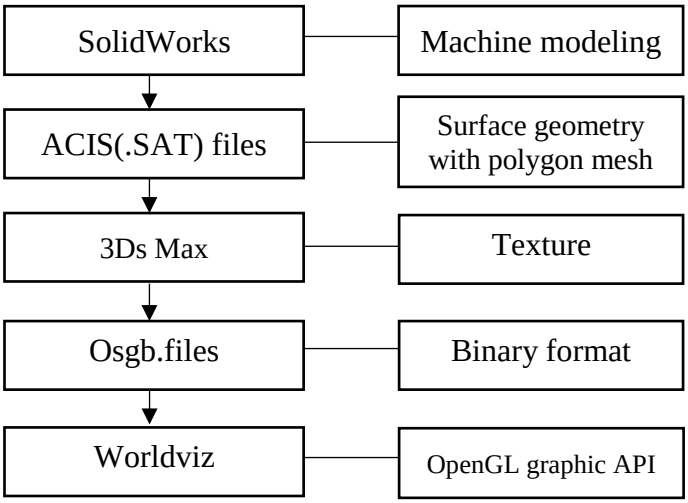

Figure 6.5. Objects modeling process

6.3.2 Dynamic modeling

In the 3D printing simulation system, 3D printer's heads need the movement in x-axis, y-axis and z-axis directions to print 3D virtual objects. To achieve it, three components of the 3D printer, including a bridge, a carrier and a holder, are assigned with motions in x-axis, z-axis and y-axis directions, respectively. Among them, the holder moves with the carrier which moves with the bridge. In order to represent the hierarchical relationships in the virtual world, a tree structure of the scene graph is used by the Worldviz software as shown in Figure 6.6. An element in the tree is called a node. Each node of the tree has an attached local transformation matrix which defines the node's position relative to the parent' node. The global transformation matrix of a component which defines node's position in the world can be gotten by multiplying the local transformation matrixes from the node itself to the node root. It can be expressed as follows:

$$M^i = M_0^i \prod_{i=0}^{n} M_i \tag{6-1}$$

Where M^i is the global transformation matrix of a component i;

M_i : The local transformation matrix of the component i;

M_0^k : The original transformation matrix of component i (matrix before being transformed).

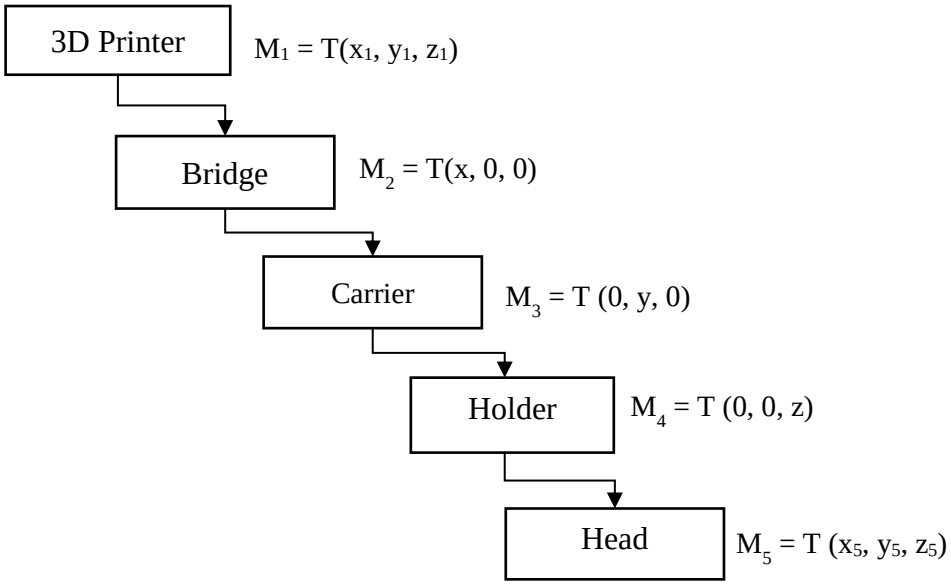

Figure 6.6 Tree structure of the 3D printer components

For example, the local transformation matrixes of the 3D printer, the bridge, the carrier, the holder and the printer heads are shown in Figure 6.6, respectively. Based on Equation 1, the global transformation matrix of the printer head is expressed as follows:

$$M^5 = M_0^5 M_4 M_3 M_2 M_1 \tag{6-2}$$

$$= \begin{bmatrix} 1 & 0 & 0 & x_1 \\ 0 & 1 & 0 & y_1 \\ 0 & 0 & 1 & z_1 \\ 0 & 0 & 0 & 1 \end{bmatrix} \begin{bmatrix} 1 & 0 & 0 & x \\ 0 & 1 & 0 & 0 \\ 0 & 0 & 1 & 0 \\ 0 & 0 & 0 & 1 \end{bmatrix} \begin{bmatrix} 1 & 0 & 0 & 0 \\ 0 & 1 & 0 & y \\ 0 & 0 & 1 & 0 \\ 0 & 0 & 0 & 1 \end{bmatrix} \begin{bmatrix} 1 & 0 & 0 & 0 \\ 0 & 1 & 0 & 0 \\ 0 & 0 & 1 & z \\ 0 & 0 & 0 & 1 \end{bmatrix} \begin{bmatrix} 1 & 0 & 0 & x_5 \\ 0 & 1 & 0 & y_5 \\ 0 & 0 & 1 & z_5 \\ 0 & 0 & 0 & 1 \end{bmatrix}$$

$$= T(x_1 + x + x_5, y_1 + y + y_5, z_1 + y + z_5)$$

Where T(x, y, z) is the translation matrix.

6.4 Haptic system

6.4.1 Interface of the phantom omni® haptic device

For the haptic interface, the Worldviz software provides a plug-in to support the phantom omni® haptic device through the use of the OpenHaptics toolkits. Working process of the phantom omni® haptic device is shown in Figure 6.7. When a user manipulates the stylus of the haptic device, the encoder output is transmitted to an interface controller at very high rates. Here, the information is processed to determine the position of the end effector. The position is then sent to the host computer running the Worldviz software application. If the supporting software determines that a reaction force is required, the host computer would send the feedback forces signals to the device. The Actuators (motors within the device) apply these forces based on the mathematical models that simulate the desired sensations.

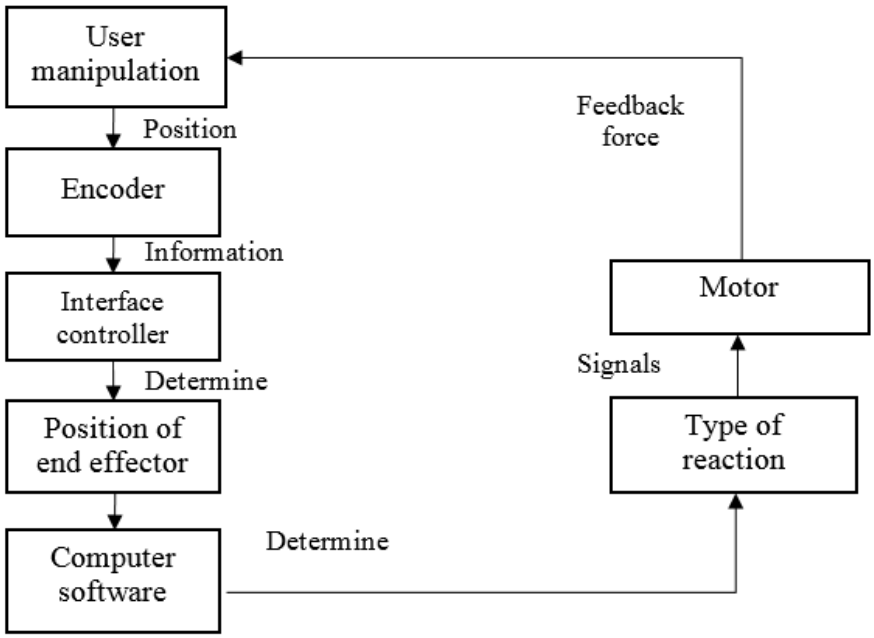

Figure 6.7. Working process of the phantom omni® haptic device

6.4.2 Haptic modeling:

In the 3D printing simulation system, the position and orientation of a virtual cursor are linked to the stylus of the haptic device so that users can move the cursor in the virtual world by manipulating the stylus of the haptic device. Here, the virtual switches on the machines are defined as the haptic objects to interact with the cursor in the virtual world. Therefore, a feedback force is provided when a user uses the cursor to touch a switch in the virtual environment. In this study, the feedback force is calculated by applying the spring-damper model and the proxy method which is based on the transform of the device end effector (the stylus of a haptic device) in the virtual environment ("OPENHAPTICS® TOOLKIT," ; Version, 2009). As shown in Figure 6.8, a virtual spring-damper system links a surface contact point (SCP) of the cursor (the proxy position) to the end-effector position of the haptic device. When the cursor is in a free space and no collision occurs, the SCP position and the end-effector position are the same as shown at t_0 position in Fig.6.8. As the cursor collides with a switch object in the virtual environment, the SCP cannot enter the body of the object and cannot follow the position of the end-effector as shown at t_1 and t_2. Therefore, the positions are no longer match and a distance between them is generated. The force is calculated using Equation 3, where x is the distance between the end-effector and SCP, v is the velocity of the end-effector, and k and b are respectively the spring and the damper constants.

$$F = -kx - bv \tag{6-3}$$

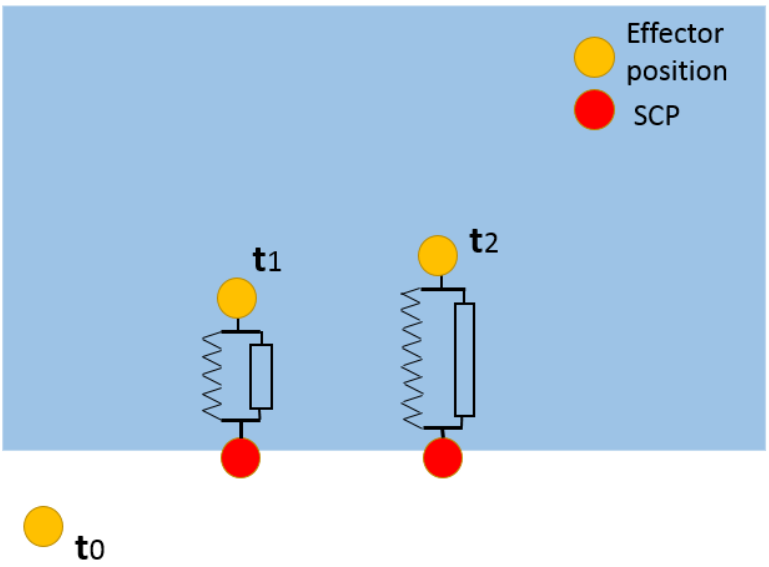

Figure 6.8. The virtual spring-damper system used for feedback force calculation

6.5 Operation demonstration

By using the technologies discussed in previous sections, a 3D printing simulation system is built for the system demonstration and training purpose. Fig. 6.9 shows an operator manipulating a haptic device to operate a virtual machine. This system is run on a conventional monitor. Based on instructions on the screen, the operator can practise 3D printing operations by touching switchers on the virtual machine. The virtual operation procedures are summarized in eight steps as shown in Fig. 6.10.

Figure 6.9. An operator operates the 3D printing simulation system

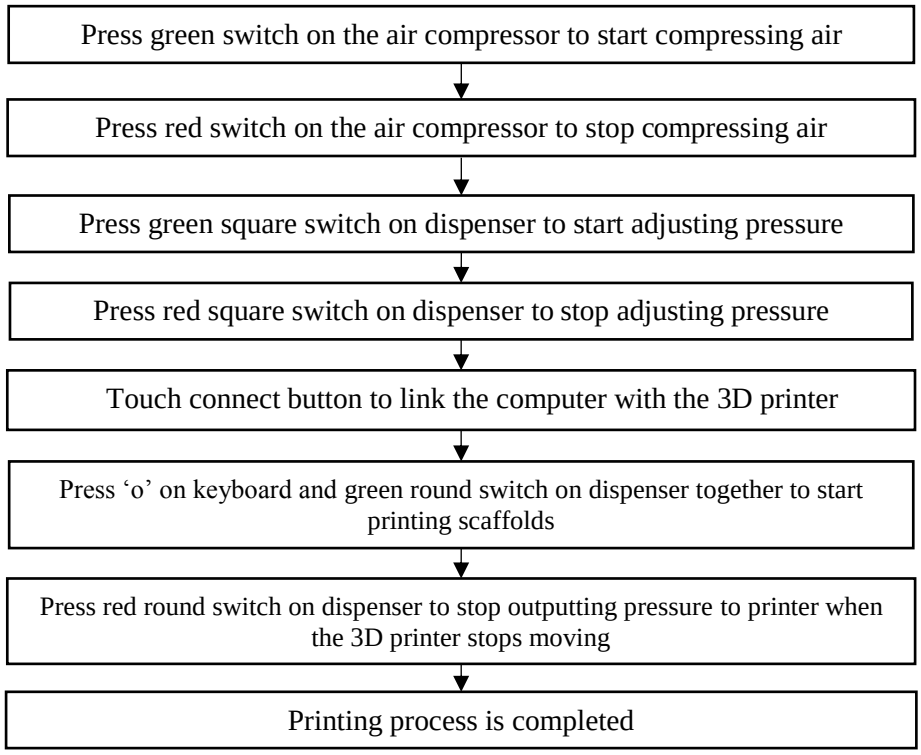

Figure 6.10. Steps of operations using the 3D printing simulation system

The initial system interface is shown in Fig. 6.11, an information bar is shown on the top right corner to provide users instructions to initialize the simulation process. Specifically, when the user presses ‘z’, names of the equipment are shown on the screen. While ‘x’ is pressed, they are hidden. It also displays that the first step to start

the printing process is to press ‘c’ on the keyboard and the next command will be shown after the last one is done. In addition, this interface has three sub-windows on the top left corners of the screen. The dial on the dispenser is magnified on the left side of the sub-windows while the dial on the air compressor is magnified on the right side of the sub-windows. The sub-window in the middle is used to help users to observe the printing process better. The operation process is demonstrated in the following part.

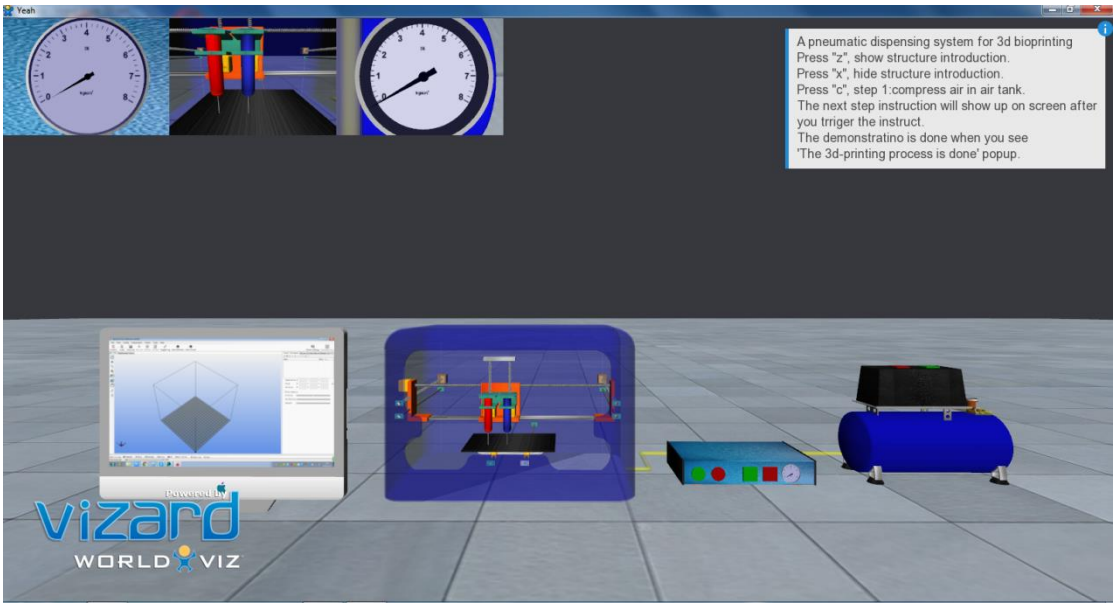

Figure 6.11. The initial screenshot of the 3D printing simulation system

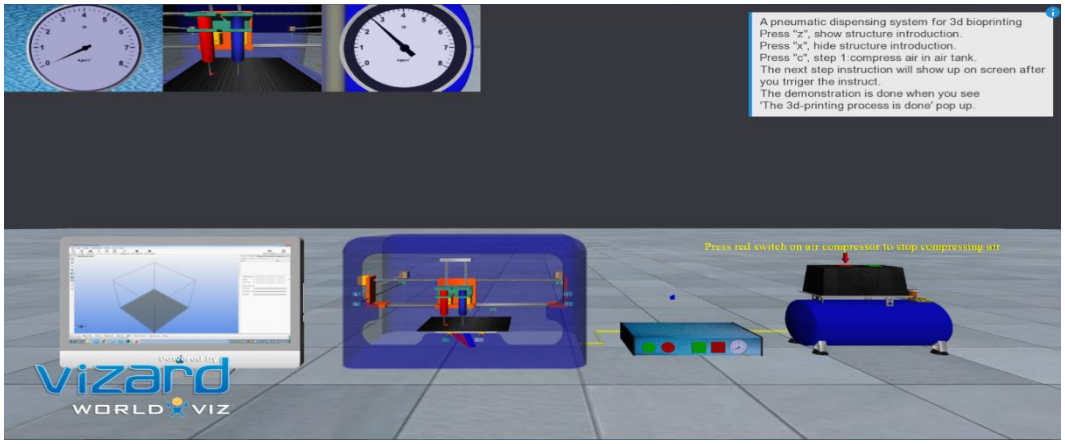

Step 1: The switch pointed by an arrow on the air compressor is used to control air compressing. An instruction on the screen guides the user to press the green switch on the air compressor to start compressing air. When the green switch is touched by the cursor using the haptic device, the pointer of the dial on the air compressor shown on the right side of the sub-window starts rotating to display real time readings of air pressure in the compressor. Meanwhile, a command is displayed on the screen as follows.

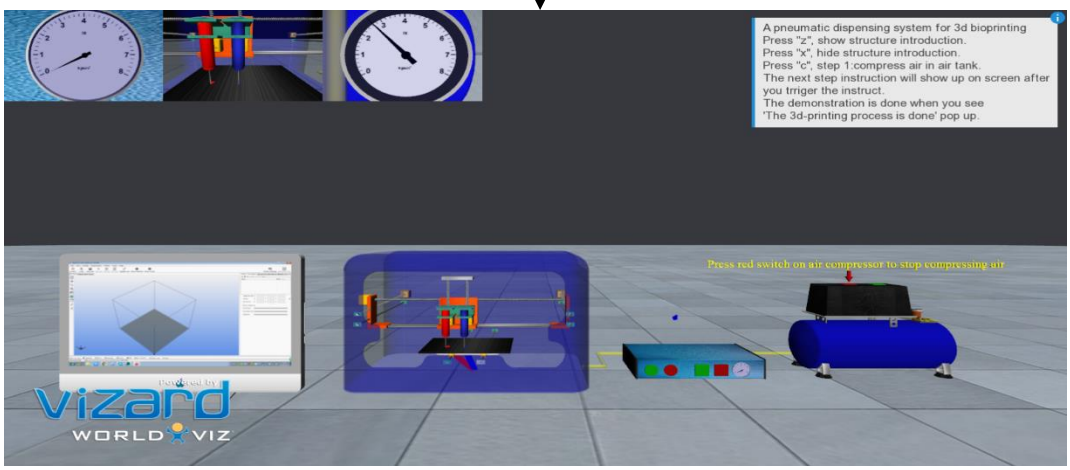

Step 2: The instruction on the screen guides the user to press the red switch on the air compressor to stop compressing air. When the red switch is touched, the pointer stops moving and the next instruction is shown as following.

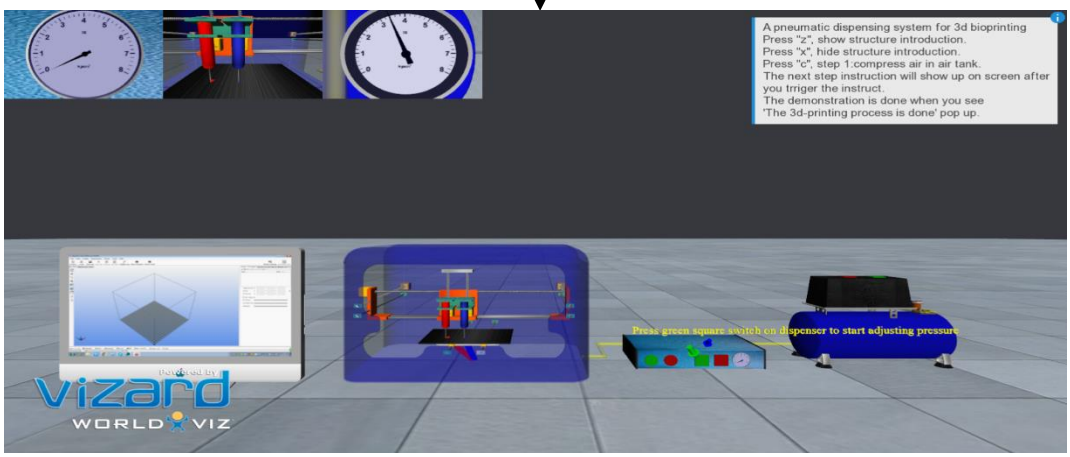

Step 3: The square switches pointed by the arrows on the dispenser are utilized to adjust an appropriate output pressure for 3D printing. An instruction on the screen guides users to press the green square for switch on dispenser to start adjusting pressure. When the green square switch is touched by the cursor, the pointer of the dial on the dispenser shown on the left sub-window starts rotating to display real time readings of the air pressure in the dispenser. Meanwhile, an instruction displays on the screen.

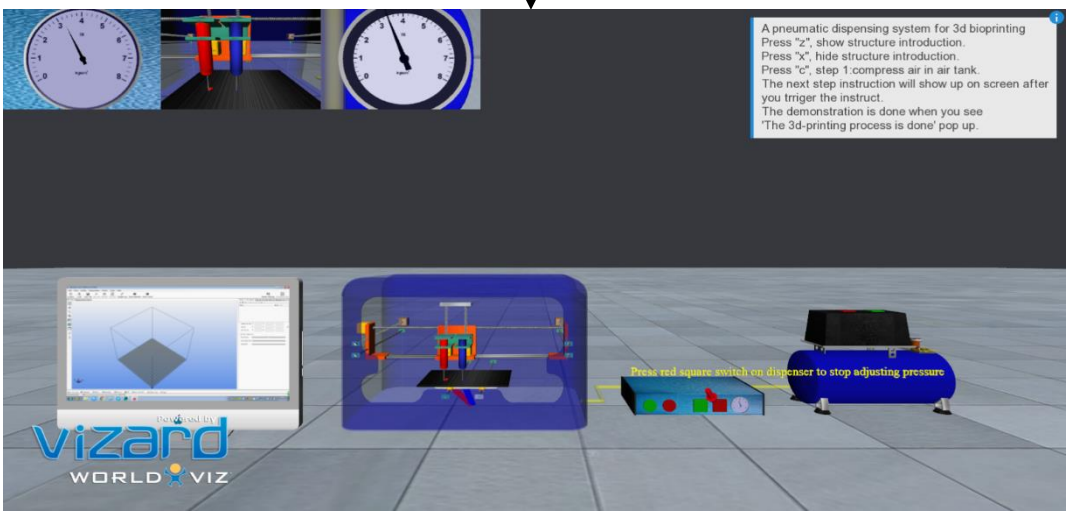

Step 4: The command on the screen guides users to press the red square for switch on dispenser to stop adjusting pressure. When the red square switch is touched, the pointer stops moving and the next instruction shows up.

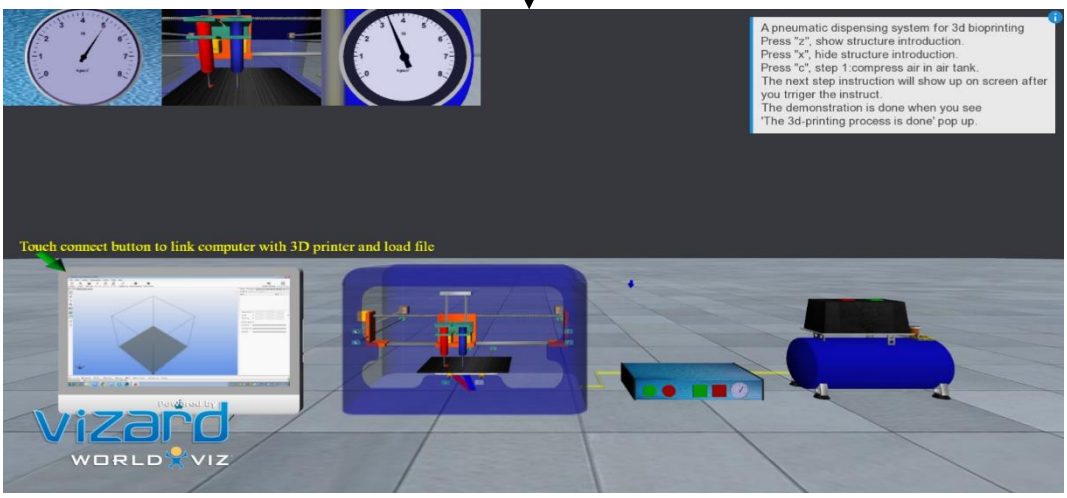

Step 5: A command on the screen tells to link the 3D printer with a computer and load a file by touching a software interface icon on the computer screen pointed by a green arrow. When it is touched, the next instruction shows up as follows.

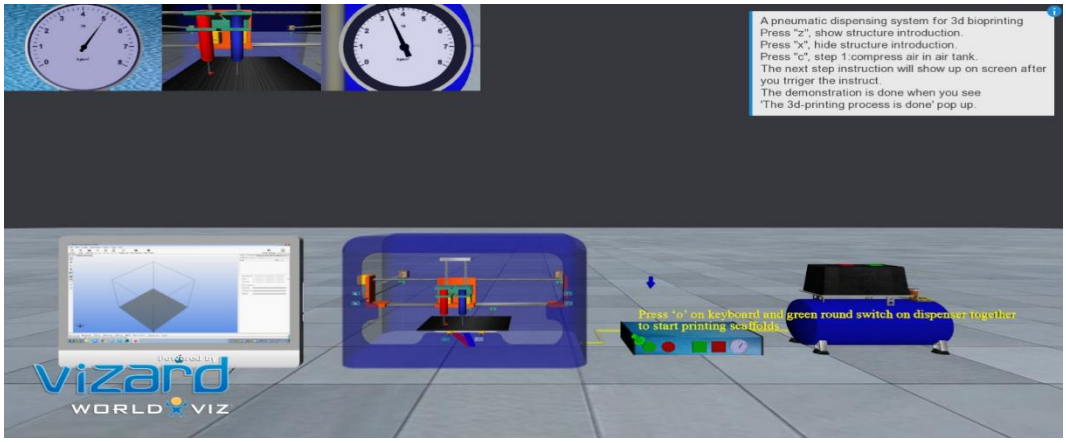

Step 6: An instruction of virtual objects printing operation is shown on the window. Two round switches on the dispenser are used to dispense air for 3D printing. When the green switch is touched and letter ‘O’ on the keyboard is pressed together, the 3D printer starts to print two virtual objects. The users can both observe the printing process by watching the middle sub-window on the screen and hear working voice of machines.

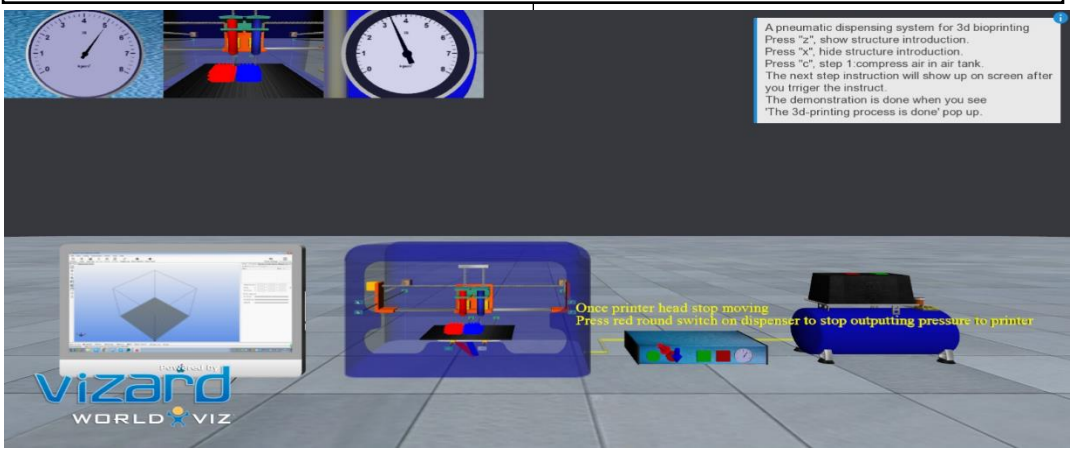

Step 7: When the printer stops moving, it is required for users to touch the red round button on the dispenser to stop outputting pressure to the 3D printer. Then, a message shown in the following window indicates that the printing process is completed.

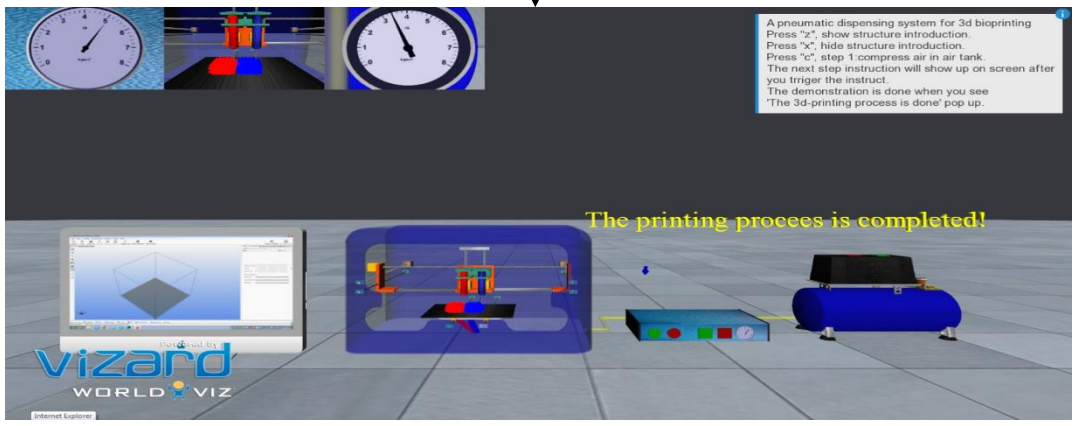

6.6 The system evaluation

Subjects and methods

This study uses a questionnaire survey method to evaluate the VR system performance by comparing users' satisfactions in using the pneumatic dispensing simulation and the traditional training operation manual. Prior to the experiment, nine participants with varied ages, genders, and nationalities were given a brief verbal introduction to the experiment. Due to the lack of knowledge of haptic devices, a training program of the haptic device is provided for users to learn the haptic device operation. Then they were asked to operate the 3D printing simulation system using the haptic device and to complete a questionnaire about their satisfaction about the system. After that, they were asked to read an operation manual of the 3D printing system for a similar questionnaire about satisfaction. The operation manual is shown in the appendix III. In the questionnaires as shown in appendix I and appendix II, a five point Likert scale which is a psychometric scale commonly employed in questionnaires for scaling responses in survey research is used to capture participants responds (ranging from 1 for "strongly disagree" to 5 for "strongly agree"). The survey results are collected as shown in Tables 1 and 2 in Appendix IV. The data from the two questionnaires are analyzed to evaluate the system performance. In addition, the subjects were also asked to comment advantages and disadvantages of the simulation system.

Statistical analysis method

Using the statistical analysis in Minitab software, the Cronbach alpha is an estimate of the reliability of a psychometric test (Cronbach, 1951). It is calculated to test reliability and internal consistency for rating questions in the questionnaires.

The t-test is used to find the statistically significant difference of means scores between two training methods.

Results analysis and discussions

Reliability: Through the data item analysis in Minitab, both of questionnaires get a high Cronbach's alpha (0.733) and (0.8233), respectively, which means that the scale of the questions has a high level of the reliability and internal consistency in the both questionnaires.

Comparison of scores in the both questionnaires

Figure 6-12 shows the mean scores, medium scores and variation of scores of question 1 in the two questionnaires. It is to test users' satisfaction of the learning environment. A statistically significant difference was found between the two methods t (8) =4.06, p-value = 0.001<0.05. Therefore, it indicates that the simulation system is more user- friendly than the operational manual.

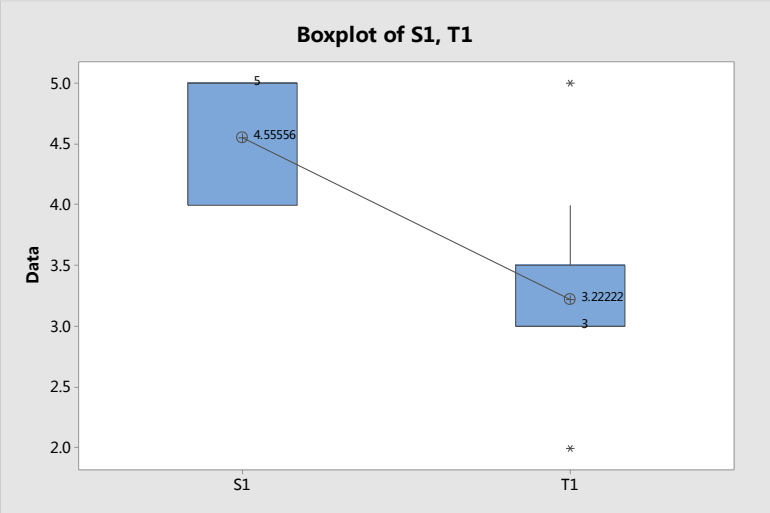

Figure 6-12. The boxplot of the scores of question 1

Figure 6-13 displays scores of question 2 about how much users understand the configuration of the 3D printing system and Figure 6-14 shows scores of question 3 about whether users obtain the basic skills to operate a 3D printing system. There is a statistically significant effect of the simulation system on the both understanding of

system configuration, t (8) =4.16, p =0.001<0.05, and learning of machines operation, t (8) =5.25, p=0.000<0.05. Therefore, the results suggest that users acquire a better understanding of the 3D printing system by using the simulation program than the operation manual.

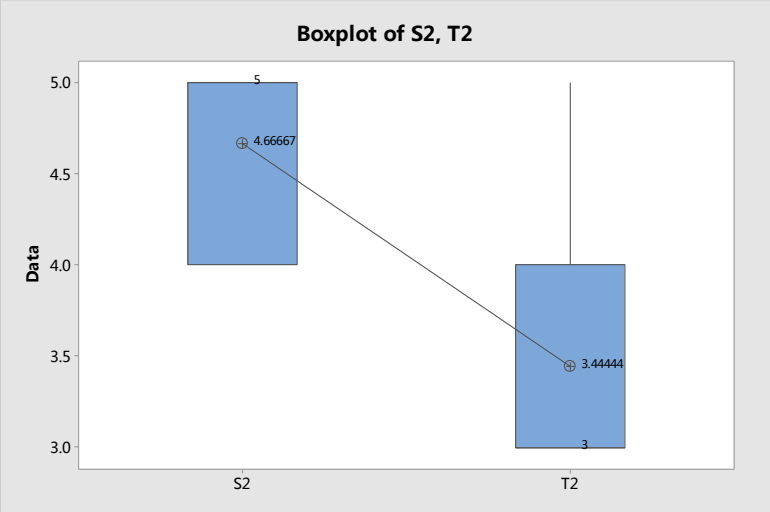

Figure 6-13. The boxplot of the scores of question 2

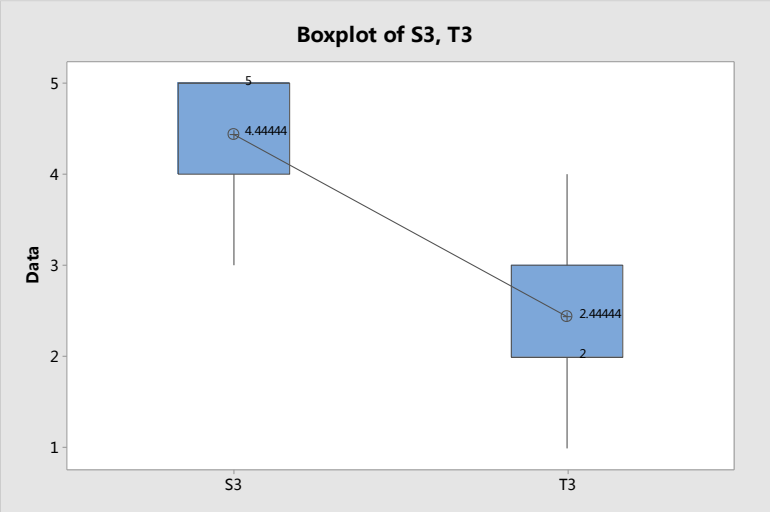

Figure 6-14. The boxplot of the scores of question 3

Figures 6-15 and 6-16 show scores of questions 4 and 5, respectively. The former is to test the degree of concentration of users while learning and the latter is to evaluate users' learning interest of the both methods. It reveals that uses are more engaged t(9) = 3.95, p = 0001<0.05 and interested t(9) = 4.71, p = 0.001<0.05 in the learning contents using the simulation system.

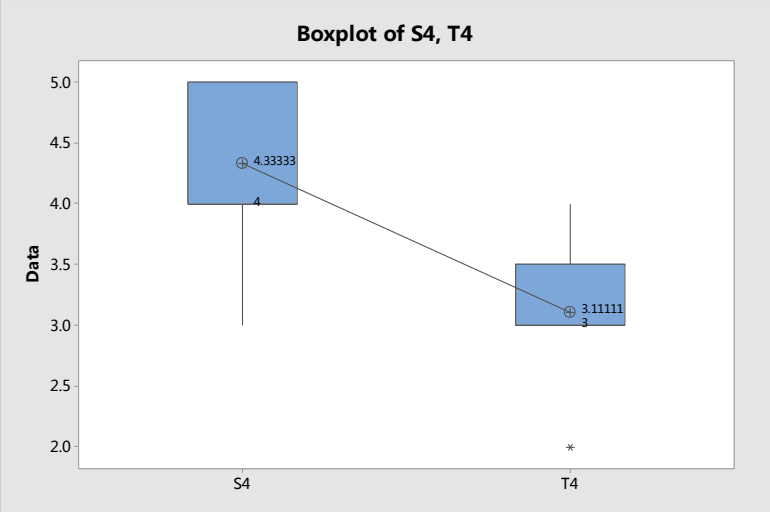

Figure 6-15. The boxplot of the scores of question 4

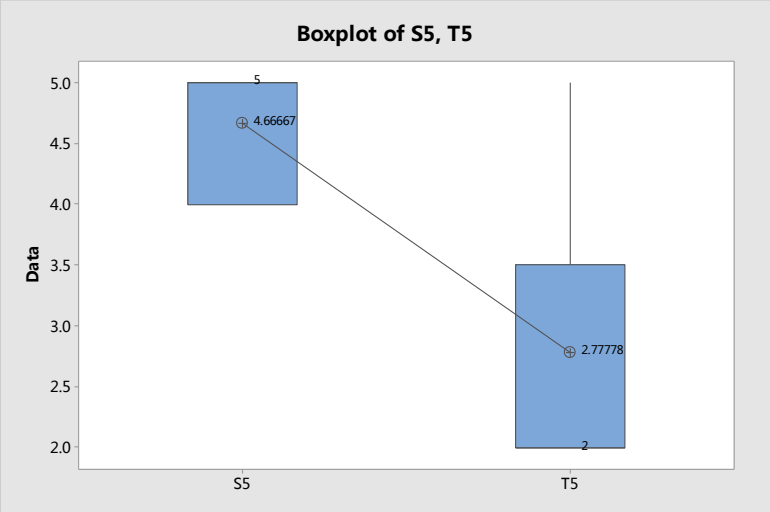

Figure 6-16. The boxplot of the scores of question 5

At the end, question 6 tests users' satisfaction of two methods and scores are shown in Figure 6-17. A statistically significant difference was found, $t(9) = 3.29$, $p = 0.006 < 0.05$, indicating that users are more enjoyable using the simulation system than the operational manual.

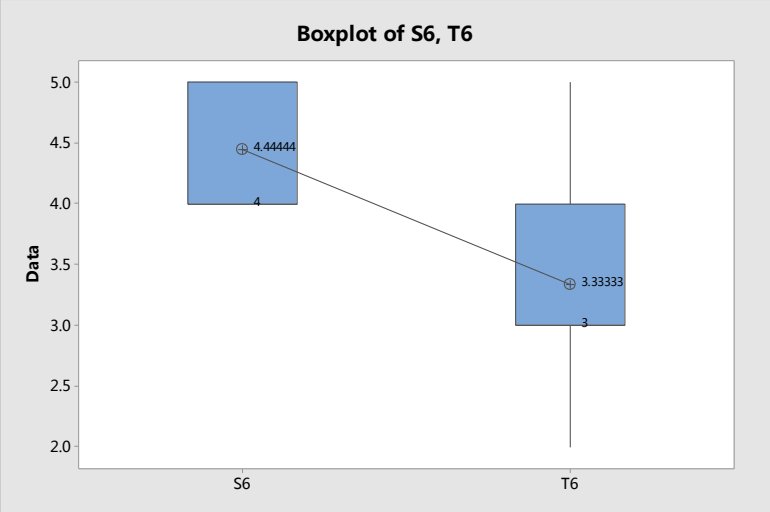

Figure 6-17. The boxplot of the scores of question 6

In the open question part, 77.8% of participants comment that the simulation system creates a friendly and realistic-learning learning environment. Using a haptic device to operate the virtual machines largely increases the learning interest. One of them also proposed that it would be more confident to operate the real 3D printing system through the simulation training. However, 55.6% of participants complained that it is not easy to accurately and fast touch the virtual switches to operate the machine using the haptic device since the monitor is a 2D display while the virtual world is a 3D space, causing the difficulty of the depth perception. This is a weakness of the 3D printing simulation system. Therefore, a Head Mounted display will be considered to solve the problem in future.

Conclusions

In conclusion, the statistical analysis reveals that the simulation systems creates a better learning environment, which significantly improves learning effect and learning interest of users compared to the traditional operation manual. Although the system has the problem, the majority of participants agreed that the 3D printing simulation system is a user-friendly, cost-effective, safe, and highly interactive learning environment.

In summary, a VR-based 3D printing simulation system is presented in the chapter. In order to provide the user an interactive and realistic interaction, a force feedback is provided by means of the Phantom Omni haptic interface. The SolidWorks software is used to build the virtual machine models and the virtual environment is developed using the Worldviz software. The haptic force feedback is calculated based on the spring-damper model and the proxy method. A questionnaire survey is conduct to evaluate performance of the system. It indicates that the system provides a flexible, cost-effective, safe, and highly interactive learning environment. It is an effective educational tool to demonstrate the system configuration and operation procedures of a pneumatic dispensing system for 3D bio-printing. It enables new users to handle a machine in the virtual environment with the force feedback to practise 3D printing operations. The next chapter summarizes the research with contributions and the future work.

Chapter 7
Conclusion and future work

7.1 Research summary

Based on the literature review of 3D bio-printing technologies, the advantages and disadvantages of the different bio-printing systems are compared and analyzed. The pneumatic dispensing system is chosen for bio-material printing in the research. Through the analysis of scaffolds fabrication requirements and parameters investigation methods, the current problems in fabricating soft scaffolds are summarized. According to the previous studies, the process parameters in the pneumatic dispensing system are first identified and classified into three groups including material parameters, experimental parameters and printer parameters, respectively. Then a mathematical deposition model is established to link the significant printing parameters with the strand width. Based on the mathematical model, three operational parameters are chosen for a 2^3 full factorial experiment to investigate effects of selected factors and their interactions on the strand width. According to conclusions of the experiments, a five-step parameters selection method is proposed. In the two verification tests for the proposed method, two operational parameters sets are successfully found to print the target strands width with the desired accuracy. A series of comparison tests are also conducted to verify the

parameters effects on the printing quality of scaffolds. In addition, based on the review of the VR technology and Haptic technology, a haptic-based simulation system for 3D bio-printing is presented and a questionnaire survey is conducted to evaluate the simulation system. It indicates that the system provides a flexible, cost-effective, safe, and highly interactive learning environment.

7.2 Research contributions

The contributions of this research are as follows:

(1) A simplified mathematical model is proposed to describe parameters' relations with the strand width.

(2) Through a full factorial experiment, it is found the nozzle sizes, dispensing pressure, and moving speed of a printer head all statistically affect strand widths. Among them, the nozzle size has the most significant influence on the strand width. The speed affects a little more on the strand width than pressure. Factors interactions are mainly embodied in between the nozzle size and speed, nozzle size and pressure.

(3) A data table is built to guide users for an initial parameter selection based on the material viscosity.

(4) By using the proposed parameter selection methods, the operational parameters can be rationally and systematically decided for the scaffolds fabrication in this research, instead of using a trial and error process reported previously.

(5) A haptic-based simulation system is developed and verified to demonstrate the system configuration and operation procedures of a pneumatic dispensing system for 3D bio-printing.

7.3 Future work

In the current research, all experiments and verification tests are carried out using the alginate solution in various concentrations. In future work, other bio-materials will be used to further verify the proposed method. Also, the data table will be expanded to provide users with more options to make a more accurate initial parameter selection.

In the 3D bio-printing simulation system, the rotary switches on the real dispenser machine are replaced by press switches on the virtual dispenser machine since the virtual cursor is defined as a single point based haptic object which is hard to achieve the spin operation in the virtual environment. To solve the problem, the surface-based haptic modeling method will be considered in future.

In addition, according to questionnaires, the participants indicated that it is hard to touch the virtual switches on the machines using the haptic device due to the difficulty to perceive the depth in a 3D virtual world using a 2D monitor display. Therefore, the system will be improved using a Head Mounted Device to provide users with a stereoscopic view of the virtual environment.

Papers published related to this research

Wenqi Zhou, Qingjin Peng, Parameter design of a pneumatic dispensing 3D printing system for soft scaffold fabrication, Proceedings of the ASME 2016 International Design Engineering Technical Conferences & Computers and Information in Engineering Conference, IDETC/CIE 2016, August 21-24, 2016, Charlotte, North Carolina, USA, DETC2016-59680. (Published).

References

Aguado B. A., Mulyasasmita W., Su J., Lampe K. J., & Heilshorn S. C. (2011). Improving viability of stem cells during syringe needle flow through the design of hydrogel cell carriers. *Tissue Engineering Part A, 18*(7-8), 806-815.

Anderson M., & Whitcomb P. (2001). Design of Experiments: Statistical Principles of Research Design and Analysis. *Technometrics, 43*(2), 236-237.

Anderson M. J., & Whitcomb P. J. (2000). Design of experiments. *Kirk-Othmer encyclopedia of chemical technology*.

Ang T., Sultana F., Hutmacher D., Wong Y. S., Fuh J., Mo X., . . . Teoh S.-H. (2002). Fabrication of 3D chitosan–hydroxyapatite scaffolds using a robotic dispensing system. *Materials Science and Engineering: C, 20*(1), 35-42.

Aras R., Shen Y., & Noor A. (2014). Quantitative assessment of the effectiveness of using display techniques with a haptic device for manipulating 3D objects in virtual environments. *Advances in Engineering Software, 76*, 43-47.

Arbabtafti M., Moghaddam M., Nahvi A., Mahvash M., Richardson B., & Shirinzadeh B. (2011). Physics-based haptic simulation of bone machining. *Haptics, IEEE Transactions on, 4*(1), 39-50.

Bamodu O., & Ye X. M. (2013). *Virtual Reality and Virtual Reality System Components.* Paper presented at the Advanced Materials Research.

Billiet T., Gevaert E., De Schryver T., Cornelissen M., & Dubruel P. (2014). The 3D printing of gelatin methacrylamide cell-laden tissue-engineered constructs

with high cell viability. *Biomaterials, 35*(1), 49-62.

Billiet T., Vandenhaute M., Schelfhout J., Van Vlierberghe S., & Dubruel P. (2012). A review of trends and limitations in hydrogel-rapid prototyping for tissue engineering. *Biomaterials, 33*(26), 6020-6041.

Blevins N. H., & Girod S. (2006). Visuohaptic simulation of bone surgery for training and evaluation.

Box G. E., Hunter J. S., & Hunter W. G. (2005). *Statistics for experimenters: design, innovation, and discovery* (Vol. 2): Wiley-Interscience New York.

Box G. E., & Wilson K. (1951). On the experimental attainment of optimum conditions. *Journal of the Royal Statistical Society. Series B (Methodological), 13*(1), 1-45.

Center H. D. (2012). Geomagic Haptic Device. from http://www.geomagic.com/en/products-landing-pages/haptic

Chang C. C., Boland E. D., Williams S. K., & Hoying J. B. (2011). Direct‐write bioprinting three‐dimensional biohybrid systems for future regenerative therapies. *Journal of Biomedical Materials Research Part B: Applied Biomaterials, 98*(1), 160-170.

Chang R., Nam J., & Sun W. (2008). Effects of dispensing pressure and nozzle diameter on cell survival from solid freeform fabrication-based direct cell writing. *Tissue Engineering Part A, 14*(1), 41-48.

Chen X., & Ke H. (2006). Effects of fluid properties on dispensing processes for electronics packaging. *Electronics Packaging Manufacturing, IEEE Transactions on, 29*(2), 75-82.

Chen X., Li M., & Ke H. (2008). Modeling of the flow rate in the dispensing-based process for fabricating tissue scaffolds. *Journal of Manufacturing Science and*

Engineering, 130(2), 021003.

Chen Y.-L., Lee H.-P., Chan H.-Y., Sung L.-Y., Chen H.-C., & Hu Y.-C. (2007). Composite chondroitin-6-sulfate/dermatan sulfate/chitosan scaffolds for cartilage tissue engineering. *Biomaterials, 28*(14), 2294-2305.

Chin Ang K., Fai Leong K., Kai Chua C., & Chandrasekaran M. (2006). Investigation of the mechanical properties and porosity relationships in fused deposition modelling-fabricated porous structures. *Rapid Prototyping Journal, 12*(2), 100-105.

Cronbach L. J. (1951). Coefficient alpha and the internal structure of tests. *psychometrika, 16*(3), 297-334.

Cruz-Neira C., Sandin D. J., & DeFanti T. A. (1993). *Surround-screen projection-based virtual reality: the design and implementation of the CAVE.* Paper presented at the Proceedings of the 20th annual conference on Computer graphics and interactive techniques.

Cui X., Boland T., D'Lima D. D., & Lotz M. K. (2012). Thermal inkjet printing in tissue engineering and regenerative medicine. *Recent patents on drug delivery & formulation, 6*(2), 149.

Cui X., Breitenkamp K., Finn M., Lotz M., & D'Lima D. D. (2012). Direct human cartilage repair using three-dimensional bioprinting technology. *Tissue Engineering Part A, 18*(11-12), 1304-1312.

Cui X., Dean D., Ruggeri Z. M., & Boland T. (2010). Cell damage evaluation of thermal inkjet printed d cells. *Biotechnology and bioengineering, 106*(6), 963-969.

Czitrom V. (1999). One-factor-at-a-time versus designed experiments. *The American Statistician, 53*(2), 126-131.

Duan B., Hockaday L. A., Kang K. H., & Butcher J. T. (2013). 3D bioprinting of heterogeneous aortic valve conduits with alginate/gelatin hydrogels. *Journal of Biomedical Materials Research Part A, 101*(5), 1255-1264.

Duan B., Kapetanovic E., Hockaday L. A., & Butcher J. T. (2014). Three-dimensional printed trileaflet valve conduits using biological hydrogels and human valve interstitial cells. *Acta biomaterialia, 10*(5), 1836-1846.

Dunietz I., Ehrlich W. K., Szablak B., Mallows C. L., & Iannino A. (1997). *Applying design of experiments to software testing: experience report.* Paper presented at the Proceedings of the 19th international conference on Software engineering.

Federer W. T. (1955). Experimental design. *Experimental design.*

Ferreira S. C., Bruns R., Ferreira H., Matos G., David J., Brandao G., . . . Souza A. (2007). Box-Behnken design: An alternative for the optimization of analytical methods. *Analytica chimica acta, 597*(2), 179-186.

Frey D. D., Engelhardt F., & Greitzer E. M. (2003). A role for" one-factor-at-a-time" experimentation in parameter design. *Research in Engineering Design, 14*(2), 65-74.

Gauvin R., Chen Y.-C., Lee J. W., Soman P., Zorlutuna P., Nichol J. W., . . . Khademhosseini A. (2012). Microfabrication of complex porous tissue engineering scaffolds using 3D projection stereolithography. *Biomaterials, 33*(15), 3824-3834.

Ghosal K., Latha M. S., & Thomas S. (2014). Poly (ester amides)(PEAs)–Scaffold for tissue engineering applications. *European Polymer Journal, 60*, 58-68.

Guillemot F., Souquet A., Catros S., Guillotin B., Lopez J., Faucon M., . . . Bellance S. (2010). High-throughput laser printing of cells and biomaterials for tissue

engineering. *Acta biomaterialia, 6*(7), 2494-2500.

Guillotin B., Souquet A., Catros S., Duocastella M., Pippenger B., Bellance S., . . . Amédée J. (2010). Laser assisted bioprinting of engineered tissue with high cell density and microscale organization. *Biomaterials, 31*(28), 7250-7256.

Gunst R. F., & Mason R. L. (2009). Fractional factorial design. *Wiley Interdisciplinary Reviews: Computational Statistics, 1*(2), 234-244.

Hinton T. J., Jallerat Q., Palchesko R. N., Park J. H., Grodzicki M. S., Shue H.-J., . . . Feinberg A. W. (2015). Three-dimensional printing of complex biological structures by freeform reversible embedding of suspended hydrogels. *Science Advances, 1*(9), e1500758.

Hoelzle D. J., Alleyne A. G., & Johnson A. J. W. (2008). Micro-robotic deposition guidelines by a design of experiments approach to maximize fabrication reliability for the bone scaffold application. *Acta biomaterialia, 4*(4), 897-912.

Hutmacher D. W. (2000). Scaffolds in tissue engineering bone and cartilage. *Biomaterials, 21*(24), 2529-2543.

Jang D., Kim D., & Moon J. (2009). Influence of fluid physical properties on ink-jet printability. *Langmuir, 25*(5), 2629-2635.

Janik H., & Marzec M. (2015). A review: Fabrication of porous polyurethane scaffolds. *Materials Science and Engineering: C, 48*, 586-591.

Jones N. (2012). Science in three dimensions: the print revolution. *Nature, 487*(7405), 22-23.

Kagawa T., Shimamoto T., Nishino H., & Utsumiya K. (2010). *A study of haptic interaction for image edition tools.* Paper presented at the Complex, Intelligent and Software Intensive Systems (CISIS), 2010 International Conference on.

Kang K., Hockaday L., & Butcher J. (2013). Quantitative optimization of solid

freeform deposition of aqueous hydrogels. *Biofabrication, 5*(3), 035001.

Karadogan E., Williams R. L., Howell J. N., & Conatser Jr R. R. (2010). A stiffness discrimination experiment including analysis of palpation forces and velocities. *Simulation in Healthcare, 5*(5), 279-288.

Katari R., Edgar L., Wong T., Boey A., Mancone S., Igel D., . . . Zambon J. P. (2015). Tissue-Engineering Approaches to Restore Kidney Function. *Current diabetes reports, 15*(10), 1-10.

Kennedy M., & Krouse D. (1999). Strategies for improving fermentation medium performance: a review. *Journal of Industrial Microbiology and Biotechnology, 23*(6), 456-475.

Keselman H., Huberty C. J., Lix L. M., Olejnik S., Cribbie R. A., Donahue B., . . . Keselman J. C. (1998). Statistical practices of educational researchers: An analysis of their ANOVA, MANOVA, and ANCOVA analyses. *Review of Educational Research, 68*(3), 350-386.

Khalil S., Nam J., & Sun W. (2005). Multi-nozzle deposition for construction of 3D biopolymer tissue scaffolds. *Rapid Prototyping Journal, 11*(1), 9-17.

Khalil S., & Sun W. (2007). Biopolymer deposition for freeform fabrication of hydrogel tissue constructs. *Materials Science and Engineering: C, 27*(3), 469-478.

Kim J. Y., & Cho D.-W. (2009). The optimization of hybrid scaffold fabrication process in precision deposition system using design of experiments. *Microsystem technologies, 15*(6), 843-851.

Kim J. Y., Yoon J. J., Park E. K., Kim D. S., Kim S.-Y., & Cho D.-W. (2009). Cell adhesion and proliferation evaluation of SFF-based biodegradable scaffolds fabricated using a multi-head deposition system. *Biofabrication, 1*(1), 015002.

Koch L., Kuhn S., Sorg H., Gruene M., Schlie S., Gaebel R., . . . Ma N. (2009). Laser printing of skin cells and human stem cells. *Tissue Engineering Part C: Methods, 16*(5), 847-854.

Koschan A., & Antony J. (2006). Taguchi or classical design of experiments: a perspective from a practitioner. *Sensor Review, 26*(3), 227-230.

Kufelt O., El-Tamer A., Sehring C., Schlie-Wolter S., & Chichkov B. N. (2014). Hyaluronic acid based materials for scaffolding via two-photon polymerization. *Biomacromolecules, 15*(2), 650-659.

Kumar P., Verma J., & Prasad S. (2012). Hand data glove: a wearable real-time device for human-computer interaction. *International Journal of Advanced Science and Technology, 43*.

Kumbar S., James R., Nukavarapu S., & Laurencin C. (2008). Electrospun nanofiber scaffolds: engineering soft tissues. *Biomedical Materials, 3*(3), 034002.

Landers R., Hübner U., Schmelzeisen R., & Mülhaupt R. (2002). Rapid prototyping of scaffolds derived from thermoreversible hydrogels and tailored for applications in tissue engineering. *Biomaterials, 23*(23), 4437-4447.

Lee J. M., & Yeong W. Y. (2015). A preliminary model of time-pressure dispensing system for bioprinting based on printing and material parameters: This paper reports a method to predict and control the width of hydrogel filament for bioprinting applications. *Virtual and Physical Prototyping, 10*(1), 3-8.

Lee K. Y., & Mooney D. J. (2012). Alginate: properties and biomedical applications. *Progress in polymer science, 37*(1), 106-126.

Lee O., Lee K., Oh C., Kim K., & Kim M. (2014). Prototype tactile feedback system for examination by skin touch. *Skin Research and Technology, 20*(3), 307-314.

Lee S.-J., Kang H.-W., Park J. K., Rhie J.-W., Hahn S. K., & Cho D.-W. (2008).

Application of microstereolithography in the development of three-dimensional cartilage regeneration scaffolds. *Biomedical microdevices, 10*(2), 233-241.

Lee W., Lee V., Polio S., Keegan P., Lee J.-H., Fischer K., . . . Yoo S.-S. (2010). On-demand three-dimensional freeform fabrication of multi-layered hydrogel scaffold with fluidic channels. *Biotechnology and bioengineering, 105*(6), 1178.

Lee Y.-B., Polio S., Lee W., Dai G., Menon L., Carroll R. S., & Yoo S.-S. (2010). Bio-printing of collagen and VEGF-releasing fibrin gel scaffolds for neural stem cell culture. *Experimental neurology, 223*(2), 645-652.

Li K.-Y., & Lin C.-F. (2007). Head mounted device: Google Patents.

Li M., Tian X., & Chen X. (2009a). A brief review of dispensing-based rapid prototyping techniques in tissue scaffold fabrication: role of modeling on scaffold properties prediction. *Biofabrication, 1*(3), 032001.

Li M., Tian X., & Chen X. (2009b). Modeling of flow rate, pore size, and porosity for the dispensing-based tissue scaffolds fabrication. *Journal of Manufacturing Science and Engineering, 131*(3), 034501.

Luftig J. T. J. T., & Jordan V. S. (1998). *Design of experiments in quality engineering*.

Lundstedt T., Seifert E., Abramo L., Thelin B., Nyström Å., Pettersen J., & Bergman R. (1998). Experimental design and optimization. *Chemometrics and intelligent laboratory systems, 42*(1), 3-40.

Marga F., Jakab K., Khatiwala C., Shephard B., Dorfman S., & Forgacs G. (2012). *Organ printing: A novel tissue engineering paradigm.* Paper presented at the 5th European Conference of the International Federation for Medical and Biological Engineering.

Melchels F. P., Feijen J., & Grijpma D. W. (2009). A poly (D, L-lactide) resin for the preparation of tissue engineering scaffolds by stereolithography. *Biomaterials, 30*(23), 3801-3809.

Michael S., Sorg H., Peck C.-T., Koch L., Deiwick A., Chichkov B., . . . Reimers K. (2013). Tissue engineered skin substitutes created by laser-assisted bioprinting form skin-like structures in the dorsal skin fold chamber in mice. *PloS one, 8*(3), e57741.

Minitab. Designing an Experiment. from http://support.minitab.com/en-us/minitab/17/getting-started/designing-an-experiment/#create-a-designed-experiment

Mironov V., Reis N., & Derby B. (2006). Review: bioprinting: a beginning. *Tissue engineering, 12*(4), 631-634.

Montgomery D. C. (2008). *Design and analysis of experiments*: John Wiley & Sons.

Motamedian S. R., Hosseinpour S., Ahsaie M. G., & Khojasteh A. (2015). Smart scaffolds in bone tissue engineering: A systematic review of literature. *World journal of stem cells, 7*(3), 657.

Murphy S. V., & Atala A. (2014). 3D bioprinting of tissues and organs. *Nature biotechnology, 32*(8), 773-785.

Murphy W. L., Dennis R. G., Kileny J. L., & Mooney D. J. (2002). Salt fusion: an approach to improve pore interconnectivity within tissue engineering scaffolds. *Tissue engineering, 8*(1), 43-52.

Myers R. H., Montgomery D. C., & Anderson-Cook C. M. (2016). *Response surface methodology: process and product optimization using designed experiments*: John Wiley & Sons.

Neter J., Kutner M. H., Nachtsheim C. J., & Wasserman W. (1996). *Applied linear*

statistical models (Vol. 4): Irwin Chicago.

OPENHAPTICS® TOOLKIT.

Park S. A., Lee S. H., & Kim W. (2011). Fabrication of hydrogel scaffolds using rapid prototyping for soft tissue engineering. *Macromolecular Research, 19*(7), 694-698.

Pati F., Jang J., Ha D.-H., Kim S. W., Rhie J.-W., Shim J.-H., . . . Cho D.-W. (2014). Printing three-dimensional tissue analogues with decellularized extracellular matrix bioink. *Nature communications, 5*.

Pflesser B., Petersik A., Tiede U., Höhne K. H., & Leuwer R. (2002). Volume cutting for virtual petrous bone surgery. *Computer Aided Surgery, 7*(2), 74-83.

Pham H. (2006). *Springer handbook of engineering statistics*: Springer Science & Business Media.

Pignolet L. H., Waldman A. S., Schechinger L., Govindarajoo G., Nowick J. S., & Labuza T. (1998). The alginate demonstration: Polymers, food science, and ion exchange. *Journal of chemical education, 75*(11), 1430.

Raimondi M. T., Eaton S. M., Laganà M., Aprile V., Nava M. M., Cerullo G., & Osellame R. (2013). Three-dimensional structural niches engineered via two-photon laser polymerization promote stem cell homing. *Acta biomaterialia, 9*(1), 4579-4584.

Ren X., Zhang Q., Liu K., Li H.-l., & Zhou J. G. (2014). Modeling of pneumatic valve dispenser for printing viscous biomaterials in additive manufacturing. *Rapid Prototyping Journal, 20*(6), 434-443.

Roy R. K. (2001). *Design of experiments using the Taguchi approach: 16 steps to product and process improvement*: John Wiley & Sons.

Saunders R. E., & Derby B. (2014). Inkjet printing biomaterials for tissue

engineering: bioprinting. *International Materials Reviews, 59*(8), 430-448.

Saunders R. E., Gough J. E., & Derby B. (2008). Delivery of human fibroblast cells by piezoelectric drop-on-demand inkjet printing. *Biomaterials, 29*(2), 193-203.

Schuster M., Turecek C., Weigel G., Saf R., Stampfl J., Varga F., & Liska R. (2009). Gelatin‐based photopolymers for bone replacement materials. *Journal of Polymer Science Part A: Polymer Chemistry, 47*(24), 7078-7089.

Sharma C., Dinda A. K., Potdar P. D., & Mishra N. C. (2015). Fabrication of quaternary composite scaffold from silk fibroin, chitosan, gelatin, and alginate for skin regeneration. *Journal of Applied Polymer Science, 132*(44).

Skardal A., Mack D., Kapetanovic E., Atala A., Jackson J. D., Yoo J., & Soker S. (2012). Bioprinted amniotic fluid-derived stem cells accelerate healing of large skin wounds. *Stem cells translational medicine, 1*(11), 792.

Smay J. E., Cesarano J., & Lewis J. A. (2002). Colloidal inks for directed assembly of 3-D periodic structures. *Langmuir, 18*(14), 5429-5437.

Sperling L. H. (2015). *Introduction to physical polymer science*: John Wiley & Sons.

Sun S.-H., & Tsai L.-Z. (2012). Development of virtual training platform of injection molding machine based on VR technology. *The International Journal of Advanced Manufacturing Technology, 63*(5-8), 609-620.

Tartarisco G., Gallone G., Carpi F., & Vozzi G. (2009). Polyurethane unimorph bender microfabricated with Pressure Assisted Microsyringe (PAM) for biomedical applications. *Materials Science and Engineering: C, 29*(6), 1835-1841.

Tekin E., Smith P. J., & Schubert U. S. (2008). Inkjet printing as a deposition and patterning tool for polymers and inorganic particles. *Soft Matter, 4*(4), 703-713.

Thomson R., Wake M., Yaszemski M., & Mikos A. (1995). Biodegradable polymer

scaffolds to regenerate organs *Biopolymers Ii* (pp. 245-274): Springer.

Tirella A., De Maria C., Criscenti G., Vozzi G., & Ahluwalia A. (2012). The PAM2 system: a multilevel approach for fabrication of complex three-dimensional microstructures. *Rapid Prototyping Journal, 18*(4), 299-307.

Tirella A., Vozzi F., Vozzi G., & Ahluwalia A. (2010). PAM2 (piston assisted microsyringe): a new rapid prototyping technique for biofabrication of cell incorporated scaffolds. *Tissue Engineering Part C: Methods, 17*(2), 229-237.

Tyssedal J. (2008). Plackett–Burman Designs. *Encyclopedia of statistics in quality and reliability*.

Underwood A. J. (1997). *Experiments in ecology: their logical design and interpretation using analysis of variance*: Cambridge University Press.

Version S. O. T. (2009). 3.0 Programmer's Guide. *Chapter, 2*, 15-30.

Visser J., Peters B., Burger T. J., Boomstra J., Dhert W. J., Melchels F. P., & Malda J. (2013). Biofabrication of multi-material anatomically shaped tissue constructs. *Biofabrication, 5*(3), 035007.

VIZARD W. (2015). WORLD VIZARD SUPPORT.

Vozzi G., Previti A., De Rossi D., & Ahluwalia A. (2002). Microsyringe-based deposition of two-dimensional and three-dimensional polymer scaffolds with a well-defined geometry for application to tissue engineering. *Tissue engineering, 8*(6), 1089-1098.

Wang Q., Chen H., Wu W., Jin H.-Y., & Heng P.-A. (2012). Real-time mandibular angle reduction surgical simulation with haptic rendering. *Information Technology in Biomedicine, IEEE Transactions on, 16*(6), 1105-1114.

Wei W. (2016). Virtual Reality Enhanced Robotic Systems for Disability Rehabilitation. *Virtual Reality Enhanced Robotic Systems for Disability*

Rehabilitation, 48.

Weibin L. (2014). *Improvement of 3D printing quality for fabricating soft scaffolds*.

Woodfield T. B., Malda J., De Wijn J., Peters F., Riesle J., & van Blitterswijk C. A. (2004). Design of porous scaffolds for cartilage tissue engineering using a three-dimensional fiber-deposition technique. *Biomaterials, 25*(18), 4149-4161.

Xing J.-F., Dong X.-Z., Chen W.-Q., Duan X.-M., Takeyasu N., Tanaka T., & Kawata S. (2007). Improving spatial resolution of two-photon microfabrication by using photoinitiator with high initiating efficiency. *Applied physics letters, 90*(13), 131106-131106.

Xu T., Jin J., Gregory C., Hickman J. J., & Boland T. (2005). Inkjet printing of viable mammalian cells. *Biomaterials, 26*(1), 93-99.

Xu T., Kincaid H., Atala A., & Yoo J. J. (2008). High-throughput production of single-cell microparticles using an inkjet printing technology. *Journal of Manufacturing Science and Engineering, 130*(2), 021017.

Yoo S.-S. (2015). 3D-printed biological organs: medical potential and patenting opportunity. *Expert opinion on therapeutic patents, 25*(5), 507-511.

Zhang C., Wen X., Vyavahare N. R., & Boland T. (2008). Synthesis and characterization of biodegradable elastomeric polyurethane scaffolds fabricated by the inkjet technique. *Biomaterials, 29*(28), 3781-3791.

Appendix I

Directions: The following items are learning outcomes related to the 3D bio-printing simulation. Please circle the number that best describes the effctiveness of the simulaiton.

Please rate your agreement with each of the statements below using the following scale:

5-strongly agree; 4-agree; 3-neutral; 2-disagree; 1- strongly disagree

	Strongly agree				Strongly disagree
1. The 3D bio-printing simulation system creates a realistic-looking learning environment.	5	4	3	2	1
2. The system helps me to understand the configuration of the 3D printing system.	5	4	3	2	1
3. The system helps me to obtain a basic capability to operate a 3D bio-printing system.	5	4	3	2	1
4. The system offers more engagement to help me understand learning content.	5	4	3	2	1
5. The system can enhance my learning motivation and learning interests.	5	4	3	2	1
6. Overall, the 3D printing system is useful learning tool.	5	4	3	2	1

OPEN-ENDED QUESTIONS

DIRECTIONS: write or list a few comments to the following questions.

What did you most enjoy or advantages of the 3D printing simulation system?

What did you least enjoy or disadvantages of the 3D printing simulation system?

Appendix II

Directions: The following items are learning outcomes related to the operation munual. Please circle the number that best describes the effctiveness of the munual.

Please rate your agreement with each of the statements below using the following scale:

5-strongly agree; 4-agree; 3-neutral; 2-disagree; 1- strongly disagree

	Strongly agree				Strongly disagree
1. The munual creates a friendly learning environment.	5	4	3	2	1
2. The munual helps me to understand the configuration of the 3D printing system.	5	4	3	2	1
3. The munual helps me to obtain a basic capability to operate a 3D bio-printing system.	5	4	3	2	1
4. The munual offers engagement to help me understand learning content.	5	4	3	2	1
5. The munual can enhance my learning motivation and learning interests.	5	4	3	2	1
6. Overall, the munual is useful learning tool.	5	4	3	2	1

Appendix III

Operation manual:

The pneumatic dispensing system consists of a computer, a 3D printer, a dispenser, and an air compressor as shown in the Figure 2. The operation procedure is shown flowchart in Figure 1.

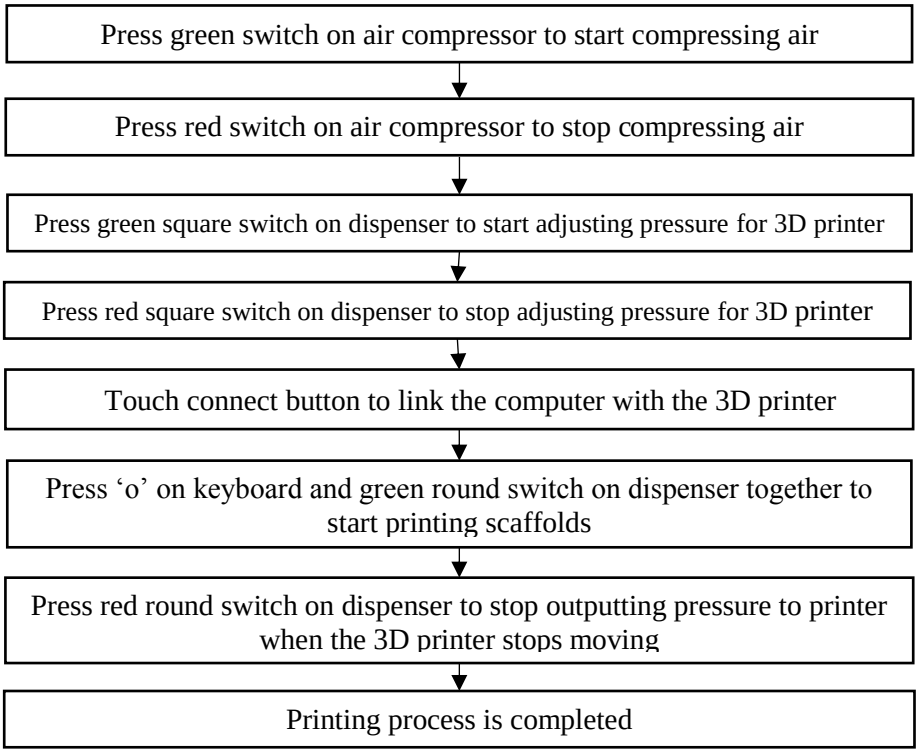

Figure 1. The operation procedures of the pneumatic dispensing system.

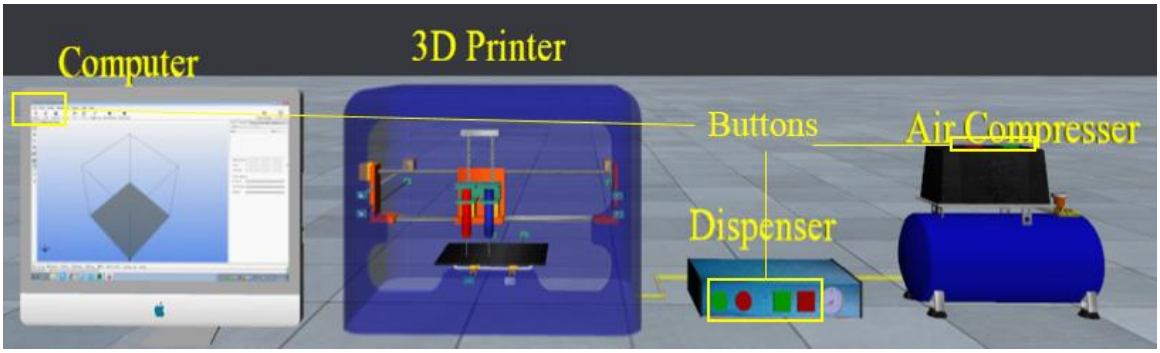

Figure 2. The system configuration of a pneumatic dispensing system.

Appendix IV

Table 1. The individual scores of questions in the questionnaires for evaluation of simulation system:

Persons / **Questions**	**Person 1**	**Person 2**	**Person 3**	**Person 4**	**Person 5**	**Person 6**	**Person 7**	**Person 8**	**Person 9**
Question 1	5	4	4	5	4	5	4	5	5
Question 2	5	4	5	5	4	4	5	5	5
Question 3	4	4	5	5	5	5	3	5	4
Question 4	5	4	4	5	4	5	3	5	4
Question 5	5	5	5	4	4	5	4	5	5
Question 6	4	4	4	5	4	5	4	5	5

Table 2. The individual scores of questions in the questionnaires for evaluation of operation manual:

Persons / Questions	Person 1	Person 2	Person 3	Person 4	Person 5	Person 6	Person 7	Person 8	Person 9
Question 1	3	3	3	4	3	3	5	2	3
Question 2	3	3	3	3	3	4	5	4	3
Question 3	3	2	2	3	2	3	4	1	2
Question 4	2	3	3	3	4	4	3	3	3
Question 5	2	3	2	2	2	4	5	3	2
Question 6	3	2	4	3	3	4	5	3	3